Computer Simulations

WS 2009

H. G. EVERTZ

BASED ON EARLIER LECTURE NOTES

BY W. VON DER LINDEN AND E. SCHACHINGER

Contents

Introduction

Traditionally, physics has been divided into two fields of activities: theoretical and experimental. Due to the development of powerful algorithms and the stunning increase of computer power, a new branch has established itself: Computational physics. Computer simulations play an increasingly important role in physics and other sciences, as well as in industrial applications. They serve different kinds of purposes, among them

- Solution of complex mathematical problems, e.g.
  - Minimization / optimization
  - Eigenvalue problems
  - High-dimensional integrals or sums (Markov Chain Monte Carlo)
- Direct Simulation of physical processes, e.g.
  - Monte Carlo Simulations of physical systems, classical and quantum mechanical
  - Molecular dynamics
  - Percolation problems: oil, forest fires, avalanches
  - Neural networks
  - Cellular automata: forest fires, traffic flow, avalanches
  - Growth processes, fractals

Within the restricted available time of one hour per week, the present lectures serve as an introduction to some of the most important techniques of computer simulations.

Chapter 1

Sampling from probability distributions

Literature

1. F.J. VESELY, *Computational Physics: An Introduction*, Springer 2001.
2. W. KINZEL and G. REENTS, *Physik per Computer. Programmierung physikalischer Probleme mit Mathematica und C*, Springer 1996 (english: Springer 1997).
3. K. BINDER and D.W. HEERMANN, *Monte Carlo Simulation in Statistical Physics: An Introduction*, Springer 2002.
4. D.P. LANDAU and K. BINDER, *A Guide to Monte Carlo Simulations in Statistical Physics*, Cambridge University Press 2009.
5. B.A. BERG, *Markov Chain Monte Carlo Simulations and their Statistical Analysis*, World Scientific 2004.
6. M.E.J. NEWMAN and G.T. BARKEMA, *Monte Carlo Methods in Statistical Physics*, Oxford University Press 1999.
7. J.S. LIU, *Monte Carlo Strategies in Scientific Computing*, Springer 2008 (mathematically oriented).

1.1 Introduction

Physical systems, like a gas, a fluid, or a more complicated system, can occur in many states x. It is often useful to describe aspects of such a system by its **statistical** properties, namely the probability distribution $\pi(x)$, and look at quantities such as the **expectation value** of some function f,

$$\langle f \rangle \; := \sum_x \; f(x)\, \pi(x) \; , \tag{1.1}$$

where f is for example the energy, or a correlation, or any other quantity. We shall denote the expectation value by angular brackets, like in quantum mechanics.

For a large or infinite state space, it can be impossible to calculate such a sum directly. Instead one can use **importance sampling**: If one finds a way to draw N states x_i from the distribution π, one can then calculate the **sample mean (average value)**, denoted by a bar

$$\overline{f} \;:=\; \frac{1}{N} \sum_{i=1}^{N} f(x_i) \;, \tag{1.2}$$

In the limit $N \to \infty$, $\overline{f}$ approaches $\langle f \rangle$. Note that this sample mean (like any quantitative result) is *meaningless* without an estimate of its error ! The variance of the distribution is

$$\sigma^2 = \left\langle \; (\, f(x) - \langle f(x) \rangle \,)^2 \; \right\rangle \;. \tag{1.3}$$

If the states x_i are drawn *independently* of each other, then the variance can be estimated by the **sample variance**

$$s^2 \;:=\; \frac{1}{N-1} \sum_{i=1}^{N} \left(f(x_i) - \overline{f} \right)^2 \tag{1.4}$$

and the error of $\overline{f}$ for large N can be estimated by $\sqrt{s^2/N}$. If the states x_i are not independent, then the error can be much larger, as we will discuss later.

One example of a very big state space is the Gibbs formulation of statistical mechanics. It uses a large number of instances x of a system (e.g., configurations consisting of positions and momenta of particles). All instances together constitute an *ensemble*, and its distribution $\pi(x)$ is the Boltzmann distribution. Analytical calculations for such systems usually have to be very limited in scope.

It is therefore highly desirable to develop and employ **numerical methods for drawing states from a given distribution** π, which might be complicated and very high dimensional.

The *dynamics* of a system is not contained in the statistical description of a system by a probability distribution $\pi(x)$. However, the probability distribution is usually the consequence of some underlying time dependent process, which on average leads to $\pi(x)$. This process is often (depending on the physical model employed) **stochastic** in nature, which means that the time evolution contains an element of randomness. Indeed, quantum mechanics is entirely of stochastic nature, as are the fundamental processes of elementary particles. Thus, stochastics is of elementary importance.

An example from classical physics is the stochastic description of the diffusion of a particle, by using an equation of motion which explicitly includes random forces. Such an equation was postulated by P. Langevin

1907 in an attempt to describe Brownian motion: the stochastic differential equation

$$m\frac{d^2}{dt^2}\mathbf{r}(t) = -\gamma\mathbf{v}(t) + \mathbf{S}(t). \tag{1.5}$$

Here, $-\gamma\mathbf{v}(t)$ describes the drag which a particle experiences in its motion, due to the viscosity of the fluid. $\mathbf{S}(t)$ is a *stochastic force* which has its origin in random collisions of the particle with the molecules of the fluid and is taken to follow some probability distribution, e.g. Gaussian, whose variance is closely related to the viscosity γ and the temperature of the fluid.

One can model such a stochastic time evolution by *sampling* the stochastic force from its desired distribution, and following the time evolution of the system by means of a direct simulation like *Molecular Dynamics*, which will be introduced in a later chapter.

Algorithms exist for drawing from some given distribution "directly", producing independent states. We will introduce important methods in this chapter. They are usually restricted to low dimensional state spaces.

For high dimensional state spaces where such direct methods become extremely inefficient, so called **Markov Chain Monte Carlo** methods have been developed. By a stochastic process, they generate a sequence of configurations x_i which together sample from the full ensemble with $\pi(x)$. We will also treat such methods in this chapter.

Monte Carlo methods have even been constructed for quantum mechanical systems. They make use of the Feynman path integral formulation to map a d-dimensional quantum mechanical system to a classically looking system in $(d+1)$ dimensional space-time, with a distribution π related to the path integral. Such **Quantum Monte Carlo** simulations also provide information about spectra and other time dependent quantities. They are beyond the scope of the present lectures. An example will be part of the advanced Computational Physics class offered in the next semester.

1.2 Direct Sampling Methods

In this section we describe different techniques to draw random numbers from a distribution $g(x)$, independent of each other. We treat the single-variable case, since random sampling from multivariate distributions can always be reduced to single variable sampling. In fact all other generators (including Monte Carlo) are built on these simple direct methods.

We are thus concerned with a *random variable* X. It is characterized by a (possibly infinite) interval $x_{\mathrm{m}in} \leq x \leq x_{\mathrm{m}ax}$ or a discrete set of x-values, which can be viewed as the outcome of "experiments", and a Cumulative Distribution Function (**CDF**) $G(\lambda)$ which specifies the probability that in a particular realization, i.e. one instance of the "experiment", the outcome satisfies $x \leq \lambda$. It is connected by

$$G(\lambda) \;=\; \int_{x_{\mathrm{m}in}}^{\lambda} dx\; g(x) \tag{1.6}$$

to the probability *density* $g(x) \geq 0$, also called the *Probability Distribution Function* (**PDF**). It is normalized ($G(x_{max}) = 1$). We want to generate realizations of such a random variable, i.e. to generate random values of x, distributed in the interval $[x_{\min}, x_{\max}]$ with density $g(x)$.

Note that with a computer program we can never generate truly random numbers. Instead we produce *"pseudorandom"* numbers, usually in sequential fashion, which should satisfy certain criteria, but will always be inadequate in some aspects. Some of the simpler criteria are statistical means, variances, etc., as well as visible correlations of subsequent numbers.

It is important to realize that the "**quality**" of any given random number generator **depends on the application** for which it is used. A generator which is very good for one application may fail badly for others, even closely related ones. One should therefore compare results employing several random number generators of *different* design, especially when precise results are desired.

1.2.1 Uniform Random Numbers

Most random sampling algorithms have as their *basic ingredient* random numbers r which are uniformly distributed in the interval $[0, 1]$, described by the PDF:

$$u(r) = \begin{cases} 1 & r \in [0,1] \\ 0 & \text{otherwise.} \end{cases} \tag{1.7}$$

This results in the cumulative distribution function

$$U(r) = \int_0^r dr'\, u(r') = \begin{cases} 0 & r < 0 \\ r & 0 \leq r < 1 \\ 1 & r \geq 1. \end{cases} \tag{1.8}$$

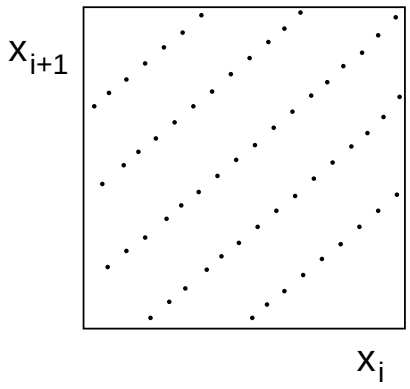

Figure 1.1: Bad generator (schematical): Pairs of random numbers lying on hyperplanes.

There are many algorithms. Among the simplest are the *linear congruential generators* (LCG) which are based on the recursion

$$x_{i+1} = (a\, x_i + c) \bmod m,$$

where the integers a, c, and m are constants. These generators can further be classified into mixed $(c > 0)$ and multiplicative $(c = 0)$ types. An LCG generates a sequence of pseudo random integers X_1, X_2,... between 0 and $m - 1$. Each X_i is then scaled into the interval $(0, 1)$ (or sometimes $[0, 1)$). When m is a prime number, the period of the generator can be up to $m-1$. It depends on the choice of parameters a, c.

One choice of parameters for the LCG sometimes used is $a = 16\,807 = 7^5$ and $m = 2^{31} - 1$. This yields a generator (called GGL or CONG or RAND0) which is given by:

$$R_n = \left(7^5\, R_{n-1}\right) \bmod \left(2^{31} - 1\right), \quad r_n = \frac{R_n}{2^{31} - 1}. \tag{1.9}$$

It produces a sequence of random numbers r_n uniformly distributed in $(0, 1)$ from a given odd *seed number* $R_0 < 2^{31} - 1$. The generator (1.9) is known to have reasonably good random properties for many purposes. The sequence is periodic, with a period of the order of $2^{31} \approx 2 \times 10^9$. This is not large enough to prevent recurrence of random numbers in large simulations (which may or may not matter). *Caution:* the least significant bits of this and most other generators have far worse properties than the most significant ones; they should thus not be used by themselves.

Another known problem of this and other linear congruential generators is that D-dimensional vectors $(x_1, x_2, \ldots, x_D)$, $(x_{D+1}, x_{D+2}, \ldots, x_{2D})$, ...formed by consecutive normalized random numbers x_i may lie on a relatively small number of parallel hyperplanes.

Operating systems and programming languages usually provide random numbers, sometimes like (1.9), sometimes of other designs. In many

cases they are good enough. But, again, it depends on the precise problem and method used whether a given generator is "good" or "bad".

1.2.2 Inverse Transformation Method

We want to draw from a probability distribution function $g(x)$. The cumulative distribution function

$$G(x) = \int_{x_{\min}}^{x} dx'\ g(x')$$

is a non-decreasing function of x and therefore it has an inverse function $G^{-1}(\xi)$. The transformation $\xi = G(x)$ defines a new random variable that takes values in the interval $[0, 1]$. It has a probability distribution function $g_\xi(\xi)$ and a cumulative distribution function $G_\xi(\xi)$. Conservation of probability implies

$$dG_\xi(\xi) \ = \ dG(x)\ .$$

(This is true for any variable-transformation $\xi = f(x)$ with a monotonically growing function f). Thus $g_\xi(\xi)d\xi = g(x)dx$ and

$$g_\xi(\xi) = g(x)\left(\frac{d\xi}{dx}\right)^{-1} = g(x)\left(\frac{dG(x)}{dx}\right)^{-1} \ = \ 1, \tag{1.10}$$

that is, ξ is *uniformly* distributed in the interval $[0, 1]$.

Therefore, if ξ is chosen as a uniformly distributed random number, then the variable defined by

$$x = G^{-1}(\xi) \ := \ \inf\{x|G(x) = \xi\} \tag{1.11}$$

is randomly distributed in the interval $[x_{\min}, x_{\max}]$ with the desired PDF $g(x)$. This provides a practical method of generating random values of x, while using a generator of random numbers which are uniformly distributed in $[0, 1]$. The randomness of x is guaranteed by that of ξ. (1.11) is equivalent to solving

$$\xi = \int_{\mathbf{x}_{\min}}^{x} dx'\, g(x'), \tag{1.12}$$

for x. This is called the *sampling equation*. The inverse transformation method is useful if $g(x)$ is given by a simple analytical expressions such that **the inverse of $G(x)$ can be calculated** easily.

Example. Consider the uniform distribution in the interval $[a, b]$:

$$g(x) = u_{a,b}(x) = \frac{1}{b-a}.$$

We need to solve

$$\xi = G(x) = \frac{x-a}{b-a}$$

for x, namely

$$x = a + \xi(b-a), \quad \xi \in [0,1].$$

As another important example consider the exponential distribution

$$g(s) = \frac{1}{\lambda} \exp\left\{-\frac{s}{\lambda}\right\}, \quad s > 0, \tag{1.13}$$

which describes, e.g., the free path s of a particle between interaction events. The parameter λ represents the mean free path. In this case, the sampling equation (1.12) is easily solved to give the sampling formula

$$s = -\lambda \ln(1-\xi) \text{ or } s = -\lambda \ln \xi. \tag{1.14}$$

The last equality follows from the fact that $1-\xi$ is also a random number distributed equally in $(0,1]$.

1.2.3 Rejection Method

The inverse transformation method for random sampling is based on a one-to-one correspondence between x and ξ values. There is another kind of sampling method, due to von Neumann, that consists of sampling a random variable from a suitable other distribution and subjecting it to a random test to determine whether it will be accepted for use or rejected. This rejection method leads to very general techniques for sampling from *any* PDF.

We want to generate random numbers following a PDF $g(x)$

$$0 \le g(x) \le 1, \quad \int_a^b dx\, g(x) = 1, \quad x \in [a,b].$$

We need to find another PDF $h(x)$,

$$0 \le h(x) \le 1, \qquad \int_a^b dx\, h(x) = 1,$$

which should satisfy

$$g(x) \le c\, h(x), \quad \forall x \in [a,b], \tag{1.15}$$

with c a constant. Thus, in the interval $[a,b]$, $c\,h(x)$ is the *envelope* of the PDF $g(x)$. (See Fig. 1.2.)

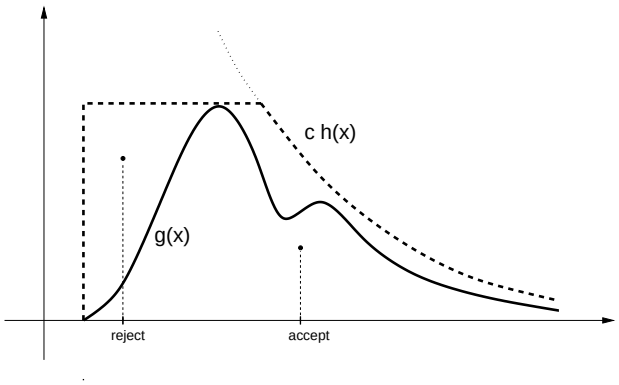

Figure 1.2: The rejection method.

The interval $[a, b]$ can also be infinite, in which case $h(x)$ cannot be a constant because of normalization. The distribution $h(x)$ needs to be *easy to sample*. In practice this means that we must be able to compute the inverse $H^{-1}(\xi)$ of the CDF $H(x) = \int_a^b h(x)dx$. In Fig. 1.2, $h(x)$ is composed of two parts, the first (e.g. $\sim 1/x^2$) taken to envelope $g(x)$ at large x, and the second constant part at small x in order to avoid the large area underneath a function like $1/x^2$ at small x (see below). The corresponding CDF $H(x)$ can still be inverted easily in an analytical way.

Random numbers distributed according to the PDF $g(x)$ are then generated according to the following procedure:

Algorithm 1 Rejection Method

begin:
Generate a trial random variable x_T from $h(x)$
Generate a uniform random number r from $u(x)$, Eq. (1.7).
if $r\, c\, h(x_T) < g(x_T)$ **then**
  accept x_T
else
  go to begin
endif

Proof: The probability of accepting a value x_T is $p(A|x_T\,\mathcal{B}) = g(x_T)/(ch(x_T))$ (with $p := 0$ when $h = g = 0$). Thus

$$\begin{aligned} p(x|\mathcal{B}) &\propto p(x = x_T|\mathcal{B})\; p(A|x_T\mathcal{B}) \\ &= h(x_T)\frac{g(x_T)}{c\, h(x_T)} \\ &\propto g(x_T). \end{aligned}$$

The accepted random numbers x_T indeed follow the PDF $g(x)$.

Probability of acceptance:

The overall probability of acceptance $P(A|\mathcal{B})$ is simply the area under $g(x)$ divided by the area under $ch(x)$, i.e. it is $\frac{1}{c}$. Formally:

$$\begin{aligned} P(A|\mathcal{B}) &= \int dx_T\, p(Ax_T|\mathcal{B}) \\ &= \int dx_T\, p(A|x_T\mathcal{B})p(x_T|\mathcal{B}) \\ &= \int dx_T\, \frac{g(x_T)}{c\,h(x_T)} h(x_T) \\ &= \int dx_T \frac{g(x_T)}{c} \\ &= \frac{1}{c}. \end{aligned}$$

Thus, the bigger c, the worse the probability of acceptance becomes. We should therefore choose the constant c as small as possible, i.e. $c\,h(x)$ should be as close to $g(x)$ as possible. If we apply rejection methods in d dimensions, we get:

$$P(A|\mathcal{B}) = \left(\frac{1}{c}\right)^d$$

which drops rapidly with increasing d. The rejection method is therefore *very inefficient in high dimensions*. Markov Chain Monte Carlo is then often the method of choice.

1.2.4 Probability Mixing

This method has its application in cases in which the PDF $f(x)$ is composed of a number of PDFs in an interval $[a, b]$:

$$f(x) = \sum_{i=1}^{N} \alpha_i\, f_i(x), \tag{1.16}$$

with

$$\alpha_i \geq 0,\ f_i(x) \geq 0, \qquad \int_a^b dx\, f_i(x) = 1, \text{ and } \sum_{i=1}^{N} \alpha_i = 1.$$

We define the partial sums

$$q_i = \sum_{l=1}^{i} \alpha_l\ .$$

Thus $q_n = 1$ and the interval $[0, 1]$ has been divided according to this figure:

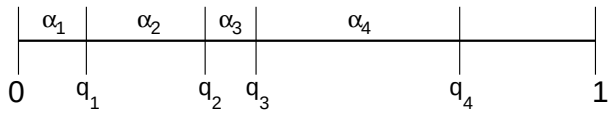

Now we choose an equally distributed random number $r \in [0, 1]$ and determine the index i for which the condition

$$q_{i-1} < r < q_i$$

is fulfilled. Then we draw a random number according to $f_i(x)$. This procedure is correct because α_i specifies the importance of the PDF $f_i(x)$. This in turn gives us the probability that the random variable X is to be sampled using the PDF $f_i(x)$.

Example: The function $h(x)$ in Fig. 1.2 is composed of two parts. We can draw from $h(x)$ by using separate generators for each of the parts.

1.3 Markov Chain Monte Carlo: Importance Sampling

Markov Chain Monte Carlo (MCMC) is an efficient approach to perform sampling in many dimensions, where often the probability density $\pi(x)$ is strongly dominated by only a small part of the total state space. Prime examples are physical systems consisting of many similar particles (electrons, atoms, ...) which interact with each other. The dimension d of state space is some multiple of the number of particles, typically $d = O(10^3 \dots 10^7)$ and larger, so that any sort of simple sampling is entirely impossible. In this lecture we will consider an especially simple model, the Ising model as an example.

In Markov Chain Monte Carlo, configurations x are created iteratively in such a way that their distribution corresponds to a desired distribution $\pi(x)$. Because of the iterative construction, consecutive configurations are usually highly correlated. Thus the samples in average values (1.2) consist of numbers which are also correlated. This is entirely permissible. It does however require careful consideration of the convergence of sample means and especially of their statistical errors.

Many methods have been developed over time for different applications, some of them very efficient. We will be concernced in details just with the basic "Metropolis-Hastings" method, which is almost always applicable. An appendix provides an overview over more modern strategies. In physics, Markov Chain Monte Carlo is often just called "Monte Carlo".[1]

1.3.1 Markov Chains

Chains of dependent events were first studied by A. Markov in 1906. We will first collect a number of definitions and properties.

Markov property

A Markov chain is specified in a discrete sequence, usually called (Markov- or Monte-Carlo-) time. It does normally *not* correspond to physical time. The Markov "time" is just $t_n = n = 0, 1, 2, \dots$. At each of these times the system is in one state x_{t_n} of the set of possible states

$$Z_1,\ Z_2,\ \dots,\ Z_k,$$

which together span the state space $\mathcal{S}$. Example: $(x_{t_1} = Z_9,\ x_{t_2} = Z_5,\ x_{t_3} = Z_8,\ \dots)$. We shall restrict our discussion to **finite state spaces**.[2]

[1] The name "Monte Carlo integration" is sometimes used for *simple* sampling with a random choice of values of the integration variable x. This should not be confused with the Importance Sampling of Markov Chain Monte Carlo.

[2] This avoids cumbersome mathematical issues. Indeed, it is realistic, since the representation of a system on a computer using a finite number of bits for the discrete or "continuous" degrees of freedom corresponds to a finite state space.

The defining **Markov property** is that the probability of being in a particular state Z_j at time t_{n+1} depends *only* on the state at the *current* time t_n, but not on any previous history.

Transition matrix

The Markov chain is specified by the initial probability distribution $\pi(x, t = 0)$ of states at time zero, and by the transition probability p_{ij} from state Z_i at time t_n to state Z_j at time t_{n+1}.
We demand that the transition probabilities do not depend on time.

Transition probabilities are organized in the *transition matrix*:

$$\boldsymbol{P} = \{p_{ij}\} = \begin{pmatrix} p_{11} & p_{12} & \dots & p_{1k} \\ \vdots & \vdots & \ddots & \vdots \\ p_{k1} & p_{k2} & \dots & p_{kk} \end{pmatrix}. \tag{1.17}$$

$\boldsymbol{P}$ is a *stochastic matrix*, *i.e.:* all elements of $\boldsymbol{P}$ obey the inequality

$$0 \leq p_{ij} \leq 1,$$

and all row-sums of the $k \times k$ matrix are equal to unity:

$$\sum_{j=1}^{k} p_{ij} = 1, \qquad i = 1, \dots, k. \tag{1.18}$$

The transition probabilities $p_{ij}^{(k)}$ from state Z_i at time t_n to a state Z_j at time t_{n+k} k steps later are simply $(\boldsymbol{P}^k)_{ij}$.

Irreducibility

A Markov chain is called *irreducible*, if for every pair of states Z_i and Z_j there is a number n, such that one can get get from Z_i to Z_j in n steps with finite probability, i.e. if the state space is not subdivided into non-communicating regions.

Periodicity

A state Z_i has period d, if any return to state Z_i occurs only in some multiple of d time steps and d is the largest number with this property. A state is *aperiodic* when $d = 1$. A sufficient condition for aperiodicity of state Z_i is that the diagonal matrix element is not zero: $p_{ii} > 0$.

In an irreducible chain, all states have the same period; so we can then speak of the chain having the period d.

Example: A transition matrix in a space of 2 states, which is irreducible but not aperiodic:

$$\begin{pmatrix} 0 & 1 \\ 1 & 0 \end{pmatrix}.$$

With this matrix one can move from any state to any state, so the chain is irreducible. But it is also periodic with period 2, since only an even number of steps will lead back to the original state.

Regular chain

The transition matrix $\boldsymbol{P}$ is called *regular* if some power of $\boldsymbol{P}$ has only strictly positive elements. This is equivalent to the chain being both irreducible and aperiodic.

Ergodicity

A Markov chain with the same properties, irreducibility and aperiodicity, is called *ergodic*.
Caution: Ergodicity is sometimes defined differently.

1.3.2 Stationarity and convergence

Stationarity, Global balance

The vector of probabilites π_i, with $\sum_i \pi_i = 1$, is called a **stationary distribution** when

$$\boxed{\pi_j \;=\; \sum_i \pi_i \, p_{ij}} \tag{1.19}$$

This means that when one starts with an *ensemble* of states occuring with probabilities π_i and performs a step of the Markov chain, then the resulting ensemble will have the same probabilities for each state.

One can write the equation (1.19) for stationarity (= "Global Balance") in matrix form:

$$\boldsymbol{\pi} \;=\; \boldsymbol{\pi}\,\boldsymbol{P}\,,$$

showing that π is a *left eigenvalue* of the transition matrix $\boldsymbol{P}$.

Convergence of a Markov chain

Theorem 1.1 *A Markov chain has a stationary* distribution *if it is irreducible. Then the stationary distribution π is* unique.

Theorem 1.2 *If the chain is also* aperiodic, *then it converges to the stationary distribution,* independent of the starting distribution.

$$\boxed{\lim_{n\to\infty} (\boldsymbol{P}^n)_{ij} \;=\; \pi_j \qquad \forall i\,.} \tag{1.20}$$

This is a central theorem for Markov chains. Equation (1.20) is equivalent to

$$\lim_{n\to\infty} \boldsymbol{P}^n \;=\; \mathbf{1}\boldsymbol{\pi}\,, \tag{1.21}$$

i.e., $\boldsymbol{P}^n$ converges to a matrix in which every row is the distribution π.

1.3.3 Detailed balance

A Markov chain is called *reversible* if it satisfies the *detailed balance* condition[3]

$$\boxed{\pi_i \, p_{ij} \;\; = \;\; \pi_j \, p_{ji}} \tag{1.22}$$

This is a sufficient condition for stationarity. Proof: We take the sum $\sum_j$ on both sides of eq. (1.22). Because of $\sum_j p_{ij} \, = \, 1$, we get eq. (1.19) immediately.

Example: Spread of a rumor

Z_1 and Z_2 are two versions of a report, namely, Z_1: Mr. X is going to resign, and Z_2: Mr. X is not going to resign. We can write the following transition matrix:

$$\boldsymbol{P} = \begin{pmatrix} 1-p & p \\ q & 1-q \end{pmatrix},$$

to the effect that:

(i) Some person receives the report Z_1. It will then pass this report on as Z_2 with a probability p and as Z_1 with a probability $(1-p)$. Consequently, the report will be modified with a probability p.

(ii) In the same way, the report Z_2 will be modified with a probability q.

Realistically $0 < p < 1$ and $0 < q < 1$. In this simple case we can analyze the Markov chain exactly, namely by diagonalizing $\boldsymbol{P}$ such that $U^\dagger \boldsymbol{P} U$ is diagonal. Then $\boldsymbol{P}^n = U \, \left(U^\dagger \boldsymbol{P} U\right)^n \, U^\dagger$, and one obtains

$$\lim_{n\to\infty} \boldsymbol{P}^n = \frac{1}{p+q} \begin{pmatrix} q & p \\ q & p \end{pmatrix}$$

and, consequently

$$\pi_1 = \frac{q}{p+q}, \qquad \pi_2 = \frac{p}{p+q}.$$

Indeed, this distribution also satisfies the detailed balance condition, namely

$$\frac{p_{12}}{p_{21}} \;\; = \;\; \frac{\pi_2}{\pi_1} \, .$$

x

[3]The same equation occurs in chemistry for concentrations and reaction rates.

No matter what the initial probabilities of the reports Z_1 and Z_2 were, they will in the end converge to π_1 and π_2. Thus the public will eventually be of the opinion that Mr. X will resign with a probability π_1 that is independent of his real intentions.

Markov chains have applications in many diverse fields, among them statistical physics, evolution of populations, Bayesian analysis of experiments, and many others.

The numerically biggest application of all is quite recent, namely the original Google page rank algorithm. This rank is the probability in the stationary distribution of a Markov chain which assigns a constant transition probability to each link on a web page, and additional tiny transition probability from any web page to any other to ensure ergodicity.

1.3.4 Metropolis-Hastings method

We want to *construct* a Markov chain such that it has a desired stationary distribution π_i. This means that we need to find a suitable transition probability matrix. The Metropolis-Hastings algorithm provides a transition matrix which *satisfies detailed balance* with respect to a given distribution π_i. If the Markov matrix is also ergodic (irreducible and aperiodic) it will then converge to π.

The Metropolis method was the first Markov chain Monte Carlo method, later generalized by Hastings. It is widely applicable since it is very simple. For specific applications, there are often much better methods, some of which are mentioned at the end of this chapter.

We construct the probability matrix p_{ij} for going from a state Z_i to some other state Z_j. Let the chain be in a state Z_i. Then we perform the following steps:

1. We *propose* to move to a state Z_j according to some *proposal probability* q_{ij}. It needs to be chosen in such a way that the Markov chain will be ergodic (irreducible and aperiodic). One needs to carefully make sure that this is indeed the case.

2. We *accept* the state Z_j as the next state of the chain with probability

$$p_{ij}^{accept} \;=\; \min\left(1,\; \frac{\pi_j\, q_{ji}}{\pi_i\, q_{ij}}\right) . \tag{1.23}$$

3. When Z_j is not accepted, then the next state of the chain will again be Z_i (!).

The overall transition matrix p_{ij} is the product of the probability q_{ij} to propose a step from i to j and the acceptance probability p_{ij}^{accept}:

$$p_{ij} \;=\; q_{ij}\, p_{ij}^{accept} . \tag{1.24}$$

Proof of detailed balance: We look at the case that the nominator in eq. (1.23) is smaller than the denominator. The opposite case is just an exchange of indices. Then

$$\begin{aligned} \pi_i \, p_{ij} &= \pi_i \, q_{ij} \, p_{ij}^{accept} \\ &= \pi_i \, q_{ij} \, \frac{\pi_j \, q_{ji}}{\pi_i \, q_{ij}} \\ &= \pi_j \, q_{ji} \end{aligned}$$

which is indeed the same as

$$\begin{aligned} \pi_j \, p_{ji} &= \pi_j \, q_{ji} \, p_{ji}^{accept} \\ &= \pi_j \, q_{ji} \, 1 \, . \end{aligned}$$

1.3.5 Making use of a single chain

With ergodicity and detailed balance satisfied, an algorithm like Metropolis will produce a Markov chain with π_i as the stationary distribution. Regardless of the original state of the chain, after a large amount of steps the final state will be from the distribution π.

One could then simulate a large number of Markov chains from some arbitrary initial state(s) (using different random numbers) and use the ensemble of final states as a sample of π. This strategy is inefficient, since it often takes a long time for the chains to "forget" the initial state, so that one must have very long chains for each individual sample, and even then the samples will still tend to be biased.

A much better strategy is to use a single chain (or a few with different initial states). First one waits for a rather long time to let the chain forget its initial state. After this “thermalization” one then takes many samples for measurements from the single chain, with a fairly small number of steps in between (described later). These samples will all be (approximately) from π because of the thermalization, but they will be more or less correlated with each other. One therefore needs a careful error analysis to make use of these numbers, which we will discuss in section 1.4.

1.3.6 Example: The Ising model

The Ising model was invented to describe ferromagnets. It is one of the simplest models of statistical mechanics. This model and related ones have applications in many other parts of physics and beyond. More information on these models as well as on Markov Chain Monte Carlo can be found in the lectures on "Phase transitions and Critical Phenomena".

The Ising model is concerned with variables called spins s_i living on a *lattice* of sites i, $i = 1, \ldots, N$, e.g. on a square or 3D lattice with N sites.

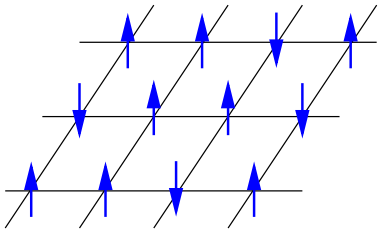

Figure 1.3: A spin configuration of the Ising model.

In the Ising model, the variables take only two values

$$s_i \in \{-1, +1\} .$$

These two values represent, for example, two spin states of an atom located at site i. A completely different incarnation of the Ising model is for example a binary alloy, where on each lattice site there is either an atom of species "A" or of species "B". The value of s_i then specifies this species. We will in the following use the language of "spins" and corresponding magnetism.

In a *ferromagnet*, spins prefer to be aligned. In the simplest Ising model, only spins on sites i and j that are nearest neighbors on the lattice interact. They have an energy

$$-J\, s_i s_j , \quad J > 0$$

which favors alignment. In addition, a magnetic field h changes the energy of each spin by $-h\, s_i$. The total energy of each configuration of spins $\mathbf{S} = (s_1, s_2, \ldots, s_N)$ is then

$$E(\mathbf{S}) = -\sum_{\langle ij \rangle} J\, s_i\, s_j \;\; - \;\; h \sum_i s_i \, . \tag{1.25}$$

The sum extends over all pairs $\langle ij \rangle$ of nearest neighbor sites.[4]

The magnetization of a spin configuration $\mathbf{S}$ is

$$M \;\; = \;\; \sum_i s_i \, . \tag{1.26}$$

For the Ising model, the spin configurations $\mathbf{S}$ are the states "x" of the probability distribution π. It is given by the *Boltzmann weight*

$$\pi(\mathbf{S}) \;\; = \;\; \frac{e^{-\beta E(\mathbf{S})}}{Z} \, , \tag{1.27}$$

[4]The expression for $E(\mathbf{S})$ can be interpreted as a quantum mechanical Hamilton operator. Then s_i represents the z-component of a quantum mechanical spin. However, there are no operators $\hat{S}_i^+$ or $\hat{S}_i^-$ which would *change* the value of s_i. The Hamilton operator is therefore already *diagonal* in the variables s_i. It is just a normal function of $\mathbf{S}$, without any operator effects, and the Ising model is in effect not quantum mechanical but a *classical* model of classical variables s_i.

where the normalization factor Z is the *partition function*

$$Z \;=\; \sum_{\mathbf{S}} \, e^{-\beta E(\mathbf{S})} \; . \tag{1.28}$$

The sum extends over all possible spin configurations. For N spins there are 2^N configurations. Therefore simple sampling is impossible except for very small toy systems.

Expectation values are given by (1.1): $\langle f \rangle \;:=\; \sum_x \; f(x)\, \pi(x)$.
Some of the interesting observables of the Ising model are:

- Internal energy

$$\langle E \rangle = \sum_{\mathbf{S}} \, \mathcal{H}(\mathbf{S}) \;\; \frac{e^{-\beta\, \mathcal{H}(\mathbf{S})}}{Z} \; , \tag{1.29}$$

- Average magnetization of a configuration

$$\langle M \rangle = \sum_{\mathbf{S}} \, M(\mathbf{S}) \;\; \frac{e^{-\beta\, \mathcal{H}(\mathbf{S})}}{Z} \; , \tag{1.30}$$

- Magnetic susceptibility

$$\chi \;=\; \frac{\partial}{\partial h} \langle M \rangle \;\; = \;\; \beta \big(\, \big\langle M^2 \big\rangle \; - \; \langle M \rangle^2 \, \big) \; . \tag{1.31}$$

In two or more dimensions, the Ising model exhibits a *phase transition*:
At low temperatures (large β), allmost all spins are aligned: the system is in an ordered, ferromagnetic state.
At high temperatures (low β), the spins take almost random values and the system is in an unordered, paramagnetic state. For a 1D system and a 2D square lattice, the model can be solved exactly. All other cases need to be examined by numerical methods or approximate analytical techniques.

1.3.7 Choice of Monte Carlo steps

Because of its many states, we need Markov Chain Monte Carlo to evaluate observables numerically, without the systematic errors of analytical approximations.

There is a lot of freedom in choosing the Markov transition matrix. Different choices can affect the efficiency of a simulation drastically, even by many orders of magnitude, especially in the physically most interesting cases.

We will stay with the simple Metropolis-Hastings method for the Ising model. Let the current state "i" of the Metropolis method be the spin configuration $\mathbf{S}$. We need to propose a change ("update") to a new state j, which here we call $\mathbf{S}'$, namely $\mathbf{S} \to \mathbf{S}'$ with some probability $q_{\mathbf{S}\mathbf{S}'}$. We will

propose the reverse transition $\mathbf{S}' \to \mathbf{S}$ with the same probability. Then $q_{ij} = q_{ji}$ for the proposal probability, and it cancels in (1.23)

$$p_{ij}^{accept} = \min\left(1,\ \frac{\pi_j\ q_{ji}}{\pi_i\ q_{ij}}\right) .$$

With $\pi(\mathbf{S}) = \frac{1}{Z} e^{-\beta E(\mathbf{S})}$ we get

$$p_{\mathbf{S}\,\mathbf{S}'}^{accept} = \min\left(1,\ \frac{e^{-\beta E(\mathbf{S}')}}{e^{-\beta E(\mathbf{S})}}\right) = \min\left(1,\ e^{-\beta \Delta E}\right) . \qquad (1.32)$$

The acceptance probability thus depends on the energy change $\Delta E = E(\mathbf{S}') - E(\mathbf{S})$. The proposed update will consist of some spin flips. If we propose to flip many spins at once, then the energy change will be large and will be accepted too rarely. For the Ising model, a suitable update proposal is to flip a *single* spin !

A single step of the Markov chain now consists of two parts:

- Choose a lattice site l at random. Propose to flip $s_l \to -s_l$, i.e. the configuration $\mathbf{S}'$ differs from $\mathbf{S}$ only in the value of s_l.
- Compute ΔE. Accept $\mathbf{S}'$ with probability (1.32). If it is accepted, the next Markov chain configuration will be $\mathbf{S}'$. If it is not accepted, the next configuration will *again* be $\mathbf{S}$.

Irreducibility of this procedure is assured: with single spin flips one can eventually get from any spin configuration to any other. With the procedure just specified, aperiodicity also holds, because the diagonal probabilites p_{ii} to stay in the same state are finite. Detailed balance is satisfied by construction. Thus this is a valid Monte Carlo procedure which will converge to the Boltzmann distribution.[5]

Obviously, the update of a single spin changes a configuration only by very little. Many such steps concatenated will eventually produce bigger changes. A useful unit of counting Monte Carlo steps is a *sweep*, defined to consist of N single spin steps, where N is the number of spins in the lattice. Observables are usually measured once every sweep, sometimes more rarely (see below).

1.3.8 Thermalization

A Markov chain is started in some configuration x_α. For instance, in an Ising model, x_α might be the configuration with "all spins up"; this is

[5] In practice, one often moves through lattice sites *sequentially* instead of at random. This violates ergodicity slightly but is usually harmless on big systems. In special cases (e.g. small system with periodic boundary conditions) it can induce a periodic Markov Chain, i.e. invalid results.

sometimes called a *cold* start. Alternatively, the Markov chain might be started in a random configuration, called a *hot* start. In any case, the initial state x_α tends to be far from the equilibrium distribution π. Therefore, the system is "out of equilibrium", and measurements $O(X_t)$ may initially have values far from their average. Theorems 1.1 and 1.2 guarantee that the system approaches equilibrium as $t \to \infty$, but we should know something about the *rate* of convergence to equilibrium. We will quantify this a little later.

One can take measurements before equilibrium is reached. This introduces a *bias* in the averages. When the number of measurements $n \to \infty$, the effect of the bias vanishes like $\frac{1}{n}$, so results eventually converge to the correct expectation values.

However, the bias can be quite large. In order to keep it small, one only starts measuring after a fairly long *equilibration phase* of some n_{therm} sweeps.

A good rule of thumb for choosing n_{therm} is about 10-20$\%$ (!) of the total number of sweeps in the simulation. Reason: It is good to have n_{therm} large to achieve a small bias, while reducing the available number of measurements by $10 - 20\%$ does not increase the statistical errors of averages significantly.

1.3.9 Parts of a Monte Carlo simulation

A Markov chain Monte Carlo consists of the following parts:

- Choose any starting configuration
- Thermalize for n_{therm} sweeps.
  The choice of starting configuration should not make a difference any more after thermalization ! This can be used as a check.
- Generate n configurations X_t, $t = 1, \ldots, n$, separated by one or more sweeps, with **measurements** $O_t := O(X_t)$. (t will from now on only count the sweeps after thermalization).
- **Analysis** of the resulting time series (see next section):
  - Compute averages.
  - Examine autocorrelations.
  - Perform error analysis.
  - Check against known results.

Thus a simulation can be divided into two parts, the data generation part and the data analysis. The interface between these two parts consists of time series of measurements of relevant physical observables taken during the actual simulation. Often a part of the analysis can be done during data generation, without the need to save complete time series.

1.4 Spectral Analysis of discrete time series

Before we analyze Monte Carlo time series, in this section we consider a generic stochastic process in discrete time, which may or may not be a Markov chain. There is a sequence of "times" $t_n = n = 1, 2, 3 \ldots$ (written without unit, for simplicity). Each time separately is associated with a random variable X_n taking real values x with some PDF $g_n(x)$.

Each *realization* of the stochastic process is a *trajectory* with coordinates $x_n = x(t_n)$. It might for example represent the motion of a particle.

Note that there is a PDF for *whole trajectories* in the space of all possible trajectories. Expectation values are defined with respect to this overall PDF. When a quantity like X_n only depends on a single time t_n, then its marginal PDF is g_n. Expectation values for single times t_n are

$$\langle X_n \rangle \;:=\; \int x\, g_n\, dx\;. \tag{1.33}$$

1.4.1 Autocorrelation function

An important issue in the analysis of time series is the question of how strongly successive x_n are correlated with each other. Another related question is that of potential periodicities in the time series. In order to examine correlations, we look at the *covariance* of quantities.

We consider only the case that all expectation values are *time-independent*:

$$\begin{array}{lcll} \langle X_n \rangle & = & \langle X_1 \rangle & =: \;\; \langle X \rangle \\ \mathrm{cov}\,(X_n, X_{n+t}) & = & \mathrm{cov}\,(X_1, X_{1+t}) & =: \;\; R(t)\;, \end{array} \tag{1.34}$$

where in the second line we have given the name $R(t)$ to the covariance. Such time-independent time series are called *"stationary"*.[6]

Since expectation values are time independent, we can write the covariance as

$$\mathrm{cov}(X, Y) \;=\; \left\langle\; (X - \langle X \rangle)\; (Y - \langle Y \rangle)\;\right\rangle \tag{1.35}$$

without time-indices. Note that the covariance measures the correlation of deviations from the expectation values. As usual,

$$\mathrm{cov}(X, X) \;=\; \mathrm{var}(X) \;=\; (\mathrm{std}(X))^2\;. \tag{1.36}$$

We define the **autocorrelation function** $\rho(t)$ (also called *autocorrelation coefficient*) between quantities separated by a "temporal" distance t as the normalized covariance of X_n at some time n with X_{n+t} at time $n + t$:

$$\rho(t) \;:=\; \frac{\mathrm{cov}(X_n, X_{n+t})}{\mathrm{std}(X_n)\,\mathrm{std}(X_{n+t})} \;=\; \frac{\mathrm{cov}(X_0, X_t)}{\mathrm{std}(X_0)\,\mathrm{std}(X_0)} \;=\; \frac{R(t)}{R(0)}, \tag{1.37}$$

[6] Caution: this is different from a "stationary Markov chain", which becomes a stationary *time series* only after and if it has exactly converged to its stationary distribution π.

It tells us how much the *fluctuations* in X (i.e. the deviations from $\langle X \rangle$) are correlated over a time distance t. We will later examine the autocorrelation function in some detail for Monte Carlo Markov Chains.

1.4.2 Estimate of autocorrelations from a realization of a time series

Let (X_n) be a discrete time series which is stationary. We want to give estimates for the most important quantities on the basis of a **realization**, i.e. a set of data

$$x_1,\, x_2,\, \ldots,\, x_N$$

under the assumption that N is large enough for reliable estimates.

An estimator for the expectation value $\langle X \rangle$ is the average value

$$\bar{x} \;=\; \frac{1}{N} \sum_{i=1}^{N} x_i.$$

One possible estimate for the autocorrelation function $\rho(t)$ is

$$\frac{\sum\limits_{j=1}^{N-t} \left(x_j - \bar{x}\right) \left(x_{j+t} - \bar{x}\right)}{\sum_{j=1}^{N-t} \left(x_j - \bar{x}\right)^2}$$

which uses $\bar{x}$ as an estimator for $\langle X \rangle$. However, this estimator tends to be unstable, since for the first bracket the term $\bar{o}$ which is subtracted is different from the average of x_i, since the sum goes only up to $i = N - t$. Similarly for the second factor, and for nominator versus denominator.

A much more stable estimator is obtained by the so-called **empirical autocorrelation function**

$$\rho^E(t) \;:=\; \frac{\sum\limits_{j=1}^{N-t} \left(x_j - \bar{x}_{(t)}\right) \left(y_j - \bar{y}_{(t)}\right)}{\sqrt{\sum\limits_{i=1}^{N-t} \left(x_i - \bar{x}_{(t)}\right)^2 \sum\limits_{j=1}^{N-t} \left(y_j - \bar{y}_{(t)}\right)^2}} \tag{1.38}$$

where

$$y_j \;:= x_{j+t}$$

is the time series shifted by t, and the averages $\bar{x}_{(t)}$ and $\bar{y}_{(t)}$ are calculated with the values of x_j and y_j which actually appear in the sums:

$$\begin{aligned} \bar{x}_{(t)} \;&:=\; \frac{1}{N-t} \sum_{j=1}^{N-t} x_j, \\ \bar{y}_{(t)} \;&:=\; \frac{1}{N-t} \sum_{j=1}^{N-t} y_j \;=\; \frac{1}{N-t} \sum_{j=1+t}^{N} x_j \end{aligned}$$

By construction, $-1 \leq \rho^E(t) \leq 1$. Large values of $|\rho^E(t)|$ indicate a large correlation (or anti-correlation) between data points at a time shift t.

For instance, when $\left|\rho^E(t)\right|$ is particularly large for $t = m, 2m, 3m$ in comparison to other times t, then there is a strong indication of a period $T = 2m$ in the data set.

The autocorrelation coefficient $\rho^E(t)$ is called "empirical" because it refers to a particular realization of the stochastic process.

1.4.3 Computing covariances by Fast Fourier Transform

The calculation of the empirical autocorrelation function is very useful for the analysis of time series, but it is very time consuming, since for each value of t, one needs to sum O(N) terms. There are $O(N)$ possible values of the time distance t. Thus the direct calculation of the autocorrelation function needs $O(N^2)$ steps. This is very expensive, since the *generation* of the time series usually takes $O(N)$ time.[7]

Fast Fourier Transform (FFT)

A very efficient alternative makes use of the so-called Fast Fourier Transform. The FFT consists of an ingenious reorganization of the terms occuring in a Fourier transform. It allows the calculation of the Fourier series of a function $f(t_i)$, $i = 1, \ldots, N$ in only $O(N \log N)$ steps instead of $O(N^2)$. It works best when N is a power of 2, or at least contains only prime factors $2, 3, 5$. FFT is provided as a routine in numerical libraries.

Convolution Theorem for periodic functions

The second ingredient in the efficient calculation of covariances and autocorrelations is the convolution theorem.

We start with functions $f(t_i)$, $g(t_i)$, with $t_i = i$ (again without units, for simplicity), defined in the range $1 \leq i \leq L$. We assume that these functions are *periodic* with period L.

The Fourier transform is

$$\tilde{f}(\omega_n) \;:=\; \frac{1}{\sqrt{L}} \sum_{j=1}^{L} \; e^{-i\omega_n t_j} \; f(t_j) \;, \tag{1.39}$$

where $\omega_n = 2\pi \frac{n}{L}$. We note that

$$\textit{If } f(t_i) \textit{ is real valued, then} \quad \tilde{f}(-\omega_n) \;=\; \left(\tilde{f}(\omega_n)\right)^* \;. \tag{1.40}$$

[7] In the analysis of Monte Carlo time series, where $\rho(t)$ will hopefully decay fast, one usually needs only values $t < O(100) \ll N$, which is however still very expensive.

We calculate the convolution

$$h(t) := \sum_{j=1}^{L} f(t-t_j)\, g(t_j) \tag{1.41}$$

$$= \sum_{j=1}^{L} \frac{1}{\sqrt{L}} \sum_{n=1}^{L} e^{i\omega_n (t-t_j)}\, \tilde{f}(\omega_n) \quad \frac{1}{\sqrt{L}} \sum_{m=1}^{L} e^{i\omega_m t_j}\, \tilde{g}(\omega_m) \tag{1.42}$$

$$= \sum_{n,m=1}^{L} e^{i\omega_n t} \quad \underbrace{\frac{1}{L} \sum_{j=1}^{L} e^{i(\omega_n-\omega_m)t_j}}_{=\delta_{n,m}} \quad \tilde{f}(\omega_n) \quad \tilde{g}(\omega_m) \tag{1.43}$$

$$= \sqrt{L} \quad \underbrace{\frac{1}{\sqrt{L}} \sum_{n=1}^{L} e^{i\omega_n t}\, \tilde{f}(\omega_n)\, \tilde{g}(\omega_n)}_{\text{inverse FT of } \tilde{f}\cdot\tilde{g}} \tag{1.44}$$

and see that in Fourier space it corresponds simply to a product.

We can now compute a convolution of periodic functions efficiently by first calculating the Fourier transforms of f and g by FFT, multiplying them, and finally computing the back-transform by FFT again, with a computational effort of $O(L \log L)$.

Correlation

We repeat the calculation for correlation functions. The only change is the sign of t_j in the argument of f:

$$C(t) := \sum_{j=1}^{L} f(t+t_j)\, g(t_j) \tag{1.45}$$

$$= \sum_{n,m=1}^{L} e^{i\omega_n t} \quad \underbrace{\frac{1}{L} \sum_{j=1}^{L} e^{-i(\omega_n+\omega_m)t_j}}_{=\delta_{n,-m}} \quad \tilde{f}(\omega_n) \quad \tilde{g}(\omega_m) \tag{1.46}$$

$$= \sqrt{L} \quad \underbrace{\frac{1}{\sqrt{L}} \sum_{n=1}^{L} e^{i\omega_n t}\, \tilde{f}(\omega_n)\, \tilde{g}(-\omega_n)}_{\text{inverse FT}} \; . \tag{1.47}$$

Autocorrelation

This is the case $f = g$.
If $f(t_i)$ is real-valued, then we get the simple and very useful result

$$\sum_{j=1}^{L} f(t+t_j)\, f(t_j) = \sqrt{L}\, \frac{1}{\sqrt{L}} \sum_{n=1}^{L} e^{i\omega_n t} \left|\tilde{f}(\omega_n)\right|^2 \; . \tag{1.48}$$

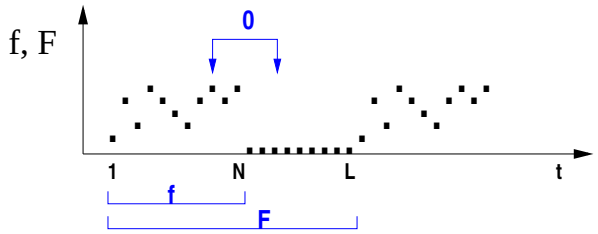

Figure 1.4: Zero Padding of a function f.

Calculation of the autocorrelation therefore involves taking the Fourier transform, calculating the absolute square, and transforming back.

Non-periodic functions

We usually want to evaluate correlations for *non*-periodic functions

$$f(t_i), \quad i = 1, 2, \ldots N,$$

given on a finite set of N points, for a finite range of time intervals, $0 \le t \le t_{max}$. The trick to do this is by so-called **zero-padding**. We define

$$F(t_i) \;:=\; \begin{cases} f(t_i), & 1 \le i \le N, \\ 0, & N+1 \le i \le L, \end{cases} \tag{1.50}$$

with $L \ge N + t_{max}$. (Similarly we extend a function $g(t_i) \to G(t_i)$.) Note that L is at most $2N$. Now the functions F and G are regarded as being periodic, with a long period L (see figure). The zeros in the definition of F ensure that $f(t+t_j)\, g(t_j) \;=\; F(t+t_j)\, G(t_j)$ in the desired range of arguments $1 \le j \le N$ and $0 \le t \le t_{max}$. Also, the right hand side is zero when $L < j \le N$ because of $G(t_j)$. Therefore, the desired correlation of f and g can be calculated as

$$\sum_{j=1}^{N-k} f(t+t_j)\, g(t_j) \;=\; \sum_{j=1}^{L} F(t+t_j)\, G(t_j) \;=\; \sqrt{L}\, \frac{1}{\sqrt{L}} \sum_{n=1}^{L} e^{i\omega_n t}\, \tilde{F}(\omega_n)\, \tilde{G}(-\omega_n)\,, \tag{1.51}$$

as long as $t \le t_{max}$.[8]

We can now compute the convolution (or correlation) of nonperiodic functions of length N by (i) zero-padding, (ii) FFT, (iii) multiplication, and (iv) back-FFT, with an effort of $O(L \log L) = O(N \log N)$ since $L \le 2N$.

[8] Sometimes one defines the convolution as $\sum_{j=1}^{N-t_{max}} f(t+t_j)\, g(t_j)$ instead of $\sum_{j=1}^{N-t} \ldots$. Then one should define $G(t_j) = 0$ for $N + 1 - t_{max} \le j \le L$.

(This page is empty.)

1.4.4 Spectrum

In order to see periodicities of a time series, it is useful to look at the Fourier transformation. We first examine a function

$$f(t_j), \quad j = 0, \pm 1, \pm 2, \ldots$$

which is now defined for times from $-\infty$ to ∞, without boundaries in time. Its Fourier transform (Fourier series) is

$$\tilde{f}(\omega) \;:=\; \frac{1}{\sqrt{2\pi}} \sum_{j=-\infty}^{\infty} e^{-i\omega t_j}\, f(t_j), \tag{1.52}$$

with continuous frequencies $\omega \in [0, 2\pi)$.[9]

The inverse transformation is

$$f(t_j) \;=\; \frac{1}{\sqrt{2\pi}} \int_0^{2\pi} e^{i\omega t_j}\, \tilde{f}(\omega)\, d\omega\,. \tag{1.53}$$

Periodicities in $f(t_j)$ become peaks in $\tilde{f}(\omega)$ and can thus easily be detected. However, $\tilde{f}(\omega)$ is in general not real valued.

It is therefore useful to examine the so-called *energy spectral density*,[10]

$$\left| \frac{1}{\sqrt{2\pi}} \sum_{j=-\infty}^{\infty} e^{-i\omega t_j}\, f(t_j) \right|^2 \;\equiv\; \left| \tilde{f}(\omega) \right|^2 \tag{1.54}$$

which by definition is real and positive.

Parseval's theorem states that the total energy in the frequency domain is the same as that in the time domain:

$$\int_0^{2\pi} \left| \tilde{f}(\omega) \right|^2 \;=\; \sum_{j,k=-\infty}^{\infty} \underbrace{\frac{1}{2\pi} \int_0^{2\pi} e^{i\omega(j-k)}}_{=\delta_{jk}}\, f(t_k)\, f^*(t_j) \tag{1.55}$$

$$\;=\; \sum_{j=-\infty}^{\infty} |f(t_j)|^2\,, \tag{1.56}$$

which is also the same as the autocorrelation of f at distance zero.

Usually, the average value of $f(t_j)$ is non-zero. Then the sum above diverges and it is better to look at the Fourier series of the autocorrelation function $R(t)$ of $f(t_j)$, which is called the *power spectral density*

$$\tilde{R}(\omega) \;:=\; \frac{1}{\sqrt{2\pi}} \sum_{t=-\infty}^{\infty} e^{-i\omega t}\, R(t) \;\;, \omega \in [0, 2\pi)\,. \tag{1.57}$$

[9] When a time step Δt is used, $\omega \in [0, \frac{2\pi}{\Delta t})$

[10] When $f(t)$ is an electromagnetic field strength, then $|f(t)|^2$ is proportional to the electric power in the field.

By the convolution theorem, this is the same as the energy spectral density $|\tilde{f}(\omega)|^2$, except at $\omega = 0$ because of the subtraction of $\langle f \rangle^2$ in $R(t)$.

Example 1: Let only one autocorrelation coefficient be non-zero:

$$R(\pm t_n) \neq 0, \quad R(t_k) = 0, \quad \forall\, k \neq n$$

for a fixed number $n \geq 1, \in \mathbb{N}$. Then

$$\tilde{R}(\omega) = \frac{R(t_n)}{\sqrt{2\pi}} \left(e^{-in\omega} + e^{in\omega}\right) = \frac{R(t_n)}{\sqrt{2\pi}} 2\cos(n\omega), \quad \omega \in \mathbb{R}.$$

Example 2: Let only the variance $R(0)$ be unequal zero:

$$R(0) \neq 0, \quad R(t_k) = 0, \quad \forall\, k \neq 0,$$

then

$$\tilde{R}(\omega) = \frac{R(0)}{\sqrt{2\pi}}, \quad \omega \in \mathbb{R}.$$

Such an uncorrelated time series is called **white noise**.

Spectrum of finite length time series

Actual time series, say $x_1, x_2, \ldots x_N$, have a finite length N, as discussed before. One can formally write this finite length series as an infinite one (similar to zero-padding)

$$f(t_j) \;:=\; x_j\, W(t_j), \;\; \text{where } W(t_j) := \begin{cases} 1, \; 1 \leq j \leq N \\ 0, \; \text{else} \end{cases} \tag{1.58}$$

using a *windowing function* $W(t_j)$. However, this affects the Fourier transform of f. By using the convolution theorem backwards, one gets

$$\tilde{f}(\omega) \;\equiv\; \widetilde{x \cdot W}(\omega) \;=\; \frac{1}{2\pi} \int d\nu\; \tilde{x}(\nu)\, \tilde{W}(\omega - \nu)\;, \tag{1.59}$$

i.e. the *convolution* of the desired $\tilde{x}$ *with the Fourier transform of the windowing function* W, which is a heavily oscillating function in case of the "square" window W. Therefore one often dampens the cut-off of finite series with smoother windowing functions when one wants to analyze the spectrum.

Reversely, when one has a signal $f(t)$ that is the convolution of some desired signal x_n with some windowing function W (e.g. a Gaussian), then one can try to *deconvolve* $f(t)$ by dividing its Fourier transform by that of W.

1.5 Statistical Analysis of Monte Carlo time series

1.5.1 Averages

When the time series data result from an importance sampling MC simulation, the expectation value $\langle O \rangle$ can be estimated as as a simple arithmetic mean over the Markov chain:

$$\bar{O} = \frac{1}{n} \sum_{t=1}^{n} O_t \; . \tag{1.60}$$

Conceptually, it is important to distinguish between the expectation value $\langle O \rangle$ which is an ordinary number, and the *estimator* $\bar{O}$ which is a random number fluctuating around the theoretically expected value. In principle, one could probe the fluctuations of the mean value directly, by repeating the whole MC simulation many times. Usually, one estimates its variance

$$\mathrm{var}(\bar{O}) \;:=\; \left\langle \left[\bar{O} - \langle \bar{O} \rangle \right]^2 \right\rangle \;\equiv\; \langle \bar{O}^2 \rangle - \langle \bar{O} \rangle^2 \tag{1.61}$$

by first estimating the variance of the individual measurement

$$\sigma_{O_t}^2 \equiv \mathrm{var}(O_t) = \langle O_t^2 \rangle - \langle O_t \rangle^2 \; , \tag{1.62}$$

by the sample variance $s^2(t)$, (1.4). If the n subsequent measurements were all uncorrelated, then the relation **would** simply be

$$\mathrm{var}(\bar{O}) = \frac{\mathrm{var}(O_t)}{n}, \tag{1.63}$$

For this relation to hold we also have to assume that the simulation is in equilibrium and time-translationally invariant. (See Sec. 1.3.) Equation (1.62) is true for any distribution of the values O_t.

Whatever form this distribution assumes, by the central limit theorem the distribution of the *mean* value is Gaussian, for uncorrelated data in the asymptotic limit of large n. The variance of the mean, $\mathrm{var}(\bar{O})$, is the squared width of this distribution. It is usually specified as the "one-sigma" squared error $\varepsilon_{\bar{x}}^2 = \mathrm{var}(\bar{O})$, and quoted together with the mean value $\bar{O}$. Under the assumption of a Gaussian distribution, the interpretation is that about 68% of all simulations under the same conditions would yield a mean value in the range $[\bar{O} - \mathrm{std}(\bar{O}), \bar{O} + \mathrm{std}(\bar{O})]$.

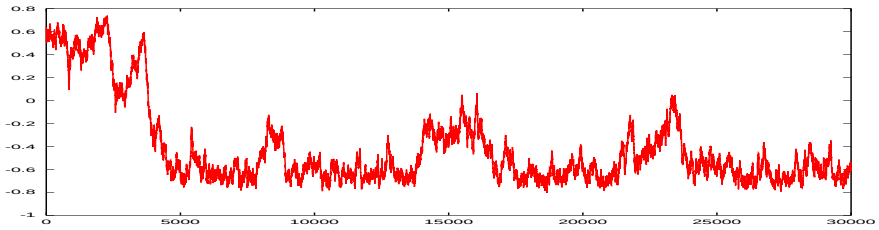

Figure 1.5: *Time series of successive measurements of the magnetization in an Ising model at low temperature. The* expectation *value of the magnetization is exactly zero. The average here is far from zero.*

1.5.2 Autocorrelations

In a simulation with very bad autocorrelations, successive measurements may for example look like Fig. 1.5. In the time series, we see long correlated regions. Furthermore, we know that the magnetization (without magnetic field) should average to zero. Therefore the negative values throughout most of the time series must be temporary, and actually most of the time series, over more than 25000 sweeps, is correlated ! As a result, the average value is far off its asymptotic value of zero.

In this example the long autocorrelations occur because at low temperature the spin configurations more or less "freeze" into a state with mostly spin-down (or mostly spin-up). With single-spin-flips, intermediate configurations with high energies must be overcome to get to the opposite magnetization. This will happen only very rarely. The situation is quite similar to the metastable behavior of real materials ($\rightarrow$ applications) even though the Monte Carlo time evolution with the Metropolis algorithm does not correspond to a physical Hamilton-evolution.

Another common reason for long Monte Carlo autocorrelations are large physical regions of similarly oriented spins. They occur close to second order phase transitions, which are physically very interesting to investigate. These regions have a typical size, which is called the *correlation length* ξ. Autocorrelation times with local updates then typically are of order $\tau \sim \xi^2$. Note though, that because of their very Markov nature, measurements from a Markov chain will *always* be autocorrelated to some smaller or larger degree[11] Thus we *always* have to take autocorrelations into account for error calculations.

As we have already discussed, they can be quantified by the **autocorrelation function**

$$\rho_O(t) \;=\; \frac{\langle O(t_0)\, O(t_0+t)\rangle \;-\; \langle O\rangle^2}{\langle O^2\rangle - \langle O\rangle^2} \;=\; \sum_{i=1}^{\infty} c_i(O)\; e^{-t/\tau_i}\;. \qquad (1.64)$$

[11] Except for the rare cases that completely independent configurations can be chosen.

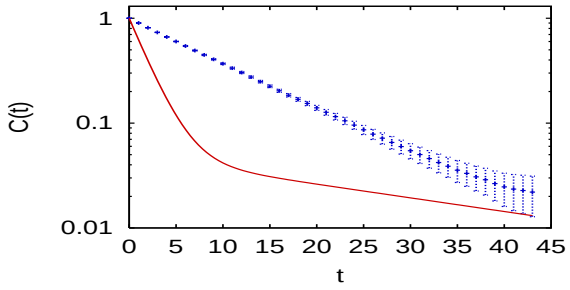

Figure 1.6: *Typical autocorrelation function. Note the log-scale.*

The last expression can be obtained by a lengthy calculation using the spectral representation of the Markov transition matrix P. It contains positive coefficients $c_i(O)$ and time scales $\tau_i = -\log \lambda_i$ which are related to the eigenvalues of the Markov matrix. These eigenvalues satisfy $|\lambda_i|^2 \in (0, 1]$ and are usually real valued. We see that the autocorrelation function is a **sum of exponentials**, and it should therefore always be analyzed on a *logarithmic* scale. Typical cases are depicted in Fig. 1.6.

The largest eigenvalue $\lambda_0 = 1$ of the Markov transition matrix corresponds to the equilibrium distribution π, since $\pi = \pi \mathbf{P}$. The next largest eigenvalue determines the largest time scale in the time evolution. It is called the *asymptotic autocorrelation time* $\tau_{exp}(O)$. For a specific operator O, the largest time scale $\tau_{exp}(O)$ occuring in $\rho_O(t)$ is determined by the largest eigenvalue with $c_i(O) \neq 0$. It sets the time scale for thermalization of O. In the autocorrelation function, plotted logarithmically, $\tau_{exp}(O)$ is the asymptotic slope, at large time separations t.

1.5.3 Statistical error and Integrated Autocorrelation time

From the autocorrelation function, one can compute the true variance of the average value $\bar{O} = \frac{1}{N} \sum_{i=1}^{n} O_i$. We now label the n measurements of O by O_i. We *assume* that the Markov chain has no memory of the initial configuration any more. Its probabilities are then time-translation invariant.

The variance of an individual measurements O_i can be expressed by *expectation values*:

$$\sigma^2_{O_i} \;=\; \langle O_i^2 \rangle - \langle O_i \rangle^2 \,.$$

We now compute the variance of the average value $\bar{O}$. If the measurements were independent, it would be equal to $\sigma^2_{O_i}/n$. In general, it is

$$
\begin{aligned}
\sigma^2_{\bar{O}} &\equiv \langle \bar{O}^2 \rangle - \langle \bar{O} \rangle^2 \\
&\equiv \frac{1}{n^2} \sum_{i,j=1}^{n} \langle O_i \, O_j \rangle \; - \; \frac{1}{n^2} \sum_{i,j=1}^{n} \langle O_i \rangle \, \langle O_j \rangle \\
&= \frac{1}{n} \frac{1}{n} \sum_{i=1}^{n} \left(\langle O_i^2 \rangle - \langle O_i \rangle^2 \right) + 2 \sum_{i=1}^{n} \sum_{j=i+1}^{n} \left(\langle O_i O_j \rangle - \langle O_i \rangle \, \langle O_j \rangle \right) \\
&= \frac{1}{n} \left[\sigma^2_{O_i} + 2 \sum_{t=1}^{n} \left(\langle O_1 O_{1+t} \rangle - \langle O_1 \rangle \, \langle O_{1+t} \rangle \right) \, \left(1 - \frac{t}{n} \right) \right]
\end{aligned}
$$

In the second line, we have inserted the definition of $\bar{O}$, and in the third line we collected diagonal terms $i = j$. The last line is obtained by using the assumed time translation invariance and writing $j = i + t$. The first bracket after the sum is equal to $\sigma^2_{O_i} \, \rho_O(t)$. We arrive at the important result that the actual variance of $\bar{O}$ is

$$
\boxed{\sigma^2_{\bar{O}} \; = \; \frac{\sigma^2_{O_i}}{n} \, 2 \, \tau_{int}(O)} \tag{1.65}
$$

with the so-called *integrated autocorrelation time*

$$
\boxed{\tau_{int}(O) \; = \; \frac{1}{2} \; + \; \sum_{t=1}^{n} r_O(t) \left(1 - \frac{t}{n} \right) .} \tag{1.66}
$$

Equation 1.65 means that the effective number of measurements in the Monte Carlo run is a factor of $2\tau_{int}$ smaller than n !

$$
n_{eff} \; = \; \frac{n}{2\tau_{int}(O)} \, . \tag{1.67}
$$

It is this *effective* number of measurements which needs to be large in order to obtain reliable averages, whereas the number of measurements n itself has no direct meaning for error estimates !

The autocorrelation function $\rho_O(t)$ can be estimated from the data by the empirical autocorrelation function $\rho^E_O(t)$, (1.38). Note that in order to estimate it reliably, the time series needs to be about O(100) times as long as the largest time scale τ_i occuring in $\rho_O(t)$! Because of the exponential decay of $\rho_O(t)$ this also implies that the factor $(1 - \frac{t}{n})$ does not matter in practice. It is therefore often omitted.

Example: Let $\rho_O(t) = e^{-t/\tau_i}$ be a single exponential, with $n \gg \tau_i \gg 1$. Then (using $\rho_O(0) = 1$ in the second line)

$$\begin{aligned}
\tau_{int}(O) &\simeq \frac{1}{2} + \sum_{t=1}^{n} \rho_O(t) \\
&= -\frac{1}{2} + \sum_{t=0}^{n} (e^{-1/\tau_i})^t \\
&= -\frac{1}{2} + \frac{1 - (e^{-1/\tau_i})^{n+1}}{1 - e^{-1/\tau_i}} \\
&\simeq -\frac{1}{2} + \frac{1}{1 - e^{-1/\tau_i}} \simeq -\frac{1}{2} + \frac{1}{1 - (1 - 1/\tau_i)} \simeq -\frac{1}{2} + \tau_i \\
&\simeq \tau_i \; .
\end{aligned}$$

For the typical case $\rho_O(t) = \sum_{i=1}^{\infty} c_i(O)\, e^{-t/\tau_i}$ this means

$$\rho_O(t) \simeq \sum_i c_i \, \tau_i \; . \tag{1.68}$$

In a logarithmic plot, $\rho_O(t)$ consists of a sum of straight lines, each of which contributes its inverse slope τ_i with a factor c_i equal to the intercept with the y-axis. Note that time scale with very small coefficients c_i can thus still be important (see Fig. 1.6).

1.5.4 Binning: Determine autocorrelations and errors

The autocorrelation function is rather cumbersome to calculate and to analyze. A much easier determination of errors can be done by *binning* the time series. The idea is that averages over very long parts of the time series, much longer than the autocorrelation time, are independent of each other (similar to independent Monte Carlo runs), and provide correct error estimates.

Since we do not know the autocorrelation time in advance, we have to use blocks of increasing lengths until the error estimate converges, which

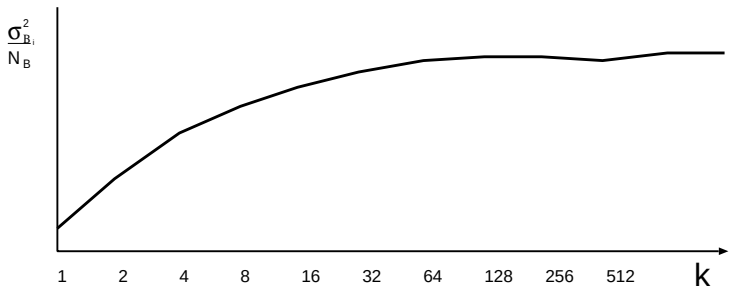

Figure 1.7: Error estimate by data binning. The value of $\frac{\sigma^2_{B_i}}{N_B}$ converges towards the true variance $\sigma^2_{\bar{O}}$ of the mean value $\bar{O}$.

means that the blocks are then long enough. We perform the following steps:

- **Cut the time series into N_B blocks of length k**, where $k = 2^1, 2^2, 2^3, ...$, $N_B = n/k$, and any remaining measurements are disregarded. The block average on the i-th block is

$$\bar{O}_{B_i} = \frac{1}{k} \sum_{t=1}^{k} O_{(i-1)k+t} \ .$$

  All blocks together have a mean value of $\bar{O}_B$. The variance of the single-block values is estimated as usual

$$\sigma^2_{B_i} = \frac{1}{N_B - 1} \sum_{i=1}^{N_B} (\bar{O}_{B_i} - \bar{O}_B)^2 \tag{1.69}$$

  When the block length $k = 1$, then $\sigma^2_{B_i}$ is the "naive" estimate $\sigma^2_{O_i}$.

- The estimate of the variance of the *mean* $\bar{O}_{B_i}$ is $\sigma^2_{B_i}/N_B$. When the block length $k \gg \tau_{int}(O)$, then the block averages are uncorrelated, and this estimate converges to the correct variance of the mean $\bar{O}$:

$$\boxed{\text{Correct error}^2 \text{ of mean:} \quad \frac{1}{N_B}\, \sigma^2_{B_i} \quad \overset{k \gg \tau_{int}(O)}{\longrightarrow} \quad \sigma^2_{\bar{O}}} \tag{1.70}$$

  This is illustrated in figure 1.7.

- The longer the block length k, the fewer the number N_B of such blocks. When N_B becomes smaller than roughly 100, then the fluctuations in the estimated variance $\frac{\sigma^2_{B_i}}{N_B}$ become too large, as can be seen in fig. 1.7 at large k.

- **Convergence criterion:** The measurement of $\bar{O}$ can be considered to be converged when $\frac{\sigma^2_{B_i}}{N_B}$ stays constant (to within a few percent) over several bin-sizes.

  Then the run has been long enough to overcome autocorrelations, and this estimate of $\sigma^2_{\bar{O}}$ as well as the estimate $\langle O \rangle \approx \bar{O}$ are reliable. Since the number of blocks N_B needs to be at least about 100 for stable results, the simulation must be considerably longer than $100\tau_{int}$ for binning to converge.

  Caution: When $\frac{\sigma^2_{B_i}}{N_B}$ has not converged, then $\bar{O}$ can be completely wrong !
  Example: Magnetization in the Ising model at low temperature: the exact value is $\langle M \rangle = 0$, but the mean $\bar{M}$ is often far from 0 because of extremely long autocorrelations.

- From (1.65), the integrated autocorrelation time for the quantity O is given by the ratio of the last and the first value in the binning plot (fig. 1.7):

$$2\tau_{int}(O) \;=\; \frac{\frac{\sigma^2_{B_i}}{N_B}(k \to \infty)}{\frac{\sigma^2_{B_i}}{N_B}(k = 1)} \tag{1.71}$$

- Note that autocorrelation times can be very different for different measured quantities. (Example: Magnetization and energy for the Ising model). The convergence has therefore to be checked independently for each measured quantity. Fortunately, the convergence criterion described above can easily be *automated* !

  However, if some quantities have not converged, then one has to carefully discuss the validity of other seemingly converged measurements (which may or may not be correct).

1.6 Summary: Recipe for reliable Monte Carlo simulations

Algorithm. We need a Markov Process that is ergodic and satisfies detailed balance.

Simulation

- *Any starting configuration* should provide the same results, unless properties like metastability are to be analyzed.
- *Thermalization:* about 10% of the total number of sweeps. This tends to avoid bias from the starting configuration, but does not increase statistical errors noticeably.
- *Sweeps with measurements.* When $\tau_{int}(O) \gg 1$, one need not measure after every sweep.

Error analysis

- Check against exact results.
- Check time series by eye ! All visible time scales must be much smaller than the simulation time.
- Binning: Check convergence for each measured quantity.
- Obtain reliable errors from binning and/or Jackknife.
- For precision results, check that the results are independent of the random number generator which is used.

Danger

When the system is too large, *autocorrelations may be much longer than the simulation*. The simulation can then *appear* to be converged (including binning !), but has in fact barely moved in phase space and is **wrong**.

⇒ **Think small !**

- One *must* start with very small systems.
- Check against exact results
- Inspect for autocorrelations (especially by eye in time series).
- *Gradually* increase system size

These essential steps are actually easy to do. They involve a few extra simulations on small systems, which run very quickly. Inspections for autocorrelations by eye are very easily done.

With these extra steps for verification, Monte Carlo calculations are very efficient and can provide reliable results even on extremely large systems.

1.7 Jackknife: General purpose error analysis with automatic error propagation

Data are often combined in complicated nonlinear ways to obtain results, including fits, and fits of fit-results, etc. It is then next to impossible to apply standard error propagation. *Example:* For the autocorrelation function, it is difficult to compute error bars. When the slope of the autocorrelation function is fitted, reliable errors on this slope are even more difficult to obtain, in part because the values of the autocorrelation function at different time distances are correlated among each other.

A surprisingly easy solution in many cases is provided by "resampling" techniques, in which partial samples of all data are taken several times and analyzed. We will concentrate on the Jackknife method.A closely related procedure is called *bootstrap*.

To explain Jackknife we will use the analysis of a Monte Carlo time series as an example. We start by cutting the data (time series) into $N_B \gtrsim 30$ blocks. The number 30 is chosen so that the relative error of the calculated error will be reasonably small, namely of order $1/\sqrt{30}$. The blocks should ideally be uncorrelated. For Monte Carlo this means that they should be much larger than the autocorrelation times (which have to be determined separately). One can also combine Jackknife and Binning.

Error calculation

Analyze the data $N_B + 1$ times: We first perform an analysis of the full data set, arriving at a number which we call $R^{(0)}$ (This number can e.g. be the autocorrelation function at some time distance t, or it can e.g. be a fitted slope of the autocorrelation function).

Then we perform *another N_B analyses, each time leaving out one of the N_B blocks*, providing results $R^{(j)}$, $j = 1, \ldots, N_B$, with an average $R^{(av)}$. The fluctuation of these results tells us about the statistical error. However, the $R^{(j)}$ are highly correlated amongst each other, since they use almost the same data. The correct variance of the overall results is given by

$$\boxed{\sigma_R^2 = \frac{N_B - 1}{N_B} \sum_{j=1}^{N_B} \left(R^{(j)} - R^{(av)}\right)^2 \ .} \tag{1.72}$$

which is $(N_B - 1)^2$ times the usual estimator of the variance of a mean.

Bias

Usually , the result $R^(0)$ is corrected for a "bias", with the overall result

$$R \;=\; R^{(0)} \;-\; \text{Bias}, \quad \text{Bias} \;=\; (N_B - 1)(R^{av} - R^{(0)}) \;. \tag{1.73}$$

However, this bias is usually much smaller than the statistical error of R and therefore unimportant. It can be used as a *diagnostic tool*: When "Bias" is of the same size as the statistical error or larger, then there is likely a *problem with the data* like an outlier, that is a strongly deviating data point.

Stability

The N_B additional analyses involve almost all the data. Therefore procedures like fits are very stable, providing a set of $N_B + 1$ stable results (e.g. for the slope of the autocorrelation function) and a reliable statistical error.

In contrast, in the more naive approach of analyzing small single bins one by one to compute a variance, quantities like fit-results may become meaningless.

We see that Jackknife is a general error analysis with automatic error propagation, even through highly nonlinear data processing like fits.
In the related *bootsstrap* method, random samples of N_B data points are taken many times and analyzed. This method cannot be used for time-series, since the sequential nature of events gets lost.

1.8 Appendix: Other Monte Carlo algorithms

This appendix provides a very quick overview over some other Monte Carlo methods, in addition to and beyond the original Metropolis method.

1.8.1 Some more advanced methods

Beyond the simple Metropolis Hastings method with local updates, many methods have been developed, which can be orders of magnitude better for suitable problems.

Gibbs sampler = Heat bath. This is a different update proposal. In an update step, most degrees of freedom are held fixed. Then the distribution π amounts to a (conditional) distribution for the remaining

degrees of freedom. They are sampled directly from this distribution. The proposed configuration is therefore always accepted. Of course this requires a method to do the sampling exactly within the restricted phase space. Note that in practice this method is not necessarily better that single site Metropolis updates.

Example: All spins in the Ising model are held fixed except for spin s_i. In the next configuration it will have value $+1$ with probability

$$\frac{e^{-\beta E(s_i=+1)}}{e^{-\beta E(s_i=+1)} + e^{-\beta E(s_i=-1)}} .$$

This probability is independent of the current value of s_i.

Overrelaxation. For continuous variables. When all other variables are held fixed, a variable x_i will see some effective potential. In overrelaxation, the proposal for the new value is not chosen at the minimum of this potential, but instead x_i "swings" beyond the minimum. This strategy anticipates that the surroundings will change in the future, likely following x_i. It can lead to faster convergence.

Fourier acceleration. Also for continuous variables. Proposals are made in Fourier space. This is efficient when the Hamiltonian is close to bilinear, where the Fourier modes are independent.

Cluster methods. For some classical model like the Ising model, and, more importantly, for a number of important Many-Particle Quantum Models (e.g. the Heisenberg model) there are efficient cluster methods with almost no autocorrelations and with other advantages. The clusters are generated stochastically, based on the current configuration. The methods work well, because these clusters turn out to be the physically relevant objects.

Introduction of additional degrees of freedom. Often, simulations become much easier when *additional* degrees of freedom are introduced. This way, barriers in phase space can be overcome, which is often advantageous, even when a large part of the extended phase space might be "unphysical". This is related to the extended ensembles discussed later. One very successful example are "Worm Methods" in Many Body quantum physics.

Exact Monte Carlo. Also called CFTP ("Coupling from the Past"). Surprisingly, it is possible to generate configurations which are guaranteed to be independent, without autocorrelations, and from the correct distribution (given a perfect random number generator). However, each new configuration takes a long time to generate.
See www.dbwilson.com/exact.

Multigrid methods. This is a very wide field in itself, with applications far beyond Monte Carlo. The strategy is to "coarse grain" the problem, finding effective degrees of freedom on a larger length scale, with some effective interaction. If the effective interaction is known precisely enough, the system can be simulated on the coarser scale.[12] When only an approximate effective interaction is known, then it can be used to generate an update proposal, which is then evaluated for the original variables and interaction.

1.8.2 Combination of algorithms

Sometimes it is advantageous to combine several Monte Carlo algorithms in order to improve performance.

Hybrid Monte Carlo:

We make use of the Metropolis-Hastings procedure, with eq. (1.23):

$$p_{ij}^{accept} \;=\; \min\left(1,\; \frac{\pi_j\, q_{ji}}{\pi_i\, q_{ij}}\right) \;.$$

Now we use as a proposal probability $q(x \to x')$ some procedure which *almost* satisfies detailed balance with respect to π. Then p_{accept} provides a *"filter"* to accept or reject these proposals in order to achieve detailed balance overall.

Example: In large scale simulations of Quantum Chromodynamics, update proposals are made by a molecular dynamics propagation of the quark and gluon degrees of freedom, and then accepted or rejected with the full QCD weight, which is very expensive to evaluate. This way, larger steps in phase space and fewer evaluations of the full weight are possible.

A variant of the Hybrid MC method is to *split a Hamiltonian*: Let

$$Z\,\pi_i \;=\; e^{-\beta H_i} \;=\; e^{-\beta H_i^{(0)}}\, e^{-\beta H_i^{(1)}} \;.$$

If one has a Monte Carlo procedure to simulate $H^{(0)}$, one can use it in order to generate update proposals, which are then filtered with $H^{(1)}$.

Example: Efficient cluster updates for the Ising model work only without magnetic field. For a small field, it makes sense to use the cluster-updates as proposals and accept or reject them according to the proposed change of magnetization.

[12] Indeed, this is the strategy in most of physics, except for elementary particle physics and cosmology !

Random Mixing of methods

When the transition matrices P_1, P_2, ... satisfy detailed balance, then so does the mixture

$$P \;:=\; \sum \lambda_i \, P_i \tag{1.74}$$

with $\lambda_i \geq 0$, $\sum \lambda_i = 1$. One can therefore mix methods with different strengths, e.g. methods which update different degrees of freedom efficiently. *Example:* Mix a method which moves in phase space efficiently with another method that ensures ergodicity.
The following statement is related.

Sequence of methods

When the transition matrices P_1, P_2, ... are *stationary* with respect to π, then so is the sequence $P_1 P_2 ....$ (Proof: $\pi P_1 P_2 = \pi P_2 = \pi$).

Again, this can be used in order to mix several methods.

Note that the analogous statement is not true for detailed balance, unless the transition matrices P_i commute.

1.8.3 Extended ensembles

Often, simulations are stopped by barriers in phase space from exploring important regions of phase space. This problem appears not only in standard Monte Carlo simulations of some probabilty distribution π, but **also in optimization problems** in a multitude of areas, which we will discuss in the next chapter.

Two successful strategies against such barriers are either to reduce their effective size, or to overcome them. Examples of these strategies are the so called *Multicanonical Ensemble* and *Tempering*. Both are versions of **umbrella sampling**.

Multicanonical ensemble

The probability of configurations with a certain energy E to appear in a Monte Carlo configuration is proportional to the Boltzmann weight $\pi(E) \sim \exp(-\beta E)$. It is also proportional to the *number of states* $N(E)$ with the energy E. This number is related to the entropy. Therefore the number of configurations with energy E in a Monte Carlo simulation is proportional to

$$\pi(E)\, N(E) \; .$$

We now consider the case of a large energy and/or entropy barrier, as sketched in fig. 1.8. The barrier between the two populated regions can often be many orders of magnitude high. For example, in the Potts model with $q > 4$, there is a first-order phase transition, with a jump in the average energy as a function of temperature. The barrier then corresponds to

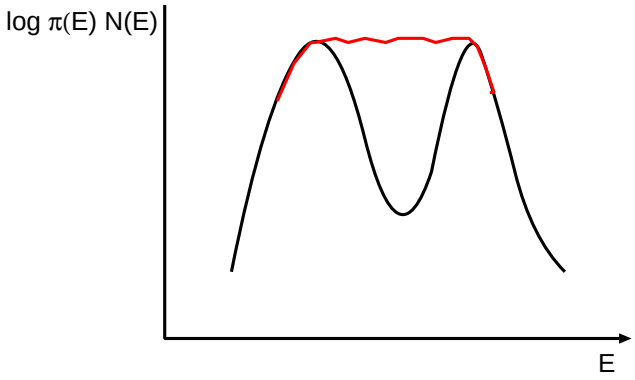

Figure 1.8: Histogram of how often specific energies occur in a Monte Carlo. There is a large barrier between small and high energies, which can be overcome by a suitably chosen new weight function.

a surface tension between ordered and disordered phases, and can reach 10^{100} already for relatively small systems. It is then *impossible* for Monte Carlo configurations to move through this barrier. Sometimes, but rarely, one can devise methods to move from one favorable region directly to the other. For the Potts model, however, one even needs to explore the barrier itself in order to measure the surface tension.

The strategy of multicanonical simulations is to **reweight energies** in such a way that the **histogram** of energies becomes approximately **flat**. A flat histogram as depicted in fig. 1.8 means that the Monte Carlo will perform a **random walk in energies** (!) and will therefore move in energies fairly quickly, much quicker than the exponentially large time required to go through the minimum. The change of weight is

$$\pi(E) \;=\; e^{-\beta E} \;\mapsto\; \tilde{\pi}(E) \;:=\; e^{-\beta E + f(E)} \;=\; W(E)\, e^{f(E)} \tag{1.75}$$

with a suitably *chosen* function $f(E)$, such that the histogram for a simulation with $\tilde{\pi}$ is approximately constant. The histogram does not need to be completely flat, it just needs to allow transitions between low and high energies. The function $f(E)$ is the difference between the two curves in fig. 1.8. In practise, this function is determined iteratively, by starting with cases (e.g. small systems) where the barrier is not high.

The Monte Carlo is now performed with the new weights $\tilde{\pi}$. Fortunately, one can still calculate expectation values with respect to the original weight π, by reweighting the measurements back:

$$\langle O \rangle_\pi \;\equiv\; \frac{\sum_x O_x \, \pi_x}{\sum_x \pi_x} \;=\; \frac{\frac{\sum_x O_x \, e^{-f_x} \, \tilde{\pi}_x}{\sum_x \pi_x}}{\frac{\sum_x e^{-f_x} \, \tilde{\pi}_x}{\sum_x \tilde{\pi}_x}} \;=\; \frac{\langle O \, e^{-f_x} \rangle_{\tilde{\pi}}}{\langle e^{-f_x} \rangle_{\tilde{\pi}}} \; . \tag{1.76}$$

Indeed, one can also determine expectation values with respect to *differ-*

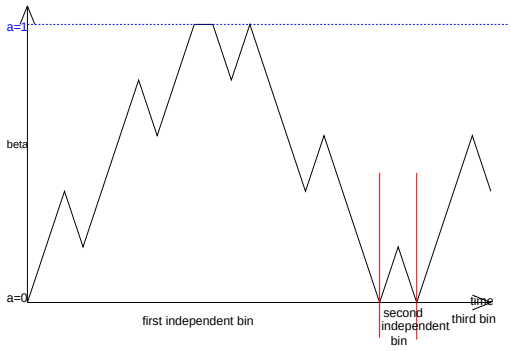

Figure 1.9: Tempering: Random walk in β.

ent temperatures.[13] The only requirement is that the probability distribution at the desired temperature is *contained* completely within the distribution that is actually simulated (fig. 1.8). I.e. one simulates an *umbrella* of all desired distributions. Note that one can also reweight in quantities other than the energy.

At the global minimum or maximum energy of phase space, one can often calculate the number (or density) of states $N(E)$. When the simulated distribution includes one of these energies, then one can *measure the density of states* $N(E)$. In normal Monte Carlo this is not possible, since the proportionality factor between the histogram of configurations and the density of states is not known.

The multicanonical technique has found important applications in optimization problems, notably in the **Traveling salesman** and related problems, and in **Protein folding**. This will be discussed in the next chapter.

Tempering

The strategy of tempering is to overcome barriers. To achieve this, one makes the **temperature a dynamical variable** with discrete values β_i of β, which can now change during a simulation. The extended phase space of the simulation now consists of the original variables x and the index i of temperature.[14]

Simulated Tempering

The partition function in this extended space for Simulated Tempering is

$$Z = \sum_i \sum_x e^{-\beta_i H_x + g_i} = \sum_i Z(\beta_i) \,. \tag{1.77}$$

One chooses constants g_i in such a way that the system approximately performs a **random walk in temperatures**.

[13] Hence the somewhat unfortunate name "multicanonical"

[14] Literally, this approach ought to be called "multicanonical", but it is not.

When it is at a sufficiently high temperature, then the system can easily overcome energy barriers. Indeed, if $\beta = 0$ is included in the simulation, the configurations will *decorrelate completely* whenever $\beta = 0$ is reached, cutting off any autocorrelations. When $\beta = 0$ is included, simulated tempering also allows the measurement of entropy, which is usually impossible in Monte Carlo. This is equivalent to the measurement of the density of states in multicanonical Monte Carlo.

When one considers only the configurations at a certain inverse temperature β_i, then (1.77) implies that they are from the normal **canonical ensemble** $\exp(-\beta_i E)$! Therefore one can directly measure observables in the canonical ensemble at any of the β_i, including the properties of the system at some low temperature, where the barriers are felt fully.

For tempering to work, the β_i need to be chosen more densely close to a phase transition. At a strong first order phase transition, the multicanonical method works better.

Parallel Tempering

In parallel tempering one simulates all inverse temperatures β_i in parallel, e.g. on different processors. Occasionally, the interchange of configurations at neighboring temperatures is proposed, and accepted with Metropolis probability according to (1.77). For such an interchange, the constants g_i *cancel*. They are therefore not required in parallel tempering and need not be determined. As a drawback, the entropy cannot be determined.

There are many applications of Tempering outside of physics, including again optimization problems like the **Traveling salesman** and **Protein folding**, as well as Bayesian **parameter determination from measured data**. This will be discussed in more detail in the next chapter.

Chapter 2

Minimization/Optimization – Problems

Literature

- W. PRESS *et al.*, *Numerical recipes*, Cambridge University Press
- F.S. ACTON, *Numerical Methods that work*, Mathematical Association of America

Optimization is of enormous importance in physics, engineering, economics, information technology and in many other fields. The layout of electric circuits on a chip, timetables, or the optimum load of a pipeline system are a few typical examples.

In general we have a problem which is determined by a set of n real parameters. Each set of parameter values specifies a *state*. Together they span the *search space*. Each state is mapped to a real number, its *cost*, by a *cost function*. One has to find the specific values of the parameters for which the cost function develops a maximum/minimum. Often, one also requires *robustness* of the solution against small fluctuations of the parameters.

If the cost function is at least once differentiable in its parameters, then mathematics will provide us with well defined (deterministic) algorithms to find at least *local* maxima/minima of the cost function. Such methods will be discussed first.

When there are too many extrema, or when the value of the cost function is not differentiable, then other methods are used, some of which have been developed from evolutionary models. One starts from some state and modifies it using *stochastic methods*. If the cost function changes to a better value, then the new state is usually taken, otherwise the old state may be modified again. This is repeated until an optimum has been found, as specified by some suitable criterion.

2.1 Quantum Mechanical Examples

We will discuss problems with many continuous degrees of freedom. Some representative examples are

1. First (not quantum mechanical), the solution of *a set of linear algebraic equations* can be viewed as a minimization problem

$$\begin{aligned} \boldsymbol{B}\,\mathbf{x} = \mathbf{b} \quad \Longleftrightarrow \quad & \min_{\mathbf{x}} \|\boldsymbol{B}\,\mathbf{x} - \mathbf{b}\|^2 \\ & = \min_{\mathbf{x}} \left[\mathbf{x}^\dagger B^\dagger B\mathbf{x} - 2\mathrm{Re}\,\mathbf{b}^\dagger \boldsymbol{B}\mathbf{x} + \|\mathbf{b}\|^2\right]. \end{aligned} \tag{2.1}$$

   For large-dimensional matrices $\boldsymbol{B}$, the direct inversion may easily exceed present computer power. We will see that iterative minimization procedures come in handy.

2. The **ground state energy** E_0 of a quantum mechanical system is given by the minimum of the energy expectation value

$$E_0 = \min_{\psi} \frac{\left\langle \psi \,\middle|\, \hat{H} \,\middle|\, \psi \right\rangle}{\langle \psi \,|\, \psi \rangle}. \tag{2.2}$$

   When expressed in a complete orthonormal basis set $\{|\Phi_i\rangle\}$ this is equivalent to

$$E_0 = \min_{\mathbf{c}} \frac{\mathbf{c}^\dagger \boldsymbol{H}\mathbf{c}}{\mathbf{c}^\dagger\mathbf{c}}, \tag{2.3}$$

   where $\mathbf{c}$ stands for the vector of expansion coefficients of the ground state vector and $\boldsymbol{H}$ is the Hamilton matrix in the basis $\{|\Phi_i\rangle\}$, *i.e.:*

$$H_{ij} = \left\langle \Phi_i \,\middle|\, \hat{H} \,\middle|\, \Phi_j \right\rangle.$$

   Special case: Variational ansatz with parameters $\boldsymbol{\eta}$, spanning some part of the total Hilbert space.

$$|\psi\rangle = |\psi(\boldsymbol{\eta})\rangle, \quad \boldsymbol{\eta} \in \mathbb{R}^n \text{ parameters}. \tag{2.4}$$

   Again the energy expectation value is to be minimized:

$$E_0 = \min_{\boldsymbol{\eta}} \frac{\left\langle \psi(\boldsymbol{\eta}) \,\middle|\, \hat{H} \,\middle|\, \psi(\boldsymbol{\eta}) \right\rangle}{\langle \psi(\boldsymbol{\eta}) \,|\, \psi(\boldsymbol{\eta}) \rangle}. \tag{2.5}$$

3. To compute static or dynamic properties of molecules or solids, one can take an entirely classical approach, in which only the positions of the nuclei are accounted for. Empirical forces among the nuclei are introduced, which mimic parts of the quantum mechanical features.

Only effective two-particle forces are employed, which, for the i-th particle, are of the form

$$\mathbf{F}_i = \sum_j \mathbf{f}(\mathbf{R}_i, \mathbf{R}_j),$$

with $\mathbf{R}_i$ being the coordinate of the i-th particle. The classical equations of motion for the nuclei read

$$m_i \ddot{\mathbf{R}}_i = \mathbf{f}(\{\mathbf{R}_i\}).$$

They can be simulated with *molecular dynamics*. The equilibrium positions determine the static properties. Such an approach is for example taken to model *proteins*.

4. Some progress towards quantum molecular dynamics consists in treating at least the forces quantum mechanically. One solves the electron dynamics quantum mechanically while the nuclei are treated as classical degrees of freedom. This approach is a significant improvement and goes beyond the classical approximation. It is known as the *Born-Oppenheimer approximation*. It is often (but not always) justified because the mass of the nuclei is roughly 2000 times heavier than that of the electrons, so that nuclei tend to move much more slowly than electrons. The dynamics is then solved in two steps.

   The first step consists in solving the electronic eigenvalue problem for fixed positions $\{\mathbf{R}_i\}$ of the nuclei. This is a many-electron problem which, though in a fixed potential, is not soluble exactly. A widespread *approximation* for such type of problems is the local-density approximation (LDA) (an effective *one-electron* approximation which, however, *misses all many-body correlation effects*) for which the so-called Kohn-Sham equations from *Density Functional Theory*

$$\begin{aligned} \hat{H}(\{n\}, \mathbf{R})\, \psi_{\mathbf{k}}(\mathbf{x}) &= \varepsilon_{\mathbf{k}}\, \psi_{\mathbf{k}}(\mathbf{x}) \\ n(\mathbf{x}) &= \sum_{\mathbf{k} \leq \mathbf{k}_{Fermi}} |\psi_{\mathbf{k}}(\mathbf{x})|^2 \end{aligned} \tag{2.6}$$

   have to be solved self-consistently. They contain the electronic density $n(\mathbf{x})$, One now argues that for low temperatures and fixed nuclei the electronic subsystem is in the ground-state. Since the motion of the nuclei is slow compared to that of the electrons, one assumes that the dynamics of the nuclei is equivalent to an adiabatic change of the potential, such that it leaves the electronic subsystem always in the eigenstate (ground state) which corresponds to the actual potential. The ground state energy $E(\{\mathbf{R}_j\})$, consisting of contributions from the electrons and the nuclei, defines the potential in which the nuclei move.

Therefore, the second step consists in computing the force on the i-th particle via the Hellmann-Feynman formula

$$\mathbf{F}_i = -\frac{\partial}{\partial \mathbf{R}_i} E(\{\mathbf{R}_j\}) = -\left\langle \psi \left| \frac{\partial}{\partial \mathbf{R}_i} \hat{H} \right| \psi \right\rangle. \tag{2.7}$$

The change in the position of the nuclei for a small time-step is then computed via the classical equations of motion, driven by the ab-initio forces.

In hindsight we can also scrutinize the reliability of the classical approximation for the nuclei. We can separate one nucleus and make a quadratic approximation to the ab-initio potential, leading to a harmonic oscillator for which the exact quantum mechanical dynamics can easily be obtained. Molecular dynamics calculations will be discussed in a later chapter.

An improvement over the Born-Oppenheimer approximation is provided by the *Car-Parrinello method*, which uses some fictitious dynamics for the system of nuclei and electrons to keep the electrons in the ground state of the nuclear potential.

Often one is just interested in the equilibrium geometry. Then one needs to minimize the ab-initio potential

$$\min_{\{\mathbf{R}_j\}} E(\{\mathbf{R}_j\}),$$

which is obviously a challenging task as it involves the self-consistent solution of the electronic eigenvalue problem for each configuration $\{\mathbf{R}_j\}$. According to (2.5), the computation of the electronic ground-state is itself a minimization problem. We can therefore cast the entire problem into the form

$$\min_{\{\mathbf{R}_i\},\mathbf{c}} \left[\frac{\mathbf{c}^\dagger \boldsymbol{H}(\mathbf{c})\mathbf{c}}{\mathbf{c}^\dagger \mathbf{c}} + \sum_{i>j} V(\mathbf{R}_i, \mathbf{R}_f) \right].$$

Contrary to (2.5), however, the Hamiltonian matrix $\boldsymbol{H}$ depends itself on the expansion coefficients $\mathbf{c}$ because of its dependence on the density $n(\mathbf{x})$. The last term in the above equation describes the bare Coulomb interaction of the nuclei.

2.2 Quadratic Problems: Steepest Descent and Conjugate Gradient

A *quadratic form* is a scalar, quadratic function of a vector and is of the form:

$$\boxed{f(\mathbf{x}) = \frac{1}{2}\mathbf{x}^T \boldsymbol{A}\mathbf{x} - \mathbf{b}^T\mathbf{x} + c.} \tag{2.8}$$

[See also Eq. (2.1).] Here, $\boldsymbol{A}$ is an $N \times N$ matrix, $\mathbf{x}$ and $\mathbf{b}$ are vectors $\in \mathbb{R}^N$, and c is a scalar constant. *We restrict the discussion to real-valued problems.*

Theorem: If the matrix $\boldsymbol{A}$ is symmetric (i.e. $\boldsymbol{A}^T = \boldsymbol{A}$) and positive definite (i.e. $\mathbf{x}^T\boldsymbol{A}\mathbf{x} > 0$ for any non-zero vector $\mathbf{x} \in \mathbb{R}^N$) the quadratic form (2.8) is *minimized* by:

$$\boxed{\boldsymbol{A}\mathbf{x} = \mathbf{b}.} \tag{2.9}$$

To prove this, we compute the gradient of $f(\mathbf{x})$:

$$\begin{aligned} \nabla f(\mathbf{x}) &= \frac{1}{2}\nabla\left(\mathbf{x}^T\boldsymbol{A}\mathbf{x}\right) - \nabla\left(\mathbf{b}^T\mathbf{x}\right) \\ &= \frac{1}{2}\boldsymbol{A}^T\mathbf{x} + \frac{1}{2}\boldsymbol{A}\mathbf{x} - \mathbf{b} \end{aligned}$$

$$\boxed{\nabla f(\mathbf{x}) = \boldsymbol{A}\mathbf{x} - \mathbf{b}} \tag{2.10}$$

Setting the gradient to zero produces (2.9), therefore $\boldsymbol{A}\mathbf{x} = \mathbf{b}$ correponds to an extremum of $f(\mathbf{x})$.

When $\boldsymbol{A}$ is not symmetric, i.e. $\boldsymbol{A}^T \neq \boldsymbol{A}$, then we see from this derivation that one will find a solution to the system $\tilde{\boldsymbol{A}}\mathbf{x} = \mathbf{b}$ with $\tilde{\boldsymbol{A}} = \frac{1}{2}\left(\boldsymbol{A}^T + \boldsymbol{A}\right)$ which is a symmetric matrix.

When the matrix $\boldsymbol{A}$ is positive definite, then $\boldsymbol{A}\mathbf{x} = \mathbf{b}$ corresponds to a *minimum* of $f(\mathbf{x})$. To see this, let us assume that $\mathbf{x}$ is a point $\in \mathbb{R}^N$ which satisfies $\boldsymbol{A}\mathbf{x} = \mathbf{b}$. Let $\mathbf{e}$ be an "error" term, i.e. a deviation from the solution vector $\mathbf{x}$.

$$\begin{aligned} f(\mathbf{x}+\mathbf{e}) &= \frac{1}{2}(\mathbf{x}+\mathbf{e})^T\boldsymbol{A}(\mathbf{x}+\mathbf{e}) - \mathbf{b}^T(\mathbf{x}+\mathbf{e}) + c \\ &= \frac{1}{2}\mathbf{x}^T\boldsymbol{A}\mathbf{x} + \frac{1}{2}\mathbf{e}^T\boldsymbol{A}\mathbf{e} + \underbrace{\frac{1}{2}(\mathbf{e}^T\mathbf{b} + \mathbf{b}^T\mathbf{e})}_{\mathbf{b}^T\mathbf{e}} - \mathbf{b}^T\mathbf{x} - \mathbf{b}^T\mathbf{e} + c \\ &= \frac{1}{2}\mathbf{x}^T\boldsymbol{A}\mathbf{x} - \mathbf{b}^T\mathbf{x} + c + \frac{1}{2}\mathbf{e}^T\boldsymbol{A}\mathbf{e} \\ &= f(\mathbf{x}) + \frac{1}{2}\mathbf{e}^T\boldsymbol{A}\mathbf{e}. \end{aligned}$$

In the second line we used the symmetry of $\boldsymbol{A}$ to write $\mathbf{x}^T\boldsymbol{A}\mathbf{e} = \mathbf{b}^T\mathbf{x}$, and also $\mathbf{b}^T\mathbf{x} = \mathbf{x}^T\mathbf{b}$. If the matrix $\boldsymbol{A}$ is positive definite, then the last term is positive for all $\mathbf{0} \neq \mathbf{e} \in \mathbb{R}^N$ and therefore $\mathbf{x}$ minimizes $f(\mathbf{x})$.

Eq. (2.9) can be solved by a number of methods. A "direct" solution can be obtained, for example, by Gaussian elimination, the Gauss-Newton method, Cholesky-decomposition, or a similar method. These methods are related to computing the minimum directly via the inverse of $\boldsymbol{A}$:

$$\nabla f(\mathbf{x}) = \boldsymbol{A}\mathbf{x} - \mathbf{b} = 0 \;\; \Rightarrow \;\; \mathbf{x} = \boldsymbol{A}^{-1}\mathbf{b}\,. \tag{2.11}$$

They require $O(N^3)$ operations, which can, however, be prohibitive for large matrices.

In the present chapter, we will examine methods which start from some initial guess $\mathbf{x}_0$ and iteratively improve it, $\mathbf{x}_n \rightarrow \mathbf{x}_{n+1}$, moving towards the minimum of $f(\mathbf{x})$ by using the **gradient** ∇f at the current $\mathbf{x}_n$. Let us estimate the computational effort for such methods. The number of degrees of freedom, i.e. the number of elements of $\boldsymbol{A}$ and $\mathbf{b}$, is of order N^2. If one of these elements is modified, the solution $\mathbf{x}$ will change. The gradient $\nabla f(\mathbf{x})$ has N components of information. *A good method based on gradients should therefore ideally need at most N iterations*. The computational effort to compute the gradient is $\mathcal{O}(N^2)$; to compute it N times, the effort is $\mathcal{O}(N^3)$.

At first glance, the two approaches seem to be similar as far as CPU time is concerned. This is not true in practice, though, since with iterative methods based on gradients, there is usually no need to really perform all N iterations. In most large problems *a much smaller number of iterations suffices* to achieve some desired accuracy. Other properties of such methods:

- Gradient methods are especially suited for sparse matrices $\boldsymbol{A}$. The effort to compute the gradient is proportional to the number m of non-zero elements (typically $\mathcal{O}(mN)$, with $m << N$); i.e. the entire approach is of order $\mathcal{O}(mN^2)$ instead of $\mathcal{O}(N^3)$.
- They can do with any amount of memory. There are three possibilities
  - keep the entire matrix in fast memory
  - read it from hard disk in portions, which can be kept in memory
  - generate the matrix elements from scratch as they are needed
- They are well suited for parallelization or vectorization.

2.3 Steepest Descent: not a good method

The most elementary gradient-based algorithm is the method of steepest descent. At each step we move in the direction opposite to the gradient of $f(\mathbf{x}_n)$, i.e. downhill, until we reach the local minimum in that direction.

This method turns out to fail easily. It can, however, be modified to become the very useful method of Conjugate Gradients, discussed in the following section. Both Steepest Descent and Conjugate Gradient are methods to minimize quadratic functions (i.e. solve linear equations). They can be generalized to more general functions, as we shall see.
The outline of Steepest Descent is as follows

Algorithm 2 Steepest descent (draft)

Choose an initial vector $\mathbf{x}_0$
for $n = 0$ to $n_{\max}$ **do**
  calculate the gradient $\mathbf{g}_n = \nabla f(\mathbf{x})\big|_{\mathbf{x}_n}$
  new search direction $\mathbf{r}_n := -\mathbf{g}_n = \mathbf{b} - \boldsymbol{A}\mathbf{x}_n$
  set $\mathbf{x}_{n+1}$ to the minimum of $f(\mathbf{x})$ in direction $\mathbf{r}_n$
  if converged **then** EXIT
end for

The quantity $\mathbf{r}_n = \mathbf{b} - \boldsymbol{A}\mathbf{x}_n$ is called the *"residual"*. Its modulus $|\mathbf{r}|$ can be used to judge how well x_n has converged to the solution $\mathbf{x}$.

When we take a step n, we choose the direction in which $f(\mathbf{x}_n)$ decreases most quickly, and this is the direction opposite $\nabla f(\mathbf{x}_n) = \boldsymbol{A}\mathbf{x}_n - \mathbf{b}$. Suppose we start at the point $\mathbf{x}_0$. Our first step is along the direction of steepest descent. Thus, we will choose a point

$$\mathbf{x}_1 = \mathbf{x}_0 + \lambda_0 \mathbf{r}_0, \quad \mathbf{r}_0 = \mathbf{b} - \boldsymbol{A}\mathbf{x}_0 = -\nabla f(\mathbf{x}_0). \tag{2.12}$$

We choose λ_0 to minimize $f(\mathbf{x})$ along the line $\mathbf{x}_0 + \lambda_0 \mathbf{r}_0$ (*"line minimum"*). The miminum is reached when the *directional derivative* $df(\mathbf{x})/d\lambda_0$ is equal to zero. By the chain rule

$$0 \stackrel{!}{=} \frac{d}{d\lambda} f(\mathbf{x}_1) = \nabla f(\mathbf{x}_1)^T \frac{d}{d\lambda}\mathbf{x}_1 \stackrel{(2.12)}{=} \underbrace{\nabla f(\mathbf{x}_1)^T}_{-\mathbf{r}_1^T} \mathbf{r}_0 \;=\; -\mathbf{r}_1^T \mathbf{r}_0 \,.$$

We find that λ_0 should be chosen such that $\mathbf{r}_0$ (the *residual*) and $\nabla f(\mathbf{x}_1)$ are orthogonal. Since we always go to the respective line minimum, successive gradients are perpendicular. This is illustrated in Fig. 2.1 which shows two successive search directions (gradients) along with the contours of $f(\mathbf{x})$. If the gradients were not orthogonal, we could still reduce $f(\mathbf{x})$ by moving further in the direction of the old gradient.

For step n the strategy reads

$$\mathbf{r}_n \;=\; -\nabla f(\mathbf{x}_n) \;=\; \mathbf{b} - \boldsymbol{A}\mathbf{x}_n \tag{2.13a}$$

$$\mathbf{x}_{n+1} \;=\; \mathbf{x}_n + \lambda_n \mathbf{r}_n \tag{2.13b}$$

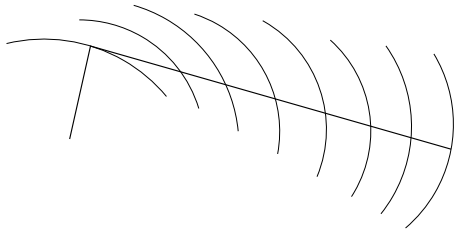

Figure 2.1: The search path follows the inverse gradient of $f(\mathbf{x}_n)$ until the line minimum is reached. There the gradient is orthogonal to the search direction.

A simple recursion relation can be derived for successive search directions:

$$\mathbf{r}_{n+1} = -\nabla f(\mathbf{x}_{n+1}) = \mathbf{b} - \boldsymbol{A}\mathbf{x}_{n+1} = \underbrace{\mathbf{b} - \boldsymbol{A}\mathbf{x}_n}_{\mathbf{r}_n} - \lambda_n \boldsymbol{A}\,\mathbf{r}_n$$

$$\Rightarrow\ \mathbf{r}_{n+1} = \mathbf{r}_n - \lambda_n \boldsymbol{A}\,\mathbf{r}_n. \tag{2.14}$$

We use the orthogonality of search directions to calculate λ_n:

$$0 \ = \ \mathbf{r}_{n+1}^T \mathbf{r}_n = \mathbf{r}_n^T \mathbf{r}_n - \lambda_n \boldsymbol{A}\,\mathbf{r}_n^T \mathbf{r}_n \tag{2.15}$$

$$\Rightarrow \ \ \lambda_n = \frac{\mathbf{r}_n^T \mathbf{r}_n}{\mathbf{r}_n^T \boldsymbol{A} \mathbf{r}_n}. \tag{2.16}$$

In summary, the Steepest Descent algorithm is given by Algorithm 3.

Algorithm 3 Steepest descent

Choose an initial vector $\mathbf{x}_0$
$\mathbf{r}_0 = \mathbf{b} - \boldsymbol{A}\mathbf{x}_0$
for $n = 0$ to $n_{\max}$ **do**
  $\lambda_n = \dfrac{\mathbf{r}_n^T \mathbf{r}_n}{\mathbf{r}_n^T \boldsymbol{A} \mathbf{r}_n}$
  $\mathbf{x}_{n+1} = \mathbf{x}_n + \lambda_n \mathbf{r}_n$
  if converged **then** EXIT
  $\mathbf{r}_{n+1} = \mathbf{r}_n - \lambda_n \boldsymbol{A} \mathbf{r}_n$
end for

We illustrate Steepest Descent by the following simple example in $N = 2$ dimensions.

$$A = \begin{pmatrix} 0.001 & 0 \\ 0 & 0.01 \end{pmatrix}, \ \ \mathbf{b} = \begin{pmatrix} 0.001 \\ 0.002 \end{pmatrix}, \ \ c = 0.0007. \tag{2.17}$$

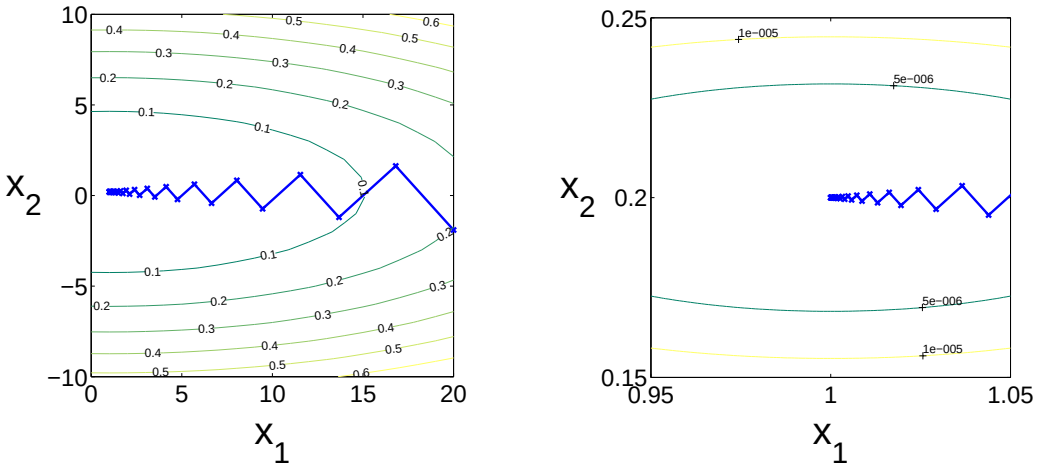

Figure 2.2: Steepest descent trajectory with initial point $(20, -1.9)$, for different resolutions.

The initial starting point is chosen to be $(20, -1.9)$. This turns out to be an unfavorable example for steepest descent, because the eigenvalues of $\boldsymbol{A}$ are very different from each other.

The trajectories are plotted in Fig. 2.2 on different scales. The coordinates of the minimum are $\xi = (1, 0.2)$. A 6 digit accuracy takes 76 iterations. We see the oscillatory trajectory on all scales (panels) in figure 2.2. This is in strong contradiction to our general consideration that a good gradient based method ought to yield the exact solution in $\mathcal{O}(N)$ steps. The shortcoming is the orthogonality of the successive search directions. If the first gradient forms an angle of 45 degrees with the x_1-axis, then so do all following directions since they are orthogonal to each other. *Due to the asymmetric eigenvalues*, the contour lines are also strongly asymmetric and the line minimum is always close to the $(x_2 = 0)$-axis. Therefore each step cannot get far ahead on the x_1-axis towards the true minimum.

In the most favorable case, namely for spherical contour lines, i.e. equal eigenvalues for both principle axes of the matrix $\boldsymbol{A}$, the iteration would reach the exact solution within one step.

The relevant parameter determining how slowly the solution converges is the ratio of the largest and the smallest eigenvalues of the matrix $\boldsymbol{A}$, which is called the *condition number* of $\boldsymbol{A}$.

In order to overcome the problem of orthogonality of locked search directions, more general directions are required which account for any non-spherical metric. This is achieved in the method of *conjugate gradients*.

2.4 Conjugate Gradient Method

Conjugate Directions

Steepest Descent often finds itself taking steps in the same direction as earlier steps. The idea is now to find a suitable set of N orthogonal *search directions* $\mathbf{d}_0, \mathbf{d}_1, \ldots, \mathbf{d}_{N-1}$. Together they form a *basis* of $\mathbb{R}^N$, so that the solution vector $\mathbf{x}$ can be expanded as

$$\mathbf{x} \;=\; \mathbf{x}_0 \;+\; \sum_{i=0}^{N-1} \lambda_i \, \mathbf{d}_i \; . \tag{2.18}$$

The goal is to take exactly one step in each search direction, with the right coefficient λ_i. After N steps we will be done. To accomplish this with low computational effort will require a special set of directions, and a new scalar product redefining "orthogonality".

For the first step, we set $\mathbf{x}_1 = \mathbf{x}_0 + \lambda_0 \mathbf{d}_0$. At step $n+1$ we choose a new point

$$\mathbf{x}_{n+1} = \mathbf{x}_n + \lambda_n \mathbf{d}_n \tag{2.19}$$

etc., until $\mathbf{x}_N = \mathbf{x}$ after N steps.

Let us collect a few simple relations which follow directly from (2.18) and (2.19). It is useful to introduce the deviation (”error vector”) from the exact solution $\mathbf{x}$

$$\begin{aligned}
\mathbf{e}_{n+1} \;&:=\; \mathbf{x}_{n+1} - \mathbf{x} && \text{(2.20a)}\\
&=\; \mathbf{e}_n \;+\; \lambda_n \mathbf{d}_n && \text{(2.20b)}\\
&=\; -\sum_{i=n+1}^{N-1} \lambda_i \, \mathbf{d}_i \; . && \text{(2.20c)}
\end{aligned}$$

Similar relations hold for the residuals $\mathbf{r}_n$, namely

$$\begin{aligned}
\mathbf{r}_{n+1} \;&:=\; -\nabla f(\mathbf{x}_{n+1}) \;=\; \mathbf{b} - \boldsymbol{A}\mathbf{x}_{n+1} && \text{(2.21a)}\\
&=\; \underbrace{\mathbf{b} - \boldsymbol{A}\mathbf{x}}_{=0} \;- \boldsymbol{A}\mathbf{e}_{n+1} && \text{(2.21b)}\\
&=\; \boldsymbol{A} \sum_{i=n+1}^{N-1} \lambda_i \, \mathbf{d}_i \; , && \text{(2.21c)}
\end{aligned}$$

and also the recursion

$$\mathbf{r}_{n+1} = \mathbf{r}_n \;-\; \boldsymbol{A}\, \lambda_n \mathbf{d}_n \; . \tag{2.21d}$$

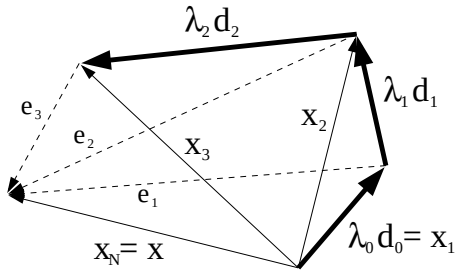

Figure 2.3: Sketch of the expansion of the solution $\mathbf{x}$ in directions $\mathbf{d}_i$ (with $x_0 = 0$). This figure is a projection from a higher dimensional space; therefore there are more than two "orthogonal" directions d_i.

The expansion is sketched in Fig.2.3.

Let us now see what would happen if we would demand that the directions d_n obey the usual 90 degree orthogonality $\mathbf{d}_i^T \mathbf{d}_j = 0$ for $i \neq j$. We want the search direction $\mathbf{d}_n$ to be orthogonal to all other search directions, including all future directions making up the error vector $\mathbf{e}_{n+1}$:

$$0 \stackrel{?}{=} \mathbf{d}_n^T \mathbf{e}_{n+1} \stackrel{(2.20b)}{=} \mathbf{d}_n^T \mathbf{e}_n + \mathbf{d}_n^T \lambda_n \mathbf{d}_n.$$

This would imply

$$\lambda_n \stackrel{?}{=} -\frac{\mathbf{d}_n^T \mathbf{e}_n}{\mathbf{d}_n^T \mathbf{d}_n}.$$

However, this equation is not useful, because this λ_n cannot be calculated without knowing the $\mathbf{e}_n$; but if we knew $\mathbf{e}_n$, then the problem would already be solved. This solution for λ_n would also mean that we totally ignore the line minima during search (e.g. when we try to reach the solution in Fig.2.1 with 2 vectors that are at 90 degrees to each other.)

Line minimum

The successful strategy is instead to still *follow each search direction* $\mathbf{d_i}$ *until the line minimum* ist reached. Thus

$$\begin{aligned} 0 &\stackrel{!}{=} \frac{d}{d\lambda} f(\mathbf{x}_{n+1}) = \nabla f(\mathbf{x}_{n+1})^T \frac{d}{d\lambda} \mathbf{x}_{n+1} \\ &= -\mathbf{r}_{n+1}^T \mathbf{d}_n \\ &\stackrel{(2.21d)}{=} -\mathbf{d}_n^T \mathbf{r}_n + \mathbf{d}_n^T \boldsymbol{A} \mathbf{d}_n \end{aligned} \tag{2.22}$$

and we get

$$\lambda_n = \frac{\mathbf{d}_n^T \mathbf{r}_n}{\mathbf{d}_n^T \boldsymbol{A} \mathbf{d}_n}. \tag{2.23}$$

This equation for the line minimum is valid for any set of search directions. It contains the current search direction $\mathbf{d_n}$ and the current residuum $\mathbf{r}_n$, which are both known.

Orthogonality

Eq. (2.22) tells us again that at the line minimum, the current search direction is orthogonal to the residuum. We rewrite this equation:

$$0 \;=\; -\mathbf{d}_n^T \mathbf{r}_{n+1} \overset{(2.21c)}{=} -\mathbf{d}_n^T \boldsymbol{A} \sum_{i=n+1}^{N-1} \lambda_i \, \mathbf{d}_i \overset{(2.20c)}{=} \mathbf{d}_n^T \boldsymbol{A} \, \mathbf{e}_{n+1} \, . \tag{2.24}$$

Our goal is that all search directions are "orthogonal". As argued above, this means that $\mathbf{d}_n$ should be orthogonal to $\mathbf{e}_{n+1}$. This is consistent with (2.24), if we **use a new scalar product**

$$(\mathbf{u}, \mathbf{v})_{\boldsymbol{A}} \;:=\; \mathbf{u}^T \, \boldsymbol{A} \, \mathbf{v} \, . \tag{2.25}$$

to define orthogonality.

We now *demand* that all search directions are mutually A-orthogonal

$$\boxed{\mathbf{d}_i^T \boldsymbol{A} \mathbf{d}_j = 0 \quad (i \neq j)} \tag{2.26}$$

We will construct such a set of conjugate directions $\mathbf{d}_i$. Since $\mathbf{u}^T \, \boldsymbol{A} \, \mathbf{v}$ is a scalar product, these vectors form an orthogonal *basis* of $\mathbb{R}^N$, in which the solution vector $\mathbf{x}$ can be expanded as in (2.18).

We are therefore also guaranteed that the solution will take *at most* N *steps* (up to effects of rounding errors).

From (2.21c) and (2.26) we can deduce

$$\mathbf{d}_m^T \mathbf{r}_n \;=\; \mathbf{d}_m^T \, \boldsymbol{A} \sum_{i=n}^{N-1} \lambda_i \, \mathbf{d}_i \;=\; 0 \;\text{ for } m < n \, , \tag{2.27}$$

meaning that the residual $\mathbf{r}_n$ is orthogonal in the usual sense (90 degrees) to all old search directions.

Gram-Schmidt Conjugation

We still need a set of N $\boldsymbol{A}$-orthogonal search directions $\{\mathbf{d}_i\}$.There is a simple (but inefficient) way to generate them iteratively: The *conjugate Gram-Schmidt process*.

Let $\{\mathbf{u}_i\}$ with $i = 0, \ldots, N-1$ be a set of N linearly independent vectors, for instance unit vectors in the coordinate directions. Suppose that the search directions $\mathbf{d}_k$ for $k < i$ are already mutually $\boldsymbol{A}$-orthogonal. To construct the next direction $\mathbf{d}_i$, take $\mathbf{u}_i$ and subtract out all components that are not $\boldsymbol{A}$-orthogonal to the previous $\mathbf{d}$-vectors, as is demonstrated in Fig. 2.4. Thus, we set $\mathbf{d}_0 = \mathbf{u}_0$ and for $i > 0$ we choose

$$\mathbf{d}_i = \mathbf{u}_i + \sum_{k=0}^{i-1} \beta_{ik} \mathbf{d}_k, \tag{2.28}$$

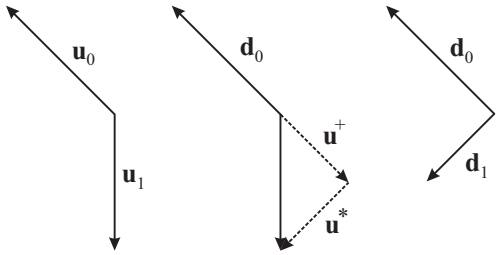

Figure 2.4: Gram-Schmidt conjugation of two vectors. Begin with two linearly independent vectors $\mathbf{u}_0$ and $\mathbf{u}_1$. Set $\mathbf{d}_0 = \mathbf{u}_0$. The vector $\mathbf{u}_1$ is composed of two components: $\mathbf{u}^*$ which is $\boldsymbol{A}$-orthogonal (in this figure: 90 degrees) to $\mathbf{d}_0$, and $\mathbf{u}^+$ which is parallel to $\mathbf{d}_0$. We subtract $\mathbf{u}^+$, so that only the $\boldsymbol{A}$-orthogonal portion remains: $\mathbf{d}_1 = \mathbf{u}^* = \mathbf{u}_1 - \mathbf{u}^+ =: \mathbf{u}_1 + \beta_{10}\mathbf{d}_0$.

with the β_{ik} defined for $k < i$. To find their values we impose the $\boldsymbol{A}$-orthogonality of the new direction $\mathbf{d}_i$ with respect to the previous ones:

$$\begin{aligned} 0 \overset{i>j}{=} \mathbf{d}_i^T \boldsymbol{A} \mathbf{d}_j &= \mathbf{u}_i^T \boldsymbol{A} \mathbf{d}_j + \sum_{k=0}^{i-1} \beta_{ik} \mathbf{d}_k^T \boldsymbol{A} \mathbf{d}_j \\ &= \mathbf{u}_i^T \boldsymbol{A} \mathbf{d}_j + \beta_{ij} \mathbf{d}_j^T \boldsymbol{A} \mathbf{d}_j \ . \qquad (2.29) \\ \beta_{ij} &= -\frac{\mathbf{u}_i^T \boldsymbol{A} \mathbf{d}_j}{\mathbf{d}_j^T \boldsymbol{A} \mathbf{d}_j}. \qquad (2.30) \end{aligned}$$

Note that in the first line, the sum reduces to the term $k = j$ because of mutual $\boldsymbol{A}$-orthogonality of the previous search vectors $\mathbf{d}_k$, $k < i$.

Equation (2.30) provides the necessary coefficients for (2.28). However, there is a difficulty in using this method, namely that all the old search vectors must be kept and processed to construct the new search vector.

Construction from Gradients

This method is an efficient version of Gram-Schmidt. We will not need to keep the old search vectors. The new ansatz here is to choose a specific set of directions $\mathbf{u}_i$, namely

$$\mathbf{u}_i := \mathbf{r}_i \ . \qquad (2.31)$$

First we now use the fact that the residual is orthogonal to all previous search directions, (2.27). Together with (2.28) we get, for $i < j$ and for as yet general $\mathbf{u}_i$:

$$\begin{aligned} 0 \overset{i<j}{=} \mathbf{d}_i^T \mathbf{r}_j &\overset{(2.28)}{=} \mathbf{u}_i^T \mathbf{r}_j + \underbrace{\sum_{k=0}^{i-1} \beta_{ik} \mathbf{d}_k^T \mathbf{r}_j}_{=0 \ (2.27)} \\ 0 &= \mathbf{u}_i^T \mathbf{r}_j \ . \qquad (2.32a) \end{aligned}$$

In the same way one gets

$$\mathbf{d}_i^T \mathbf{r}_i = \mathbf{u}_i^T \mathbf{r}_i. \tag{2.32b}$$

With our particular choice $\mathbf{u}_i = \mathbf{r}_i$, (2.32a) becomes

$$\mathbf{r}_i^T \mathbf{r}_j = 0, \quad i \neq j \; . \tag{2.33}$$

We see that all residue vectors $\mathbf{r}_i$ will actually be orthogonal to each other.

We can now compute the Gram-Schmidt coefficients (2.30). The recursion (2.21d) implies

$$\mathbf{r}_i^T \mathbf{r}_{j+1} \; = \; \mathbf{r}_i^T \mathbf{r}_j - \lambda_j \mathbf{r}_i^T \boldsymbol{A} \mathbf{d}_j \; .$$

The last term corresponds to the denominator in (2.30). Because of the orthogonality (2.33), it simplifies to

$$\mathbf{r}_i^T \boldsymbol{A} \mathbf{d}_j \quad = \quad \begin{cases} \frac{1}{\lambda_i} \mathbf{r}_i^T \mathbf{r}_i, & i = j \\ -\frac{1}{\lambda_{i-1}} \mathbf{r}_i^T \mathbf{r}_i, & i = j+1 \\ 0, & \text{otherwise}, \end{cases}$$

Thus we obtain all the coefficients needed in (2.28):

$$\beta_{ij} = \begin{cases} \frac{1}{\lambda_{i-1}} \frac{\mathbf{r}_i^T \mathbf{r}_i}{\mathbf{d}_{i-1}^T \boldsymbol{A} \mathbf{d}_{i-1}}, & i = j+1 \\ 0, & i > j+1. \end{cases}$$

Most of the β_{ij} terms have now become zero. It is no longer necessary to store old search vectors to ensure $\boldsymbol{A}$-orthogonality. We now denote, for simplification, $\beta_i = \beta_{i,i-1}$ and plug in λ_{i-1} from (2.23) to get the final form of the coefficients:

$$\begin{aligned} \beta_i &\overset{(2.23)}{=} \frac{\mathbf{r}_i^T \mathbf{r}_i}{\mathbf{d}_{i-1}^T \mathbf{r}_{i-1}} \\ &\overset{(2.32b)}{=} \frac{\mathbf{r}_i^T \mathbf{r}_i}{\mathbf{r}_{i-1}^T \mathbf{r}_{i-1}}. \end{aligned}$$

Putting all our results together we obtain the Conjugate Gradient algorithm, which is presented in symbolic form as algorithm 4.

Comments

Note that the first step of the Conjugate Gradient method is the same as for steepest descent. Convergence is again estimated by the norm of $\mathbf{r}_n$.

The computationally most expensive part of the algorithm is one Matrix-vector multiplication $\boldsymbol{A}\mathbf{d}_n$ per step. It can be implemented efficiently, especially for sparse matrices. All other parts are vector-vector multiplications. Because of rounding errors, orthogonality can get lost during the iteration.

Algorithm 4 Conjugate Gradient method for quadratic functions

Choose a suitable initial vector $\mathbf{x}_0$
Set $\mathbf{d}_0 := \mathbf{r}_0 = -\nabla f\big|_{\mathbf{x}_0} = \mathbf{b} - \boldsymbol{A}\mathbf{x}_0$
for $n = 0$ to N **do**
  $\mathbf{a}_n = \boldsymbol{A}\mathbf{d}_n$
  $\lambda_n = (\mathbf{r}_n^T\mathbf{r}_n)/(\mathbf{d}_n^T\mathbf{a}_n)$
  $\mathbf{x}_{n+1} = \mathbf{x}_n + \lambda_n\mathbf{d}_n$
  $\mathbf{r}_{n+1} = \mathbf{r}_n - \lambda_n\mathbf{a}_n$
  $\beta_{n+1} = (\mathbf{r}_{n+1}^T\mathbf{r}_{n+1})/(\mathbf{r}_n^T\mathbf{r}_n)$
  $\mathbf{d}_{n+1} = \mathbf{r}_{n+1} + \beta_{n+1}\mathbf{d}_n$
  if converged **then** EXIT
end for

It can therefore be advantageous to occasionally calculate the residue directly as $\mathbf{r}_{n+1} = \mathbf{b} - \boldsymbol{A}\mathbf{x}_{n+1}$, which involves a second matrix multiplication.

In each step, the Conjugate Gradient algorithm invokes one multiplication with $\boldsymbol{A}$. The solution is thus in fact constructed in the space spanned by the vectors $\{\mathbf{r}_0, \boldsymbol{A}\mathbf{r}_0, \boldsymbol{A}^2\mathbf{r}_0, \boldsymbol{A}^3\mathbf{r}_0, \dots\}$, which is called a *Krylov space*. There are a many other related methods also acting in Krylov space. One of the most important ones is the closely related *Lanczos algorithm* for computing low lying eigenvalues of a big (sparse) matrix. It was developed before CG. Other methods exist for nonsymmetric matrices.

The numerical stability and convergence of CG is again governed by the *condition number* of the matrix $\boldsymbol{A}$. It can be improved greatly by a class of transformations called *Preconditioning*. Instead of solving $\boldsymbol{A}\mathbf{x} = \mathbf{b}$, one solves the equivalent equation $\boldsymbol{M}^{-1}\boldsymbol{A}\mathbf{x} = \boldsymbol{M}^{-1}\mathbf{b}$. The ideal case would be the exact solution $\boldsymbol{M}^{-1} = \boldsymbol{A}^{-1}$, giving the identity matrix $\boldsymbol{M}^{-1}\boldsymbol{A}$ with condition number unity. Much simpler transformations can already improve convergence greatly, e.g. just taking $\boldsymbol{M}$ to be the diagonal of $\boldsymbol{A}$.

2.5 Conjugate Gradient for General Functions

We are now prepared to apply the conjugate gradient idea to general functions $f(\mathbf{x})$. To this end we expand $f(\mathbf{x})$ in each iteration about the actual reference point $\mathbf{x}_n$ of the n^{th} step, to second order

$$f(\mathbf{x}) \simeq f(\mathbf{x}_n) + \mathbf{b}_n^T(\mathbf{x} - \mathbf{x}_n) + \frac{1}{2}(\mathbf{x} - \mathbf{x}_n)^T\boldsymbol{A}_n(\mathbf{x} - \mathbf{x}_n) \tag{2.34a}$$

$$\mathbf{b}_n = \nabla f(\mathbf{x})\big|_{\mathbf{x}_n} \tag{2.34b}$$

$$(\boldsymbol{A}_n)_{ll'} = \frac{\partial^2}{\partial x_l \partial x_{l'}} f(\mathbf{x})\big|_{\mathbf{x}_n}, \tag{2.34c}$$

where the matrix $\boldsymbol{A}_n$ is called the Hessian. Since (2.34) is a quadratic form it can easily be cast into the form (2.8), on which CG (Conjugate Gradi-

ent) for quadratic problems was based, with one significant modification though: The matrix (Hessian) $\boldsymbol{A}_n$ changes from iteration to iteration as does the vector $\mathbf{b}_n$. All equations in algorithm 4 are still valid with the only modification that the matrix $\boldsymbol{A}$ corresponds to the Hessian $\boldsymbol{A}_n$ of the Taylor expansion about the reference point $\mathbf{x}_n$. The iteration scheme 4 remains valid, with the modification that $\boldsymbol{A}$ has to be replaced in each iteration by the respective Hessian $\boldsymbol{A}_n$. This implies that we have to be able to compute the Hessian. Is is available analytically only in rare cases, and the numeric computation is inefficient. Fortunately, $\boldsymbol{A}_n$ enters only in conjunction with the iteration scheme for the gradients and in the expression for λ_n. These steps can be modified. First of all, we replace the update rule for $\mathbf{r}_{n+1}$ by the definition

$$\mathbf{r}_{n+1} = -\nabla f(\mathbf{x})\big|_{\mathbf{x}_{n+1}}.$$

Here we merely require the knowledge of the gradient instead of the Hessian. Secondly, the parameter λ_n is obtained more directly via

$$\min_{\lambda} \; f(\mathbf{x}_n + \lambda \mathbf{d}_n) \; \Rightarrow \lambda_n,$$

which is approximately solved numerically. Equations (2.26), (2.27), and (2.33) are, however, no longer valid for $|i-j| > 1$, since the matrix $\boldsymbol{A}$ changes from iteration to iteration. If the conjugacy relation (2.26) was still valid then the arguments given for quadratic problems would still hold and convergence would be reached within at most N steps. This is, of course, not the case for arbitrary non-quadratic functions.

The corresponding algorithm is presented below.

Algorithm 5 Conjugate Gradient method for general functions

Choose a suitable initial vector $\mathbf{x}_0$
$\mathbf{r}_0 = \mathbf{g}_0 = \nabla f\big|_{\mathbf{x}_0}$
$\mathbf{d}_0 = \mathbf{r}_0 = -\nabla f\big|_{\mathbf{x}_0}$
for $n = 0$ to $n_{\max}$ **do**
  $\min_\lambda \; f(\mathbf{x}_n + \lambda \mathbf{r}_n) \quad \Rightarrow \lambda_n$
  $\mathbf{x}_{n+1} = \mathbf{x}_n + \lambda_n \mathbf{d}_n$
  $\mathbf{r}_{n+1} = -\nabla f\big|_{\mathbf{x}_{n+1}}$
  $\beta_{n+1} = (\mathbf{r}_{n+1}^T \mathbf{r}_{n+1})/(\mathbf{r}_n^T \mathbf{r}_n)$
  $\mathbf{d}_{n+1} = \mathbf{r}_{n+1} + \beta_{n+1} \mathbf{d}_n$
  if converged **then** EXIT
end for

2.6 Stochastic Optimization

Nonlinear problems often have more than one minimum. Gradient methods like Conjugate Gradient (CG) only yield a *local* minimum in the vicinity of the initial point. If there are not too many minima, one can start CG at different initial points (chosen at random) to obtain the global minimum. However, there are many problems not accessible to this procedure. If there are many minima, then CG with random start points is very inefficient.

Combinatorial problems. Traveling Salesman.

Some examples that are not suited for gradient-based methods are the following combinatorial problems:

- The *Traveling Salesman* problem (TSP). There are N cities. A salesman has to visit each city once, and the length of the trip has to be minimized. The function to be minimized is of the form

$$f(\{i\}) = \sum_{\nu=1}^{N} \left| \mathbf{x}_{i_{\nu+1}} - \mathbf{x}_{i_\nu} \right|, \quad (i_{N+1} := i_1)$$

  with $\left| \mathbf{x}_{i_{\nu+1}} - \mathbf{x}_{i_\nu} \right|$ the distance between two consecutive cities within the list $\{i\}$. The locations $\mathbf{x}_i$ of the cities are fixed. The total distance travelled depends on the *order* in which the cities are visited. The notation $\{i\}$ stands for a list of indices in this order. The number of possible sequences is $N!$. For large N, they cannot be enumerated directly.

  More realistic applications contain additional terms and constraints in the cost function.

- Redistribute the integer numbers from $1 - 16$ in a way that the sums along all edges have the same value. There are $16!$ possible index arrangements.

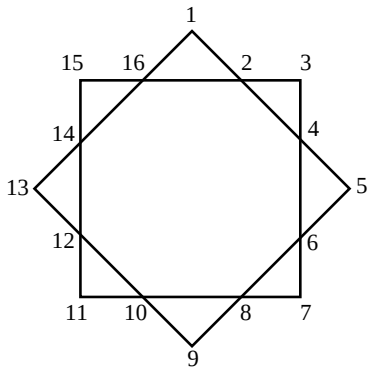

- Time tables at schools

Note that in these combinatorial examples, there is a *discrete* set of possibilities. Therefore the function to be minimized does not have any derivative in the space of possibilities, and methods like Conjugate Gradient cannot be applied.

Complexity classes

Combinatorial problems (and related others like search problems) can be extremely hard computationally. There is a large area of computer science dealing with just the *classification* of such problems. One of the "simplest" complexity classes is called "**P**" the class of all problems which can be solved in *polynomial time*, i.e. the number of steps to solve the problem grows with the "size" (like the number N of cities in the traveling salesman problem) "only" polynomially. The Traveling Salesman probably does not belong to this class, which means that there are cases which require an *exponential* number of steps.

A more difficult fundamental class is called **NP**. It is the class of problems for which the solution, once specified, can be *verified* in polynomial time. This definition says nothing about how long it may take to find the solution, which might be exponentially long. (Note that NP stands for *non-deterministic polynomial* because such problems could be solved on a non-deterministic Turing machine (which can branch at every step) in polynomial time. It does *not* stand for "non-polynomial".)

The most difficult problems in NP are called **NP-complete**, namely those to which every other problem in NP can be transformed in polynomial time. All NP-complete problems are equivalent in this sense. It is known that the Traveling Salesman is in fact an *NP-complete* problem, as are many other problems in graph-theory, networks, sorting, partitioning, data compression, etc..

It is very likely (but not proven) that NP is larger than P, i.e. that there are indeed problems which can not be solved in polynomial time. If NP where the same as P, then there would be a polynomial time algorithm for *all* the myriad important problems known to be NP-complete.

There are other problems which are known to be outside P, and others which are not solvable even on a quantum computer (called **QMA**). In fact, there are so many proposed complexity classes that one speaks of the *complexity zoo*. However, for almost all of these classes, their supposed relationship is not mathematically *proven* ! One does not even know for sure whether there are problems that a quantum computer can solve faster (in the sense of polynomial versus non-polynomial) than a classical one.

It is also important to note that the classification is in terms of *worst case* problems of a given type. A "typical" or an "average" instance of a problem class may be much easier to solve. For example, the Traveling Salesman problem can sometimes be solved for thousands of cities. The situation becomes still better when one allows approximations to the optimum.

On the other hand, problems with "polynomial time" solutions may in practice involve such high powers of N that they become intractable - which may already be the case for N^3 when N is very large.

There is a great variety of optimization methods for such difficult problems. We will introduce some of the most fundamental ones.

No method is perfect

It is important to realize that *no method provides a* guarantee to find the global optimum of an arbitrary function, except by exhaustive search. In order to gain some confidence in any solution, it is therefore always advisable to perform several independent optimizations, with different starting points and different random number sequences.

2.6.1 Classical Simulated Annealing

Literature:

- S. KIRKPATRICK, C.D. GELLAT, JR., and M.P. VECCHI, *Simulated Annealing*, Science **220**, 671 (1983).

The most well known stochastic optimization algorithm is Simulated Annealing. Its approach is borrowed from physics, specifically from thermodynamics. The method models the way that liquids freeze and crystallize during an annealing process. At high temperatures, the particles can move freely. Differences of potential energies of various configurations are overcome by the particles due to their high kinetic energy. When the liquid is cooled down slowly, an ordering process sets in, thermal mobility is lost and some optimal configuration (e.g. an ideal crystal) may be achieved. This is a configuration where the cost function (free energy) attains its absolute minimum. However, if the liquid is cooled down too quickly, no ideal crystal is obtained and the systems ends in some local minimum of the energy (meta-stable state). This corresponds to a poly crystalline or amorphous state. We try to find the global minimum by simulating the slow cooling process on the computer. To this end we introduce an *artificial temperature* T and an artificial (!) *probability distribution* $p_E(\mathbf{x}|T)$, where $\mathbf{x}$ now is some point in the parameter space of the problem. The cost function to be minimized is denoted by $f(\mathbf{x})$ and can depend on a set of variables $\mathbf{x}$ that is either discrete or continuous. In Classical Simulated Annealing (CSA), we *choose*

$$p_E(\mathbf{x}|T) = \frac{1}{Z} e^{-f(\mathbf{x})/T}, \tag{2.35}$$

which corresponds to a Boltzmann distribution. Thus we treat f like an *energy* in statistical mechanics. Here Z is a normalization factor which corresponds to the partition function of the canonical ensemble, $Z = \sum_{\mathbf{x}} e^{-f(\mathbf{x})/T}$. We can also define the expectation value of $f(\mathbf{x})$ at a given temperature T by

$$\langle f \rangle_T = \sum_{\mathbf{x}} p_E(\mathbf{x}|T)\, f(\mathbf{x}). \tag{2.36}$$

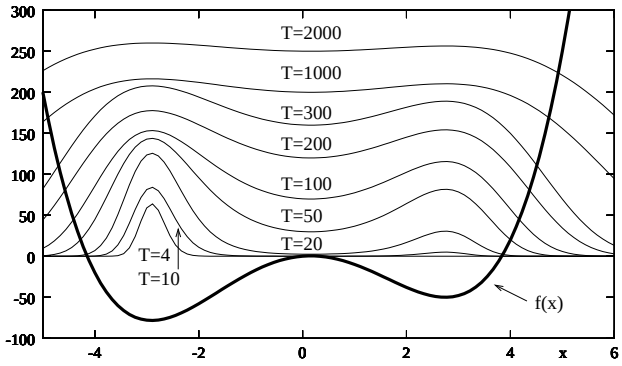

Figure 2.5: Example of a cost function $f(x)$ with two minima (thick solid line) and the Boltzmann weight $p_E(x|T)$ (thin solid lines, without scale) for various temperatures T.

In order to find the minimum, we will employ a Monte Carlo simulation with the weight function (2.35). As an example, figure 2.5 shows the cost function (thick solid line)

$$f(x) = x^4 - 16x^2 + 5x \; . \tag{2.37}$$

Figure 2.5 also depicts the Boltzmann weight (thin solid lines) for various temperatures. At temperatures much higher than the potential barrier, $T \gg 50$, the Boltzmann distribution is rather flat. As soon as the temperature is lower than the potential barrier, e.g. at $T = 20$, the weight outside the double-well is almost zero and two separate peaks develop. If the temperature is even lower than the difference of the two minima, e.g. at $T = 10$, the weight in the local minimum becomes negligible and the probability is concentrated merely around the global minimum.

It is the purpose of the distribution p_E to assign a high probability to states $\mathbf{x}$ where $f(\mathbf{x})$ is small, i.e. states $\mathbf{x}$ close to the global minimum. A *"random walker"* will spend a long time near the optimum state. The important difference with respect to gradient based methods like CG is the possibility for the walker to also go *uphill* and thus leave a local minimum. The probability to do so depends on temperature. The minimum of $f(\mathbf{x})$ as well as the corresponding state $\mathbf{x}$ are found by cooling.

An implementation of the Classical Simulated Annealing (CSA) method requires the following three parts

1. **Move in configuration space**
2. **Probability Distribution and Acceptance of states**
3. **Cooling scheme**

ad 1: Move in configuration space In the vicinity of the current point $\mathbf{x}_n$ (n is the step index) we create a trial point $\mathbf{x}_t$ at random.

For *continuous* problems, the probability distribution of the trial point $\mathbf{x}_t$ is typically chosen to be a Gaussian

$$p_x(\mathbf{x}_t - \mathbf{x}_n) \propto \prod_i e^{-(\mathbf{x}_t - \mathbf{x}_n)_i^2/(2\sigma^2)} \tag{2.38}$$

of a certain variance σ around the current point $\mathbf{x}_n$. If the curvature of $f(\mathbf{x})$ in various directions differs significantly, it is expedient to use a p_x which employs different variances in different directions, or, more generally, the covariance matrix $\boldsymbol{C}$ of $f(\mathbf{x})$ instead of the variance σ:

$$p_x(\mathbf{x}_t - \mathbf{x}_n) \propto \exp\left\{\frac{1}{2}(\mathbf{x}_t - \mathbf{x}_n)\boldsymbol{C}^{-1}(\mathbf{x}_t - \mathbf{x}_n)\right\}.$$

As an example for a *discrete* problem, we look a the Traveling Salesman. The tour is represented by a list of indices $\{i_1, i_2, \ldots, i_N\}$ indicating the order in which the cities are visited. One possibility is the so-called *lin-2-opt* move. It consists in reversing a part of the trajectory:

$$\{i_1 \ldots i_{\nu-1}, \underline{i_\nu, i_{\nu+1} \ldots i_{\mu-1}, i_\mu}, i_{\mu+1} \ldots i_L\} \longrightarrow \{i_1 \ldots i_{\nu-1}, \underline{i_\mu, i_{\mu-1} \ldots i_{\nu+1}, i_\nu}, i_{\mu+1} \ldots i_L\}. \tag{2.39}$$

The advantage of such a move is that the change in cost function can be small and is computed quickly. Here it is

$$f(\{i'\}) - f(\{i\}) = \overline{\mathbf{x}_{i_{\nu-1}}\mathbf{x}_{i_\mu}} + \overline{\mathbf{x}_{i_\nu}\mathbf{x}_{i_{\mu+1}}} - \overline{\mathbf{x}_{i_{\nu-1}}\mathbf{x}_{i_\nu}} - \overline{\mathbf{x}_{i_\mu}\mathbf{x}_{i_{\mu+1}}},$$

with $\overline{\mathbf{x}_{i_\nu}\mathbf{x}_{i_\mu}} = \left|\mathbf{x}_{i_\nu} - \mathbf{x}_{i_\mu}\right|$ the distance between the cities ν and μ in configuration $\{i\}$.

ad 2: Probability Distribution and Acceptance of states We are free to choose any procedure which will lead us to the minimum, while providing the possibility to also move uphill. In Classical Simulated Annealing one chooses the Boltzmann Distribution (2.35). A common choice for the acceptance step is to use the *Metropolis probability*

$$q = \min\left\{1, \frac{p_E(\mathbf{x}_t|T)}{p_E(\mathbf{x}_n|T)}\right\}, \tag{2.40}$$

which happens to satisfy detailed balance. We thus generate a Markov chain with which we can calculate expectation values *at a given temperature* T

$$\langle f(\mathbf{x})\rangle_T \;=\; \lim_{n\to\infty}\frac{1}{n}\sum_{i=1}^{n} f(\mathbf{x}_i) \tag{2.41}$$

by averaging over the Markov chain.

Real problems often display several different (length) *scales in parameter space*. Consider as an example the traveling salesman. Towns will typically come in several agglomerations. The distance from one town to another strongly depends on whether the town is in the same agglomeration or not. Thus we have two different length scales:

- Distance between towns of the same agglomeration.
- Distance between different agglomerations.

The existence of different scales is reflected by the way the "energy" decreases when we lower the temperature. At extremely high temperatures, agglomerations do not play a role. The salesman travels at random. In the cooling procedure, the order of the agglomerations to be visited will be decided on first. Only then the trip inside each agglomeration is fixed.

In order to learn more about the behaviour of the system, we use the analogy with statistical physics. We denote the cost function $f(\{i\})$ explicitely as an *energy* $E(\{i\}) \equiv f(\{i\})$. During the simulation for one specific temperature T we calculate

$$\langle E \rangle \simeq \frac{1}{n} \sum_{\{i\}} E(\{i\}), \quad \text{and} \quad \langle E^2 \rangle \simeq \frac{1}{n} \sum_{\{i\}} E^2(\{i\}),$$

with the variance

$$\langle \Delta E^2 \rangle := \langle E^2 \rangle - \langle E \rangle^2.$$

Here, $\sum_{\{i\}}$ indicates the sum over configurations simulated at the current temperature. This allows us to introduce a *specific heat* C_H defined as

$$C_H := \frac{\partial \langle E \rangle}{\partial T} = \frac{\langle \Delta E^2 \rangle}{T^2}. \tag{2.42}$$

The last equality follows from (2.35) and (2.36). The specific heat is large when the energy changes quickly as a function of temperature (see fig. 2.6). In a statistical physics system this is typically associated with a phase transition. We get a first cooling rule: Away from "phase transitions" we can cool down quickly, since the energy (and thus the Boltzmann weight) varies slowly. However, we have to be careful in the vicinity of such "phase transitions", and the specific heat C_H with its rapid variation around phase transitions is a good indicator of critical regions.

ad 3: Cooling Strategy An important step is the choice of the initial temperature T_0. At this temperature it should be possible to cover the best part of the configuration space and it is a rough rule of thumb that at this temperature approximately 80% of the configurations should be accepted. This can easily be achieved by choosing some value for T_0 and performing n steps. When more than 80% of the steps are accepted, then T_0 is a good choice as an initial temperature, otherwise we double T_0 and try again.

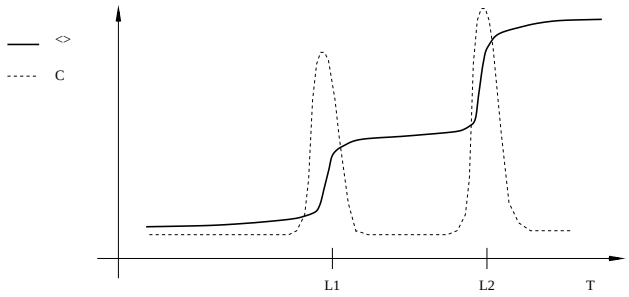

Figure 2.6: Cost function (solid line) and "specific heat" (dotted line) of the traveling salesman problem with two length scales L_1 and L_2

To proceed in the simulation, we let the walker do a n steps at every fixed temperature T_k.

One simple choice for the temperature sequence is to lower it according to a simple formula, e.g.

$$T_k = \frac{T_0}{k^q} \tag{2.43}$$

with some exponent q. Sometimes even a very fast exponential cooling like $T_k = T_0\, q^k$ is used. A fixed cooling sequence has the drawback of not taking into account any "phase transitions", where the simulation could get stuck.

One can devise a more adaptive cooling strategy which takes into account the rate of change of the function f, i.e. the "specific heat". We need to make sure that the walker can move *back and forth* in energy space. Therefore the energies in the canonical distribution of configurations at temperature T_k should overlap those in the canonical distribution at the next temperature T_{k+1}. The widths of these distributions is related to the specific heat and one can deduce that the step in temperature should be bounded

$$\frac{T_k - T_{k+1}}{T_k} \;<\; \frac{\delta}{\sqrt{C_H}} \tag{2.44}$$

where δ is a small number related to the desired acceptance rate.

During the annealing process it is expedient to choose the trial points in such a way that an acceptance rate of about 50% is achieved. We can for example measure the acceptance rate during $N = 100$ steps. If it is below 40% we decrease the size of the moves, if it is above 60% we increase the size of the moves, otherwise the proposal distribution is acceptable. (Note that changing the proposal distribution during the update violates detailed balance, but does not disturb the search for the global minimum).

Algorithm 6 Classical Simulated Annealing (CSA)

Choose a suitable initial vector $\mathbf{x}_0$
$T_0 = T_0^E$
for $j = 0$ to $j_{\max}$ **do**
  for $l = 0$ to n **do**
    generate trial state $\mathbf{x}_t$ according to $p_x(\mathbf{x}_t - \mathbf{x}_n)$
    compute $q = \min(1, p_E(\mathbf{x}_t)/p_E(\mathbf{x}_n))$
    if $q = 1$; $\mathbf{x}_{n+1} = x_t$; **else**
      random number $r \in [0, 1)$
      if $q > r$; $\mathbf{x}_{n+1} = \mathbf{x}_t$; **else** $\mathbf{x}_{n+1} = \mathbf{x}_n$;
  end for
  determine T_{j+1}
  if converged **then** EXIT
end for

2.6.2 Fast Simulated Annealing

One shortcoming of the CSA method is that due to the exponential character of the Boltzmann distribution, only *short moves*, or rather small modifications, are allowed. Therefore it takes a long time to escape from a local minimum.

Instead of the Boltzmann function *Fast Simulated Annealing* (FSA) uses the CAUCHY function as a probability distribution. The D-dimensional Cauchy distribution is given by

$$p_x(\Delta\mathbf{x}|T) = \frac{T}{[(\Delta\mathbf{x})^2 + T^2]^{\frac{D+1}{2}}}, \tag{2.45}$$

where D is the dimension of the vector $\mathbf{x}$ of parameters. Due to its long ranging tails (namely an unbounded variance), the Cauchy distribution has the advantage to allow occasionally larger changes in configuration space, while the short range moves are still Gaussian distributed with a variance $\sigma^2 = 2\,T^2/(D+1)$.

Formally, it has been shown that under some assumptions on the function to be minimized the Boltzmann distribution may need a temperature schedule $T(t) \sim \frac{1}{\ln(t+1)}$, (which means an exponential number of steps !), whereas under the same assumptions the Cauchy distribution needs only $T(t) \sim \frac{1}{t+1}$.

In figure 2.7 b), CSA and FSA are compared based on the double well potential (2.37) discussed before. The temperature entering the proposal distribution is adjusted every 100 steps to ensure 50% acceptance rate. For each annealing step n, the lowest energy (value of the cost function) is stored in $E(n)$. The entire annealing procedure, covering $n_{\max} = 10000$ steps is repeated 1000 times and average $\langle E(n)\rangle$ is computed for each value of n separately. We see that FSA is indeed superior.

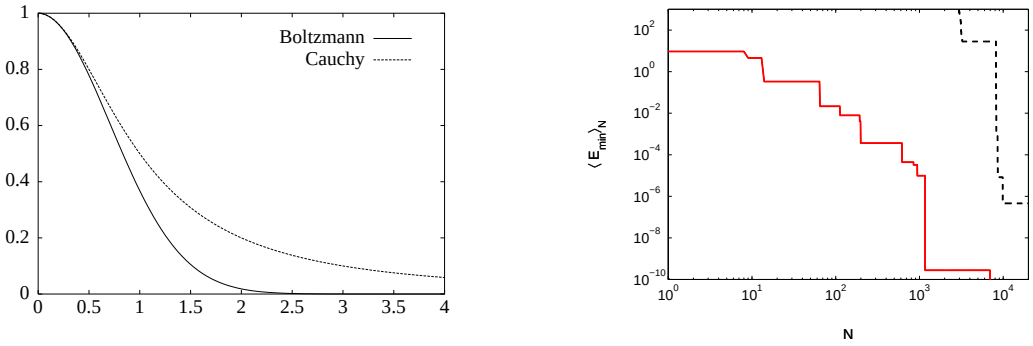

a) b)

Figure 2.7: a) Comparison between Boltzmann (Gauss) and Cauchy distribution. b) Average minimum energy $\langle E_{\min} \rangle_N$reached in step N for Fast Simulated Annealing (FSA, solid red curve) and Classical Simulated Annealing (CSA, dashed black curve).

2.6.3 Other variants

Alternative Acceptance methods

Note that for optimization purposes one does not need detailed balance! (It does however help in order to map the region of attraction of the optimum, i.e. its stability.) The proposals mentioned here do *not* satisfy detailed balance nor stationarity. Thus they do not lead to a simultation of the canonical distribution of a statistical system. Nevertheless they are well suited for finding the minimum of f.

- *Threshold Acceptance:* A new configuration $\mathbf{x}_t$ is generated. If the cost function satisfies $f(\mathbf{x}_t) < f(\mathbf{x}_n) + T$, with T some tolerance level (threshold), then $\mathbf{x}_t$ is accepted. This allows rather effectively to leave local minima. During the iteration the threshold is continuously reduced.

- *Deluge Algorithms:* Accept new configurations $\mathbf{x}_t$ only if $f(\mathbf{x}_t) > T$ with T the acceptance level. T is continuously increased during the iterations; the landscape is 'flooded' until only the summits of the mountains, and finally only the summit of the biggest mountain is above the water level.

Multicanoncial ensemble

This method, describe in more detail in section 1.8.3, moves through parameter space efficiently by using an auxiliary cost function $\tilde{f}(\mathbf{x})$ which is almost constant. It is constructed from the actual cost function $f(\mathbf{x})$ by mapping and then "filling up" its local minima. Trapping can be avoided in this way, so that the global minimum of $f(\mathbf{x})$ can be found better. This method is quite successful for, e.g., protein folding.

Tempering

A severe drawback of Simulated Annealing is that the temperature is always lowered. Once the walker is stuck in a local minimum, it will stay there. In *Tempering* (section 1.8.3) the temperature is allowed to fluctuate randomly like any other parameter, between a very low and a very high bound. The temperature steps are not prescribed from outside, but instead decided with Metropolis decisions. When the temperature is high, a local minimum can be left. Tempering is therefore somewhat like an automatic multiple run of Simulated Annealing with many starting configurations and many temperature sequences.

2.7 Genetic algorithms

A genetic algorithm takes its approach from nature. It simulates the natural evolution of a *population* of individuals (candidate solutions) from generation to generation, with steps of inheritance, mutation, and selection. There are many varieties of such algorithms.

Each individual solution is characterized by a "genome", representing one point in the parameter space of the cost function ("*fitness*") to be optimized. The genome is traditionally represented by a set of bits, but it can also be comprised of real or integer numbers, or more complicated objects. The cost function needs to be evaluated very often, and an efficient implementation is therefore important.

Initialization.

The optimization starts with an initial *population* of typically hundreds or thousands of individuals. They can be chosen at random, or according to initial guesses, in areas of parameter space where solutions are likely to be found. For each individual, the cost function is evaluated.

Iteration.

The following steps are then iterated:

- *Selection.* A part of the population is selected. This selection is based on fitness. However, it is not appropriate to select just the best solutions. One needs to include some randomness in the selection in order to insure genetic variety in the population. Otherwise the method will quickly tend towards a local optimum instead of the global one.
- *Reproduction.* Pairs of solutions are selected. The genomes are combined to generate one or more new solution, for example by a *crossover*, where up to some bit position, the bits from the first solution are taken, and then those from the second one.

- *Mutation.* Some information in the new solution is randomly mutated, often with carefully chosen probabilities and mutation steps.

- *Evaluation and Selection.* For each new solution, the cost function is evaluated. The new generation is then selected based on the cost function, either completely from the new generation, or including the previous one. It will on average have higher fitness than the previous generation.

Termination.

The above iteration is ended when a suitable condition has been reached. Common choices are

- A good enough solution is found.

- The quality of solutions has reached a plateau and does not improve any more.

- A maximum cost (number of iterations, computer time) has been reached.

Genetic algorithms can often find *good* solutions quickly, even when the cost function has a difficult shape.

Optimizing the method.

Similar to other methods, these algorithms have a *tendency towards a local optimum instead of the global one*. Of course this depends on the shape of the cost function. One needs to maintain sufficient genetic diversity to counteract such tendencies, for example by imposing a penalty for populations that are too homogeneous.

Genetic algorithms tend to be efficient at finding the neighborhood of an optimum solution, but less efficient at finding the optimum itself. It can be helpful to *combine* genetic evolution of a population with steps in which an optimum is approached more directly.

In general, the details of the algorithm, such as selection processes and mutations, as well as data representations should be *tuned* to the class of problems to be solved. For example, when the genome is specified by integer numbers, with the usual power-of-two representation in bits, then mutations of one or a few bits are likely to cause a catastrophic change of the cost function. It is much better to use *Gray coding*. In this representation of the integer numbers, sequential integers differ by only 1 bit (!). Mutations of one or a few bits will then lead to nearby integer numbers.

Applications.

Genetic algorithms are particularly good for complicated combinatorial problems. Common applications include the following

- Time tables and scheduling (including the Travelling Salesman problem).
- Design of networks (Electronic circuits, computer networks, locations of mobile-phone transmitters, water distribution, ...)
- Molecular structure optimization, protein folding.
- Data fitting.
- Preparation of neural networks.

Related Methods.

- *Ant colony optimization* uses many agents (ants) to find local optima in parameter space and to move on from there.
- *Particle swarm optimization* simulates the way that e.g. a swarm of fish or a flock of birds communicates. Many individuals are simulated which fly through parameter space. In each step, the information on good solutions that an individual finds is communicated to its neighbors up to some distance. Each individual adjusts its course and speed to this information. Often the overall best solution found so far is communicated to each individual immediately in order to improve convergence.
- *Simulated Annealing* can be seen as a limiting case of a genetic algorithms, with a population of only one individual.

Optimization of average fitness.

In some situations it is appropriate to formulate the problem such that one has to optimize the *average* fitness of a population instead of the maximum fitness. An example is again the set of locations of mobile-phone transmitters. Instead of viewing the complete set as an "individual", and simulating a populations of such sets, one can declare each transmitter to be an individual, characterized by its location. An examples of algorithms which optimize the average fitness are *Bacteriological algorithms*, which take their clues from populations of bacteria.

Chapter 3

Molecular Dynamics

Literature

- D.FRENKEL, B. SMIT, *Understanding Molecular Simulation*, Academic Press, 2001
- D.C. RAPAPORT, *The Art of Molecular Dynamics Simulation*, Cambridge University Press, 2004

It is an important field of research to describe macroscopically observable properties of matter on the basis of microscopic kinematics and dynamics of molecules. However, the simultaneous motion of a large number of interacting bodies cannot be described analytically. In order to arrive at practical solutions quickly, one can make simplifiying assumptions like in thermodynamic calculations. Then it is hard to estimate the influence of those simplifications on the solutions. In complex situations, direct numerical simulations are a better alternative. There are essentially two methods to determine physical quantities over a restricted set of states, namely Monte Carlo (MC), which samples from a static ensemble [1]and which we have treated before, and Molecular Dynamics (MD).

3.1 Overview

3.1.1 Equations of motion

The general idea of Molecular Dynamics is to let a system evolve in time by *integrating the equations of motion* of many individual interacting particles together. It is widely used to study classical systems. With some approximations, quantum systems can be studied as well. (See also chapter 2.1). One is interested in the motion of atoms in molecules and solids. Due to their much lighter mass, the electron dynamics is often much faster than

[1]Except for Quantum Monte Carlo, which samples from a (d+1) dimensional system, with (imaginary) time as the extra dimension.

that of the nuclei and it is in most cases a good approximation to treat the dynamics of the nuclei classically, i.e. by Newton's equation of motion

$$\ddot{x}_{i\alpha}(t) \;=\; \frac{1}{m_i}\, F_{i\alpha}[\mathbf{r}(t),t] \;=:\; f_{i\alpha}[\mathbf{r}(t),t], \tag{3.1}$$

where $x_{i\alpha}$ is the α-th coordinate of particle i. The vector $\mathbf{r}$ stands for the collection of coordinates $\{x_{i\alpha}\}$. Similarly, we introduce the vector $\mathbf{f}$ for the set $\{f_{i\alpha}\}$, and get the equation of motion:

$$\ddot{\mathbf{r}}(t) = \mathbf{f}[\mathbf{r}(t),t]. \tag{3.2}$$

On an atomic scale, the *forces* acting on the nuclei originate from the direct Coulomb interaction between the nuclei plus the indirect contribution stemming from electrons. The latter is either approximated by parameterized two-particle potentials (e.g. Lennard-Jones) or it is determined quantum mechanically from the electronic ground state (Car-Parrinello, see also chapter 2.1). "Molecular Dynamics" is also applicable for integrating the equations of motion on macroscopic scales, with appropriate forces and time scales, up to the simulation of the motion of whole galaxies, subject only to gravitation.

MD is widely used for studying many-particle systems. It is a simulation of the system as it develops over a stretch of time. The dynamics coincide (more or less) with the actual trajectories. This is a big advantage over Monte Carlo calculations, which do not usually incorporate actual dynamics, since the evolution from one Monte Carlo configuration to the next usually has nothing to do with the real time evolution of a system. Molecular dynamics calculations resemble actual experiments on a system, including preparation, time evolution, and measurements.

3.1.2 Equilibrium and Nonequilibrium

MD is most often used to extract *equilibrium* properties of a system. Since Newton's equations of motion are solved, the *energy is constant* during a simulation. The system follows trajectories of constant energy in phase space. This is the *microcanonical ensemble*. After an initial equilibration, the average of measured quantities over a long time should sample the whole ensemble (ergodic hypothesis).

Although the microcanonical ensemble is simulated, one usually defines an *effective temperature*, using the average kinetic energy per degree of freedom,

$$\left\langle \frac{1}{2} m_i\, v_{i\alpha}^2 \right\rangle \;=:\; \frac{1}{2} k_B T_{eff}\ .$$

In a system of N particles, one averages over the total number of degrees of freedom N_f, where $N_f \simeq 3N$ in 3 dimensions, to define an instantaneous

temperature at time t:

$$T_{eff}(t) \;:=\; \frac{1}{k_B N_f} \sum_{i=1}^{N} m_i \, \mathbf{v}_i^2 \; . \tag{3.3}$$

The relative fluctuations of this temperature will be of order $\sqrt{N_f}$. One can also sample the actual canonical ensemble of fixed temperature, as discussed later.

Molecular Dynamics can also be used to simulate *Nonequilibrium properties*, for example the time evolution starting at a special initial state, and/or with non-conservative external forces, and other time dependent phenomena. One prominent example is the Weather Forecast (which also includes non-particle equations of motion like fluid dynamics). We shall touch on some aspects of nonequilibrium systems in subsequent chapters.

3.1.3 Boundary conditions

For finite systems, *boundary conditions* are important. Most equilibrium MD simulations are performed for periodic boundary conditions (pbc), which means that the finite system is surrounded by identical systems with exactly the same configuration in phase-space. Forces act across the boundary of neighboring replicas. The angular momentum is not conserved when pbc are imposed. Another common situation are open boundary conditions (obc). The reason for pbc is that otherwise too many particles are at the surface of the system. For example, in a simple cubic crystal of 1000 atoms, almost 50% of the atoms are in the outer layer, and for 10^6 atoms there are still 6% on the surface.

3.1.4 Time scales

The time integration is restricted to *finite times* for any simulation because it becomes inaccurate after some time. There is a tradeoff between accuracy, corresponding to small time steps, and overall integration time. As a matter of fact, each individual MD trajectory will deviate rather quickly from the true trajectory which the system would follow in reality. However, with proper integration schemes, ensemble averages remain useful much longer. The applicability of MD is limited by the times and systems sizes which can be reached. Of course, the limits depend on whether one simulates argon atoms with time scales of 10^{-14} seconds or galaxies with time steps of many years.

For liquid argon, which can be described reliably by simple Lennard-Jones pair forces, the typical time step used in the numerical integration of the equations of motion is about 10^{-14} seconds, which means that with 10^6 time steps, a total simulation time of about 10^{-8} seconds can be covered.

The physical correlation time has to be much smaller than this simulation time in order to yield reasonable averages.

In addition, the influence of any finite system size will become noticeable after some time. One should expect to observe differences when the particles have travelled on average more than half the linear system size. In practice such effects tend to show up at larger time scales.

3.2 MD at constant energy

If the forces acting on the particles depend on the their mutual relative position, then energy and total momentum are conserved. Trivially, particle number and volume are conserved as well. The time averages thus correspond to the microcanonical or (NVE) ensemble. The rough structure of the algorithm is

- Initialize, then loop:
- Calculate forces
- Integrate equations of motion for a small time step τ.
- After an initial equlibration time, perform measurements.

3.2.1 Initialization

The number N of particles and the finite size volume are specified. As an example, we will use periodic boundary conditions with a box of size L^3.

For equilibrium calculations, a "temperature" is usually of greater interest than the total energy and is therefore specified as an input parameter. The particles are assigned positions and velocities. Typically the positions are chosen on a regular grid or at random, while the velocities $\mathbf{v}_i$ are generated according to the Boltzmann distribution

$$p(v_\alpha) \propto e^{-mv_\alpha^2/(2k_BT)}.$$

A vanishing total momentum is achieved by subtracting the mean momentum from all particle momenta. We will discuss later how to actually simulate a canonical ensemble.

3.2.2 Force calculation

This is usually the most time-consuming part of an MD-simulation.

As an example, we will consider the Lennard-Jones pair potential

$$u^{ij}(r) \;=\; 4\varepsilon \left[\left(\frac{\sigma}{r}\right)^{12} - \left(\frac{\sigma}{r}\right)^{6} \right] . \tag{3.4}$$

between particles i and j, with r the distance between them. All particles shall have the same mass m.

From now on, we express everything as dimensionless quantities in terms of *reduced units*, taking σ as the unit of length, ε as the unit of energy, and m as the unit of mass. (Then the unit of time is $\sigma\sqrt{m/\varepsilon}$ and the unit of temperature is ε/k_B.) The advantage of this rescaling is that many combinations of the actual particle density $\rho = N/L^3$, temperature T, and parameters ε and σ in fact correspond to the same set of reduced parameters, i.e. the same physical situation. In reduced units, the Lennard-Jones potential becomes

$$u^{ij}(r) \;=\; 4 \left[\left(\frac{1}{r}\right)^{12} - \left(\frac{1}{r}\right)^{6} \right] . \tag{3.5}$$

Every particle interacts with every other particle. With pbc, this includes the interaction with the infinite number of replicas („periodic images") of every particle.

Cut-off

For an interaction which decays quickly with distance like the Lennard-Jones potential, it is convenient to *cut off* the force at some radius r_c. When $r_c \leq \frac{L}{2}$, then a particle i interacts with at most one copy of particle j (see figure 3.1).

(A sharp cut-off of the *potential* would cause an infinite force at distance r_c, unless all energies are shifted to obtain zero potential at r_c first).

The cut-off neglects interactions beyond r_c. Their total contribution to the energy can be estimated approximately as

$$u_{tail} = \frac{N\rho}{2} \int_{r_c}^{\infty} dr\; 4\pi r^2 \left(u(r) - u(r_c)\right) . \tag{3.6}$$

We can now calculate the force on particle i. Let us assume that we use p.b.c. and cut off the forces at some radius $r_c \leq \frac{L}{2}$. We now loop over all

Figure 3.1:
Periodic boundary conditions in 1d, with two particles i and j.

other particles $j \neq i$ and calculate the smallest distance between i and j on the periodic lattice. (e.g. in direction x: $r_x = \min(|x_i - x_j|,\, L - |x_i - x_j|)$. The force in x-direction is then

$$f_x(r) \;=\; -\frac{\partial u(r)}{\partial r_x} \;=\; -\,\frac{\partial r}{\partial r_x}\,\frac{\partial u(r)}{\partial r}\;,\; =\; -\,\frac{r_x}{r}\,\frac{\partial u(r)}{\partial r}\;, \tag{3.7}$$

which for our Lennard Jones system becomes

$$f_x(r) \;=\; \frac{48 r_x}{r^2}\left(\frac{1}{r^{12}} - \frac{1}{2r^6}\right)\;. \tag{3.8}$$

Improved scaling for finite range interactions

We need to repeat the force calculation for all N particles. The computational effort therefore scales like N^2, which can become very large, especially considering that the time integration step will only scale like $O(N)$. In fact, there are better methods for force calculations which indeed just scale like N (!)

A simple and very good approach for finite range interactions are *cell lists*. Let r_c be the maximum range of the force (e.g., the cut-off). We divide our box of size L^3 into cells of size r_c^3 (or slightly larger). At each time step, we allocate each particle to the corresponding cell, which is an $O(N)$ operation. Each particle i in a cell interacts only with particles j in the same cell or in immediately neighboring cells. At finite density, these are a finite number of particles j to consider. When the system becomes larger at finite density, then the number of cells grows, but the number of neighbors to consider remains the same on average. If M is the average number of particles per cell, the force calculation will now scale like $\frac{N}{M}O(M^2)$.

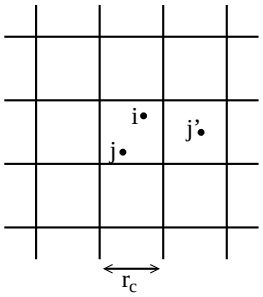

Figure 3.2:
Cells: particle i interacts only with particles in the same or in neighbouring cells when the interaction does not extend beyond r_c.

Improved scaling for infinite range interactions

Coulomb interactions are an important case. They are long range, and often cannot be cut off without large undesirable effects. Thus the force calculations scale like N^2. (For such forces, one does not usually employ p.b.c. because this can lead to infinitely large forces)[2].

Fortunately, also for this case there are methods to reduce the scaling to about $O(N)$, for example the strangely named "Particle-Particle/Particle-Mesh (PPPM)" method. In this method the short distance forces on some particle i are calculated directly. The essential idea to calculate large distance contributions efficiently is to employ a hierarchical grid, which becomes coarser and coarser at larger distances. For each region of the grid, the contribution of all particles is subsumed in one "effective" particle. Indeed, this is similar to the well-known combination of atoms of a large body in the center of mass, e.g. when one wants to know the effect of all the atoms in the moon on some particle on the earth. (Note that for non-constant distances, this is not exact). The additional idea in PPPM is to do this combination on a hierarchical scale. The number of grid points to be considered grows like $\log N$, and the whole method scales like $N \log N$. In this way the forces for all particles i are calculated, with hierarchical grids that have to be adjusted to the position of i.

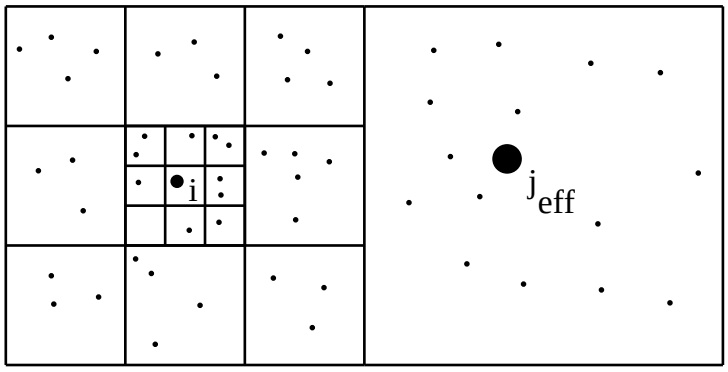

Figure 3.3:
Hierarchical grid for PPPM.

3.2.3 Time integration: Verlet and Leap-frog algorithm

We will integrate the equations of motion in discrete time steps of length τ. We will concentrate on one of the most widely used algorithm, which is both simple and reliable, the Verlet algorithm. We start with a Taylor expansion of the coordinates of a particle:

[2]Related to the question of why the sky is not infinitely bright !

$$\mathbf{r}(\tau) = \mathbf{r}(0) + \tau\ \dot{\mathbf{r}}(0) + \frac{\tau^2}{2}\ddot{\mathbf{r}}(0) + \frac{\tau^3}{6}\dddot{\mathbf{r}}(0) + \mathcal{O}(\tau^4)$$
$$\mathbf{r}(-\tau) = \mathbf{r}(0) - \tau\ \dot{\mathbf{r}}(0) + \frac{\tau^2}{2}\ddot{\mathbf{r}}(0) - \frac{\tau^3}{6}\dddot{\mathbf{r}}(0) + \mathcal{O}(\tau^4)$$
$$\Rightarrow \quad \mathbf{r}(\tau) + \mathbf{r}(-\tau) = 2\mathbf{r}(0) + \tau^2\ \mathbf{f}[\mathbf{r}(0), 0] + \mathcal{O}(\tau^4).$$

The Verlet algorithm cuts away the $O(\tau^4)$ part. Thus

$$\mathbf{r}(\tau) = 2\mathbf{r}(0) - \mathbf{r}(-\tau) + \tau^2\ \mathbf{f}[\mathbf{r}(0), 0] \tag{3.9}$$

at each time step. At the very first step, one would need $\mathbf{r}(-\tau)$, which is not known. Instead one employs the initial condition with a simpler discretization

$$\mathbf{r}(\tau) = \mathbf{r}(0) + \tau\ \mathbf{v}(0) + \frac{\tau^2}{2}\ \mathbf{f}[\mathbf{r}(0), 0]. \tag{3.10}$$

for the first time step. The corresponding discretization error is $\mathcal{O}(\tau^3)$, which occurs, however, only once, while the $\mathcal{O}(\tau^4)$ error is encountered in each time step and also adds up to $\mathcal{O}(\tau^3)$.

VERLET ALGORITHM

$$\mathbf{r}(t+\tau) = 2\mathbf{r}(t) - \mathbf{r}(t-\tau) + \tau^2\ \mathbf{f}[\mathbf{r}(t), t], \qquad t = \tau, 2\tau, \ldots$$

with Equation (3.10) to obtain $\mathbf{r}(\tau)$ initially. Note that this method does not use velocities, except at the first step. In order to calculate velocities, e.g. for the kinetic energy, one can use

$$\mathbf{r}(t+\tau) - r(t-\tau)\ =\ 2\tau\ \mathbf{v}(\tau)\ +\ O(\tau^3)\ . \tag{3.11}$$

There is an alternative formulation of the Verlet algorithm which is more robust against rounding errors. From

$$\frac{\mathbf{v}(\tau/2) - \mathbf{v}(-\tau/2)}{\tau} = \dot{\mathbf{v}}(0) + \mathcal{O}(\tau^2)$$

we obtain

$$\mathbf{v}(\tau/2) = \mathbf{v}(-\tau/2) + \tau\ \mathbf{f}[\mathbf{r}(0), 0] + \mathcal{O}(\tau^3).$$

We use, likewise, for the positions

$$\frac{\mathbf{r}(\tau/2 + \tau/2) - \mathbf{r}(\tau/2 - \tau/2)}{\tau} = \dot{\mathbf{r}}(\tau/2) + \mathcal{O}(\tau^2)$$

which leads to

$$\mathbf{r}(\tau) = \mathbf{r}(0) + \tau\ \mathbf{v}(\tau/2) + \mathcal{O}(\tau^3).$$

This approach is called the leap-frog[3] algorithm due to the way r and v interchange in time. Space-coordinates are computed at $0, \tau, 2\tau, \ldots$ and velocities are provided at intermediate times $\tau/2, 3\tau/2, \ldots$.

LEAP-FROG ALGORITHM

$$\begin{aligned} \mathbf{r}(t+\tau) &= \mathbf{r}(t) + \tau \cdot \mathbf{v}(t+\tau/2) && t = 0, \tau, \ldots \\ \mathbf{v}(t+\tau/2) &= \mathbf{v}(t-\tau/2) + \tau \cdot \mathbf{f}[\mathbf{r}(t), t] && t = \tau, 2\tau, \ldots \\ \mathbf{v}(\tau/2) &= \mathbf{v}(0) + \frac{\tau}{2} \cdot \mathbf{f}[\mathbf{r}(0), 0]. \end{aligned}$$

Next we consider one more modification. We use

$$\begin{aligned} \mathbf{r}(t+\tau) &= \mathbf{r}(t) + \tau \cdot \mathbf{v}(t) + \frac{\tau^2}{2}\ddot{\mathbf{r}}(t) + \mathcal{O}(\tau^3) \\ &= \mathbf{r}(t) + \tau \cdot \mathbf{v}(t) + \frac{\tau^2}{2}\mathbf{f}[\mathbf{r}(t), t] + \mathcal{O}(\tau^3) \end{aligned}$$

and

$$\mathbf{v}(t+\tau) = \mathbf{v}(t) + \tau\ddot{\mathbf{r}}(t+\tau/2) + \mathcal{O}(\tau^3).$$

This approach would require the knowledge of $\ddot{\mathbf{r}}(t+\tau/2)$, which can be approximated by

$$\frac{\ddot{\mathbf{r}}(t+\tau) + \ddot{\mathbf{r}}(t)}{2} = \ddot{\mathbf{r}}(t+\tau/2) + \mathcal{O}(\tau^2)\ .$$

We obtain the

VELOCITY-VERLET ALGORITHM

$$\begin{aligned} \mathbf{r}(t+\tau) &= \mathbf{r}(t) + \tau \cdot \mathbf{v}(t) + \frac{\tau^2}{2}\mathbf{f}[\mathbf{r}(t), t] \\ \mathbf{v}(t+\tau) &= \mathbf{v}(t) + \tau\frac{1}{2}\left\{\mathbf{f}[\mathbf{r}(t), t] + \mathbf{f}[\mathbf{r}(t+\tau), t+\tau]\right\}. \end{aligned}$$

[3]German: bockspringen

This form is equivalent to the other two schemes as long as all computational steps are performed with infinite accuracy, but it is less susceptible to numerical errors.

3.2.4 Stability

Several properties are important for a good time integration scheme. They are all satisfied by the Verlet-algorithm and its variants.

First of all, energy needs to be conserved, both short-term and long-term. This is a very difficult requirement for MD methods. In fact, there are a number of schemes (like so-called „predictor-corrector" schemes) which use higher order expansions in τ and thus seem to allow bigger time steps τ. However, their long-term performance is worse than that of the Verlet algorithm ! A fairly recent approach with a better behaviour has been adapted from Quantum Monte Carlo, namely the use of time evolution operators looking like $\exp(tH)$, together with approximations like the Baker-Hausdorff equation ("Trotter-Suzuki-approximation").

One criterion that such methods often do not satisfy is the *time reversal symmetry* of Newton's equations of motion. Another one is that of *preservation of volume in phase space*. All trajectories of a system that correspond to a particular energy E are contained in a specific volume in phase space. If we let Newton's equations of motion act on all points in this volume, we end up with exactly the same volume. A method which does not conserve phase space volume will eventually spread over all of phase space, and thus cannot conserve energy.

There is, however, a bigger stability concern. The trajectories of systems studied by MD depend sensitively on the initial conditions, even with exact time evolution.

When $\vec{x}(0)$ is perturbed by a small amount $\delta\vec{e}$, where $\vec{e}$ is a unit vector, then $x(t)$ will typically change by $\delta^{\lambda(\vec{e})}\vec{e}$. There are as many exponents $\lambda(\vec{e})$ as there are directions in phase space. For a Hamiltonian system, one exponent will always be zero (corresponding to $\vec{e} \parallel \vec{x}(0)$), and the others will occur in pairs $\pm lambda$. The largest positive λ is usually called *the* Lyapunov exponent.

Thus two trajectories which are initially close will diverge from each other as time progresses ! This is the so-called *Lyapunov-instability*. Therefore even tiny integration errors in MD will lead the simulated trajectory to diverge from the true one.

For the calculation of, e.g., trajectories of satellites in space this can be devastating. Fortunately, one is usually interested in averages, over particles and over time, which behave much better. There is also strong numerical evidence that MD trajectories do closely follow so-called shadow-orbits, which are true trajectories of systems with slightly different initial conditions. In addition, the Verlet algorithm can be shown to *exactly* follow

(up to numerical imprecision) the true time evolution of a Hamiltonian which differs from the desired Hamiltonian only by terms of order τ.

3.2.5 Measurements

The equilibrium thermodynamic (ensemble) average of any quantity is obtained via averaging over time. For an observable O the expectation value reads

$$\langle O \rangle = \lim_{T \to \infty} \frac{1}{T} \int_0^T dt\, O(t).$$

For instance, the inner energy $U = \langle E \rangle$. We have already mentioned the kinetic energy, which defines the so-called instanteneous temperature. One can also measure the pressure. For pairwise additive interactions one can write

$$P \;=\; \rho k_B T \;+\; \frac{1}{dV} \left\langle \sum_{i<j} \mathbf{r}_{ij}\, \mathbf{f}(\mathbf{r}_{ij}) \right\rangle \;, \tag{3.12}$$

where d is the dimensionality of the system and V is the volume. This is actually the relation for a canonical ensemble, but is often employed also at constant E.

Other important quantities are correlation functions like the so-called radial distribution function $g(r)$, which is proportional to the density-density correlation function. Care has to be taken to evaluate these correlations efficiently, in order to avoid $O(N^2)$ scaling.

3.3 Example: Harmonic Oscillator

Here we consider the harmonic oscillator since it allows to *asses the stability of the algorithm analytically*. The equation of motion for the 1D harmonic oscillator is

$$\ddot{x} = -\omega^2\, x.$$

For $t > 0$ the Verlet algorithm reads

$$x(t+\tau) - 2x(t) + x(t-\tau) = -\tau^2 \omega^2\, x(t), \tag{3.13}$$

For $t = 0$ we need to specify the initial conditions. We have $\dot{v} = f$ and, therefore, $v(\tau) \simeq v(0) + \tau f[x(0)]$. We take the initial condition $v(0) = 0$ and the initial Verlet time step then is

$$x(\tau) = x(0) - \frac{\tau^2}{2} \omega^2 x(0). \tag{3.14}$$

Eqs. (3.13) can be expressed in matrix form if we use the assignment $x_n = x(n\,\tau)$ for $n \in \mathbb{N}_0$:

$$\underbrace{\begin{pmatrix} -2 & 2 & 0 & & & \\ & 1 & -2 & 1 & & \\ & & 1 & -2 & 1 & \\ & & & 1 & -2 & \ddots \\ & & & & \ddots & \ddots \end{pmatrix}}_{=:\boldsymbol{M}} \mathbf{x} = -\tau^2\omega^2\mathbf{x}.$$

(Zero matrix elements are supressed.) Thus, the eigenvalue equation $\boldsymbol{M}\mathbf{x} = \lambda\mathbf{x}$ has to be solved for the given eigenvalue $\lambda = -\tau^2\omega^2$. We will now solve this equation analytically. Since $x(t) = e^{i\omega t}$ is the exact solution for the harmonic oscillator, we try the ansatz

$$x_n = e^{i\alpha\, n}. \tag{3.15}$$

The general condition (3.13) for $\tau > 0$ reads

$$e^{i\alpha(n+1)} - 2e^{i\alpha n} + e^{i\alpha(n-1)} = -(\tau\omega)^2\, e^{i\alpha n}$$

or rather

$$e^{i\alpha} - 2 + e^{-i\alpha} = -(\tau\omega)^2.$$

Hence, α is given by

$$1 - (\tau\omega)^2/2 = \cos(\alpha). \tag{3.16}$$

This implicit equation for α has real solutions only for

$$-1 \leq (\tau\omega)^2/2 - 1 \leq 1$$

or rather

$$0 \leq \tau\omega \leq 2.$$

In other words, the discretization has to obey at least

$$\tau \leq \frac{2}{\omega}, \tag{3.17}$$

otherwise α becomes complex and the solution (3.15) obtains exponentially increasing components, as we will see later. However, the time evolution becomes imprecise already much earlier. Equation (3.16) always has two roots, namely $\pm\alpha$. Hence, the general solution obeying the initial condition reads

$$x(n\tau) = Ae^{i\alpha n} + Be^{-i\alpha n} = a\cos(\alpha n + \varphi),$$

with parameters which are fixed by the initial condition $x(t=0) = x(0) = a\cos(\varphi)$. We still have to satisfy $v(0) = 0$, i.e. eq. (3.14).

$$\begin{aligned} a\cos(\alpha + \varphi) &\stackrel{!}{=} a\cos(\varphi) - \frac{(\tau\omega)^2}{2} a\cos(\varphi) \\ &= a\cos(\varphi)\left[1 - \frac{(\tau\omega)^2}{2}\right]. \end{aligned}$$

Because of Eq. (3.16), the last line is also equal to $a\cos(\varphi)\cos(\alpha)$. Thus

$$\begin{aligned}\cos(\alpha+\varphi) &= \cos(\varphi)\cos(\alpha)\\ \cos(\alpha)\cos(\varphi)-\sin(\alpha)\sin(\varphi) &= \cos(\varphi)\cos(\alpha)\\ \sin(\varphi) &= 0.\end{aligned}$$

The solution therefore reads

$$x_n = x_0\cos(\alpha n). \tag{3.18}$$

(In the original continuum representation this would read $x(t) = x(0)\cos(\frac{\alpha}{\tau}t)$, which would correspond to the exact solution if $\frac{\alpha}{\tau} = \omega$.) For $\tau\omega \ll 1$, Eq. (3.16) yields

$$\begin{aligned}1-(\tau\omega)^2/2 &\simeq 1-\frac{\alpha^2}{2}\\ \alpha &\simeq \tau\omega.\end{aligned}$$

Thus the numerical solution indeed approaches the correct solution for $\tau \to 0$. Obviously, there is a tradeoff between the accuracy and the total time that can be simulated by a fixed number of iterations.

Figures 3.4 and 3.5 show the time dependence of $x(t)$ for different parameters $\tau\omega$. We see that the simulation is stable over many periods, if $\tau\omega \ll 1$, while it goes off course at larger τ. As anticipated, the trajectory diverges for $\tau\omega > 2$.

We now estimate the number of periods until the discretization error becomes significant. The result of the Verlet algorithm oscillates with frequency α/τ. According to Eq. (3.18) the position at time $t = n\tau$ is given by $x^v(t) = x_0\cos(\alpha n)$. A characteristic time t^* at which the result has become completely wrong is when $x^v(t^*) = -x(t^*)$, i.e. when the phase error is π:

$$\begin{aligned}|\omega t^* - \alpha t^*/\tau| &= \pi\\ t^* &= \frac{\pi}{|\omega-\alpha/\tau|}.\end{aligned}$$

The number N^* of periods $T = 2\pi/\omega$ corresponding to t^* is:

$$N^* = \frac{t^*}{T} = \frac{\omega\tau}{2\,|\omega\tau-\alpha|}.$$

Together with an expansion of Eq. (3.16) to order α^4, with $\cos\alpha \simeq 1-\frac{\alpha^2}{2}+\frac{\alpha^4}{24}$ this leads after a few lines to

$$|\omega\tau-\alpha| = \frac{(\omega\tau)^3}{24},$$

and hence

$$N^* = \frac{12}{(\omega\tau)^2}. \tag{3.19}$$

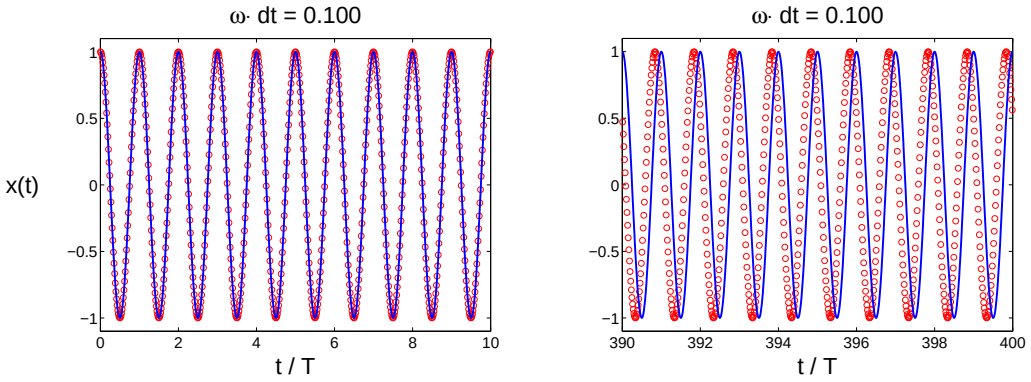

Figure 3.4: Simulation of the harmonic oscillator with $\omega\tau = 0.1$. The exact solution is represented by the blue line, and the MD results by red circles. According to Eq. (3.19) it takes $N^* = 1200$ cycles for the Verlet algorithm to go completely off course.

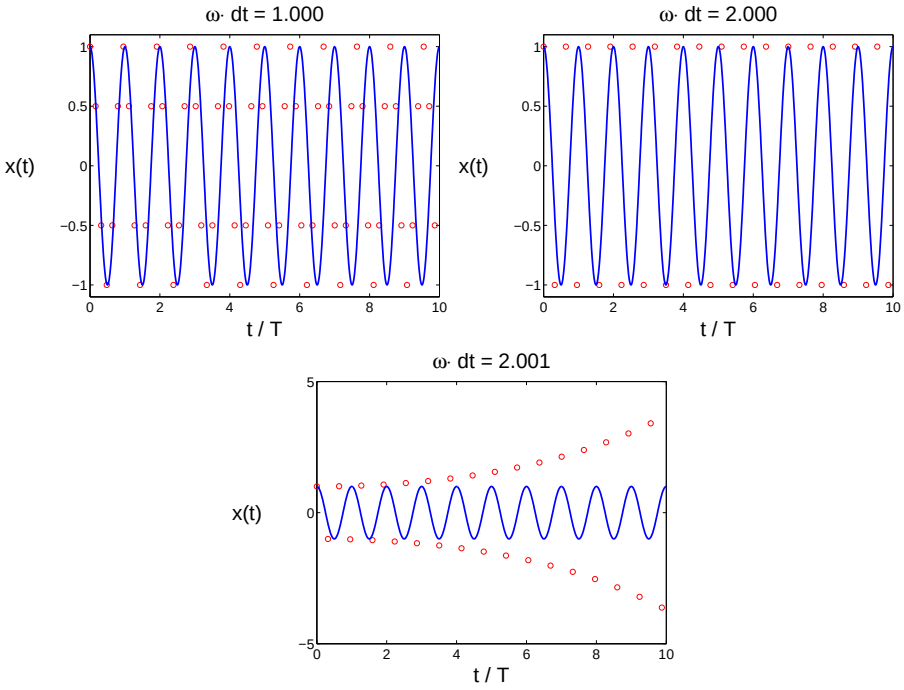

Figure 3.5: Top left: Simulation of the harmonic oscillator with the foolish choice $\omega\tau = 1$. The result of formula (3.19), $N^* = 12$, is corroborated by the simulation. Top right and bottom: Simulations for $\omega\tau = 2$ and $\omega\tau = 2.001$. Obviously, the phase becomes complex for $\omega\tau > 2$ leading to an exponential increase of the amplitude.

Alternatively, if a certain number N^* of stable periods is required, the condition for the discretization reads

$$\omega\tau \ll 2\sqrt{\frac{3}{N^*}} ,$$

or

$$\frac{T}{\tau} \gg \pi\sqrt{\frac{N^*}{3}},$$

which gives the number of partitions of one period. For example, $N^* = 1000$ corresponds to $T/\tau = 57$ partitions.

3.4 Generalizations

Canonical ensemble

The "effective temperature" can be adjusted in an MD simulation by rescaling all velocities during equilibration. However, this is still the microcanonical ensemble of constant energy

In order to obtain a true canonical ensemble, one can employ the "Anderson thermostat": The system is coupled to a heat bath. The coupling works through occasional impulsive forces that act on randomly selected particles. It can be considered to be a Monte Carlo move which transports the system from one energy to another. The collisions with the heat bath are designed such that all constant energy shells are visited according to their Boltzmann weight.

Hybrid Monte Carlo

Molecular dynamics, even a not-so-good scheme, can be employed to greatly improve the performance of some *Monte Carlo* calculations. In this method, the Molecular Dynamics evolution is used to provide a new *proposal configuration* for the next Monte Carlo step. In order to provide the MC configuration with dynamics, artificial momenta are introduced, and chosen randomly according to some distribution. The only requirement on the MD simulation is time reversal symmetry. By way of a fairly long time evolution, the system can move far in phase space, while keeping its total energy (actual energy plus small artificial kinetic energy) approximately constant, so that the new configuration will likely be accepted in the Monte Carlo step. Changes of energy are achieved by changing the articificial momenta. This method has for example been in very successful use for QCD-Simulation.

Nonequilibrium simulations

Molecular dynamics is also able to to look at the time evolution of a system starting from a special initial situation and/or with external non-conservative driving forces. Then there is no time averaging, so that great care has to be taken to integrate the equations of motion as precisely as possible.

Agent based simulations

The general approach of a simulation of invidual ”particles”, interacting and following specific rules in their time evolution has been carried over into many other fields, where one usually speaks of ”agent based simulations”, including e.g. financial markets, evolution, or the flow of dense crowds of people at large events.

Beyond Molecular Dynamics

When Molecular Dynamics is not feasible, e.g. because the necessary integration times cannot be reached with sufficiently small time steps, then one has to resort to coarser pictures. They are based on the more traditional formulation of solid bodies or of fluids as continuous media obeying differential equations like e.g. the Navier-Stokes equation. For solid matter, these are often treated by the *Finite Element Method (FEM)*. There, space is partitioned into finite regions (the „elements”), for example triangles on surfaces. The differential equation to be solved is rephrased as a variational problem. The solutions are approximated by a linear combination of a *finite* set of functions. The coefficients of this linear combination are then the solution of a (linear or nonlinear) minimization problem, for which techniques like conjugate gradient can be used.

For liquids the difficulties are greater. Depending on the precise problem, *Computational Fluid Dynamics (CFD)* uses a large variety of discretizations of space and of integration methods, often with phenomenological additional interactions, for example to describe turbulence. MD, on the other hand, can describe turbulence directly, on a microscopic scale, although currently only with unrealistic parameters like extremely large forces, in order to make it fit within the space and time available.

Chapter 4

Cellular Automata

Literature

- J. VON NEUMANN, *The Theory of Self-reproducing Automata*, in: *Essays of Cellular Automata*, ed.: A.W. BURKS, University of Illinois Press, Urbana (1970).
- S. WOLFRAM, *Theory and Application of Cellular Automata*, World Scientific, Singapore (1986).
- J. SCHMELZER, G. RÖPKE, and R. MAHNKE, *Aggregation Phenomena in Complex Systems: Principles and Applications*, J. Wiley, 1999.
- J. KROPP, H.J. SCHELLNHUBER, *The Science of Disasters*, Springer 2002.

4.1 Dynamics of Complex Systems

The ubiquitous strategy in the description of complex physical systems consists in devising a model with fewer yet relevant degrees of freedom, for example by disassembling it into small and tractable parts (key elements) which may interact in one way or other. Such a simplified procedure has been the key success factor of natural sciences for several centuries but it is nonetheless an approximation. Complex systems which have been addressed successfully by disintegration are, e.g.

- ISING, HEISENBERG model for magnetism,
- VAN DER WAALS model for fluids,
- Spring models for lattice vibrations,
- LANDAU theory for phase transitions.

An alternative approach are the artificial systems of Cellular Automata (CA). They have been invoked to study

- Chemical reactions,
- Phase separation,
- Self criticality,
- Avalanches,
- Chaos in physical systems.

Cellular automata are artificial mathematical models of dynamical systems, discrete in space and in time, whose behavior is completely specified in terms of some local law. A cellular automaton can be thought of as a stylized universe. Space is represented by a uniform grid, with each cell containing a few bits of data; time advances in discrete steps and the laws of the 'universe' are expressed in a look-up table, through which at each step each cell computes its new state from that of its close neighbors. Thus, the system's laws are usually *local* and *uniform*.

The first cellular automaton was conceived by the mathematician J. VON NEUMANN in the late 1940's. He constructed an automaton which qualified as a universal computer (property of *universality*: the computer can emulate any desired function of any other computer by the use of a set of logical rules, and, particularly, it can reproduce itself; the standard example is the *Turing machine*); it was very complex and consisted of two hundred thousand cells in any of 29 states. J.H. CONWAY suspected that a cellular automaton with universal computing capabilities might be simpler. His cellular automaton is the famous *Game of Life* (discussed later). It has only two states per cell, either filled or empty, 'alive' or 'dead. It is indeed a universal computer.

4.2 One Dimensional Cellular Automata

Cellular automata are useful to analyze and understand the laws that govern complex phenomena. Non-linear phenomena are often described by reaction-diffusion equations. Non-linear space-time dynamics of interacting particles, chemical or biological systems can generate numerous local and non local effects far from equilibrium such as steady-state multiplicity, oscillations like limit cycles, propagating fronts, target patterns, spiral waves, pulses as well as stationary spatial patterns. In 1D these processes can be described generally by

$$\frac{\partial}{\partial t}\rho(r,t) = f[\rho(r,t)] + \frac{\partial^2}{\partial r^2}\rho(r,t),$$

where f stands for the reaction function.

An alternate approach in discrete space-time is provided by 1D cellular automata. The simplest case is a 1D array of cells which take on the values

zero and one. In each time step the value of each cell is modified according to some simple rules.

A simple example:

- States: zero and one.
- Neighborhood: the two neighbor cells and the cell C under observation are denoted like NCN.
- Update rules: we have three relevant cells which can each be in two possible states. Thus, we need $2^3 = 8$ rules, e.g.

$$\begin{array}{lll} 0\ 0\ 0 \to 0 & \qquad & 1\ 0\ 0 \to 1 \\ 0\ 0\ 1 \to 1 & & 1\ 0\ 1 \to 1 \\ 0\ 1\ 0 \to 1 & & 1\ 1\ 0 \to 0 \\ 0\ 1\ 1 \to 0 & & 1\ 1\ 1 \to 0. \end{array}$$

This is called the "01101100" rule. We start with a configuration of only one cell having the value one and find the following time series:

$$\begin{array}{ll} \text{Time } 0: & \cdot\ \cdot\ \cdot\ \cdot\ \cdot\ \cdot\ \cdot\ \cdot\ 1\ \cdot\ \cdot\ \cdot\ \cdot\ \cdot\ \cdot\ \cdot \\ \text{Time } 1: & \cdot\ \cdot\ \cdot\ \cdot\ \cdot\ \cdot\ \cdot\ 1\ 1\ 1\ \cdot\ \cdot\ \cdot\ \cdot\ \cdot\ \cdot \\ \text{Time } 2: & \cdot\ \cdot\ \cdot\ \cdot\ \cdot\ \cdot\ 1\ \cdot\ \cdot\ \cdot\ 1\ \cdot\ \cdot\ \cdot\ \cdot\ \cdot \\ \text{Time } 3: & \cdot\ \cdot\ \cdot\ \cdot\ \cdot\ 1\ 1\ 1\ \cdot\ 1\ 1\ 1\ \cdot\ \cdot\ \cdot\ \cdot \\ \text{Time } 4: & \cdot\ \cdot\ \cdot\ \cdot\ 1\ \cdot\ \cdot\ \cdot\ 1\ \cdot\ \cdot\ \cdot\ 1\ \cdot\ \cdot\ \cdot \\ \text{Time } 5: & \cdot\ \cdot\ \cdot\ 1\ 1\ 1\ \cdot\ 1\ 1\ 1\ \cdot\ 1\ 1\ 1\ \cdot\ \cdot \\ \text{Time } 6: & \cdot\ 1\ \cdot\ \cdot\ \cdot\ 1\ \cdot\ \cdot\ \cdot\ 1\ \cdot\ \cdot\ \cdot\ 1\ \cdot \end{array}$$

with the zeros replaced by dots. This very primitive CA already shows signs of *self organization*, *i.e.* certain patterns evolve in the time series.

Other examples are shown in the Figures below. The result of the example above corresponds closely to the result in Fig. 4.1 for the (01111000) rule.

S. WOLFRAM studied these linear CAs quite extensively.
He categorized the cellular automata into four classes:

- **Class 1:** After a finite number of steps, a homogeneous general final state is reached (all cells are either dead or alive).
- **Class 2:** Initially simple local patterns evolve, they sometimes transform in vertical stripes. Frozen configurations are found where initial activity ceases and stable structures reign.
- **Class 3:** The states distribute seemingly without rules but now and then typical patterns can be observed.

- **Class 4:** This class displays behavior which is not disordered, but complex, and some times long-lived. CAs of this class are capable of propagating information and this class contains universal automata. The processes depend heavily on the initial conditions.

A CA can be viewed as an idealization of the reaction-diffusion equation for discrete time where the state ρ is mapped on a finite set of possible values only. CAs are in general deterministic, but stochastic forces can be included as well (*stochastic cellular automata*). Such systems can exhibit phase transitions as function of the noise level. Updating rules are employed either sequentially or in parallel.

Algorithm 7 MATLAB Code: 1D Binary CA

```
N = 601;
M = 300;
A = zeros(1,N); A((N+1)/2) = 1;
B = zeros(M,N); B(1,:) = A;
rule = [0 1 1 1 1 1 1 0];
ii = [1: N]';
ind = [(ii-1) ii (ii+1)];
ind(1,1) = N; ind(N,3) = 1;
for l = 2: M
  A = rule(bi2de(A(ind))+1);
  B(l,:) = A;
end
spy(B);
```

Figures 4.1 and 4.2 display signs of *self organization*. Indeed, they show *fractal structures*, i.e. they look similar on all length scales (beyond the underlying lattice scale). Fig. 4.3 looks the most complex. It is a standard example for a chaotic structure created by deterministic local CA. The analysis of the structure of such objects is part of *complexity theory*, initiated by KOLMOGOROV. (He coined the notion of complexity of an object as a measure for the smallest length of a binary program which is able to to generate the object.)

4.3 Two-dimensional Cellular Automata

The generalization to 2D CAs is straight forward. On a square lattice, when the 4 nearest neighbors are incorporated into the update rule, then there are $2^{2^4} = 65536$ possible update rules. The number of rules grows rapidly with the number of neighbors and with the spatial dimension. When all 8 neighbors are used, then there are $2^{2^8} \simeq 10^{77}$ rules, and when the center site is included, there are $2^{2^9} \simeq 10^{170}$ rules. Therefore PACKARD and WOLFRAM

Figure 4.1: Cellular automaton for rule (01111000).

Figure 4.2: Cellular automaton for rule (01101001).

Figure 4.3: Cellular automaton for rule (01101010) with chaotic behavior on the left hand side and fairly regular structures on the right hand side.

even proposed to resort to random sampling of rules with the expectation that the selected rules are representative.

We have already encountered one example of a two-dimensional Cellular Automaton, namely the Ising model with its Monte Carlo evolution (when done in parallel for every site). This model exhibits complicated behaviour, including *criticality* (discussed below).

4.3.1 Game of Life

The most famous Cellular Automaton is probably the proposal by Conway, the Game of Life. It is a simple 2D-system, with one bit per cell. In the time evolution, the next state of each cell depends deterministically on the states of the eight nearest neighbors. Conway had the following objectives, in trying to devise a universal computer:

- He wanted to make sure that no simple pattern would obviously grow without limit.
- He wanted to ensure, nevertheless, that some simple pattern do grow widely. There should be patterns that look like they might grow forever.
- There should be simple patterns that evolve for a long time before stabilizing. A pattern is stabilized by either vanishing completely or by producing a constellation of stable objects.

There are three rules:

- A dead cell with exactly 3 living neighbors becomes a living cell (birth).
- A living cell with 2 or 3 living neighbors stays alive (survival).
- In all other cases, a cell dies or remains dead (overcrowding or loneliness).

This CA can indeed be shown to be a universal computer !

The game is played on a 2D grid of square cells (like a chessboard) extending infinitely in every direction or on a finite grid with periodic boundary conditions. A cell can be alive or dead and a living cell is represented by a marker. A dead cell is empty. Each cell on the grid has a neighborhood consisting of the eight cells in every direction (including diagonals).

The history of this 2D "world" is determined by the initial configuration. Many different objects can be constructed and can interact. like e.g. ”blinkers”, ”gliders”, ”glider guns”, ”spaceships”, etc. A multitude of corresponding programs and applets can be found on the web.

Algorithm 8 MATLAB Code: Game of Life

```
L = 20;
A = unidrnd(2,[L,L])-1;
            % initial configuration
i1 = [2:L, 1]; i2 = [L, 1:L-1];
            % n.n. tableaux with pbc
while (1)
  N = A(i1,:) + A(i2,:) + A(:,i1) + A(:,i2) + ...
  A(i1,i1) + A(i1,i2) +A(i2,i1) + A(i2,i2);
  A = N==3 | (N==2 & A==1);
  spy(A);
  pause(0.25);
end
```

4.4 Traffic Flow

Simulations of traffic flow based on CA have gained considerable importance. Here we will show that rather simple stochastic Cellular Automata can reproduce features of real traffic including jamming transition from low density laminar flow to high density congested flow, where stop-and-go waves are dominant.

Modern versions of CA for traffic flow are called *particle hopping models*. Studies of traffic flow based on CA trace back to the year 1956 but they received wide attention in 1992 with papers by SCHRECKENBERG. The 1D road is represented by a string of cells, which are either occupied by exactly one car or empty. If all cars are updated simultaneously (parallel update), then the particle hopping model is formally analogous to a 1D CA described before. NAGEL and SCHRECKENBERG introduced the following CA for 1D traffic with periodic boundary conditions (pbc, circular lane) called *stochastic traffic cellular automata* (STCA). In this model, the space coordinate i of the road, the time t and the velocity $v_i(t)$ are discrete variables. The length of the road is L. Each particle (the total number N is fixed) can have an integer velocity v between 0 and some maximum velocity v_{max}. A configuration is characterized by the position of the particles (cars) and their respective velocities. Each cell has a value v between -1 and v_{max}, where $v = -1$ represents an empty cell (no car), while other values indicate the presence of a car with velocity v.

The update rule consists of four steps which are executed *consecutively*:

1. *Acceleration*: If the velocity v is lower than v_{max} and if the distance to the next car (# of empty sites ahead) is larger than $v + 1$, the speed is increased by one ($v \to v + 1$).

2. *Slowing down*: Let d be the distance to the next car ahead. If $d \leq v$, then the speed is reduced to $d - 1$ ($v \to d - 1$) (No accidents!).

3. *Stochastic breaking*: With probability p_{sb} the velocity of a moving vehicle is reduced by one ($v \to v - 1$).

4. *Propagation*: Each car proceeds by the value of its velocity v.

The dynamics of the traffic flow is determined by the density

$$\rho = \frac{\#\text{cars}}{\#\text{sites}},$$

by the initial configuration, and by the probability p_{sb}.

The traffic flow consists of undisturbed motion with more or less constant velocity (laminar flow), at low densities. We find car clusters (small jams) at high densities, which are formed randomly due to fluctuations of velocity. One can also observe the phenomenon of 'congestion from nowhere'.

Non-interacting Cars

We start out with very low traffic density, which corresponds to *isolated cars*. The motion describes a random walk in which with probability $q = 1 - p_{sb}$ the speed increases by one and with probability $p_{sb} = 1 - q$ the car decreases its speed. In N steps the mean number of acceleration steps is Nq. Starting with velocity zero, it takes on average $N = \frac{v_{\max}}{q}$ steps until the car reaches the maximum speed allowed. After this 'equilibration' phase in which a car reaches the maximum speed the behavior is fairly simple. Starting from either $v = v_{\max}$ or $v = v_{\max} - 1$, the speed after the intermediate step 1 will be $v_{\max}$. After all four substeps it will be $v_{\max} - 1$ with probability p_{sb} and $v_{\max}$ with probability $q = 1 - p_{sb}$. The car can never reduce its speed to $v_{\max} - 2$ or lower, once it has reached $v \geq v_{\max} - 1$. Hence, after the equilibration phase, the average speed for 'non-interacting' cars is

$$\langle v \rangle = v_{\max}(1 - p_{sb}) + (v_{\max} - 1)p_{sb} = v_{\max} - p_{sb}.$$

Interacting Cars

If there is a sufficient density of cars on the road, they will interact. When a car gets too close to the car in its front, it has to slow down. This can cause the next car to get too close and also slow down, a little later, and so on. The result is a pattern of breaking and slow movement which proceeds *backwards* along the road (!), as can be seen in Fig. 4.5 and beyond.

The higher the density of cars, the more severe the breaking becomes. Hence the average speed will *decrease* with higher density of cars. As a function of $v_{\max}$ the average speed saturates quickly: fast cars do not travel any faster than slower ones on a full road.

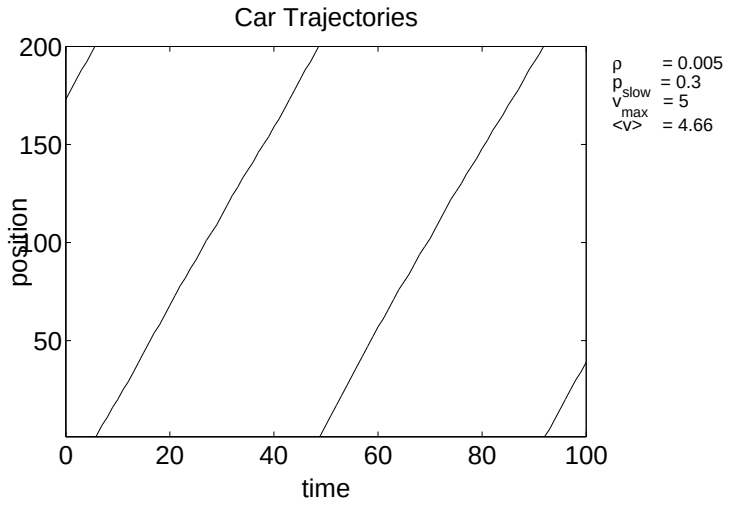

Figure 4.4: One car is on the road. It slows down stochastically with $p_{sb} = 0.3$ and has a maximum speed $v_{\max} = 5$. The average speed $\langle v \rangle = 4.66$ agrees with the general formula $\langle v \rangle = v_{\max} - p_{sb}$.

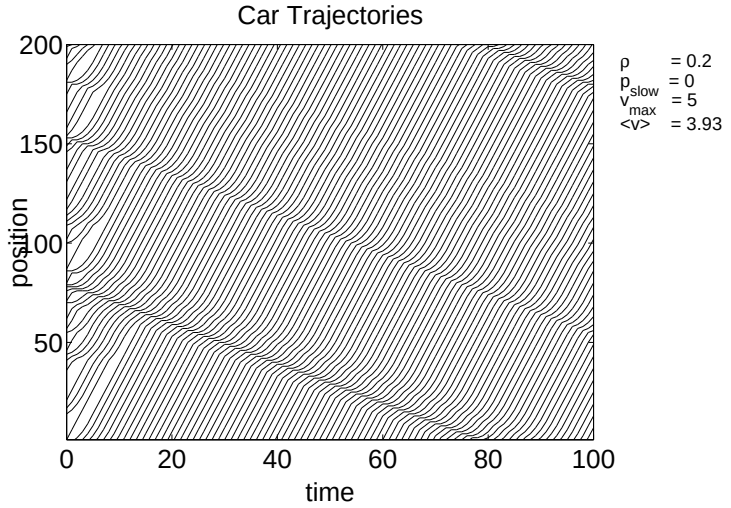

Figure 4.5: Parameters are $\rho = 0.2$, $p_{sb} = 0$, and $v_{\max} = 5$. The average speed is reduced to $\langle v \rangle = 3.93$ due to the presence of other cars. Apart from occasional minor slowing downs, the traffic is still laminar.

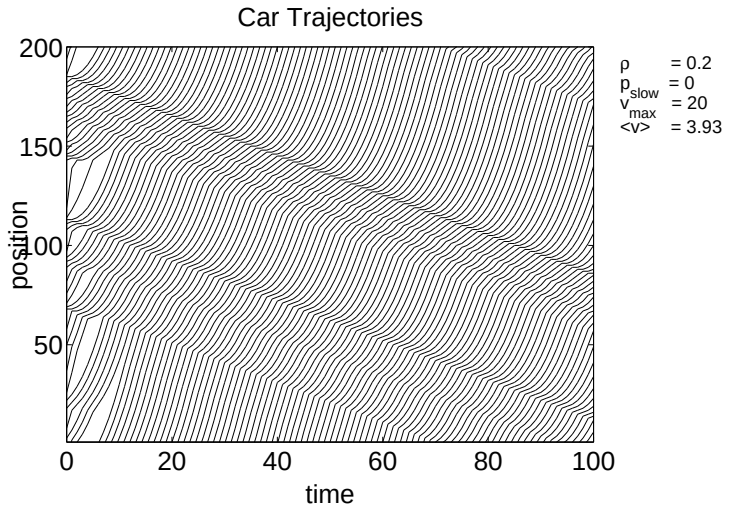

Figure 4.6: Parameters are $\rho = 0.2$, $p_{sb} = 0$, and $v_{\max} = 20$. Although the maximally allowed speed has been increased significantly, the traffic flow looks very similar to that of the previous figure. It is laminar with an average speed of $\langle v \rangle = 3.93$, the same as before !

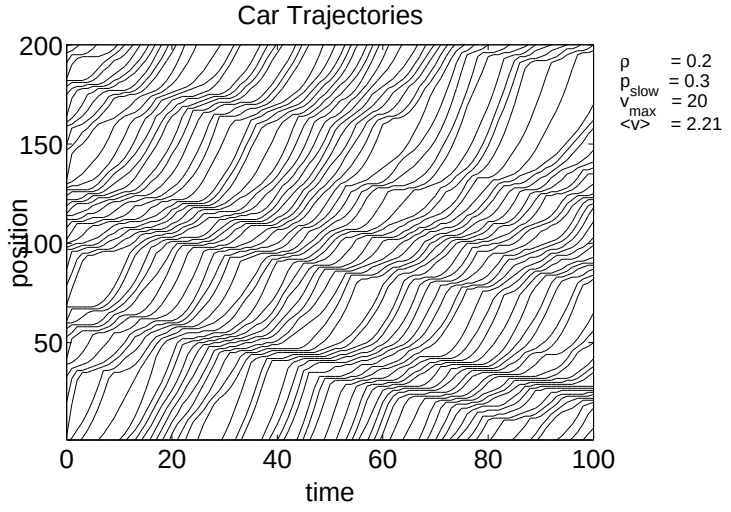

Figure 4.7: Parameters are $\rho = 0.2$, $p_{sb} = 0.3$, and $v_{\max} = 20$. The stochastic slowing down leads to an erratic traffic flow with congestion and a reduced average speed of $\langle v \rangle = 2.21$.

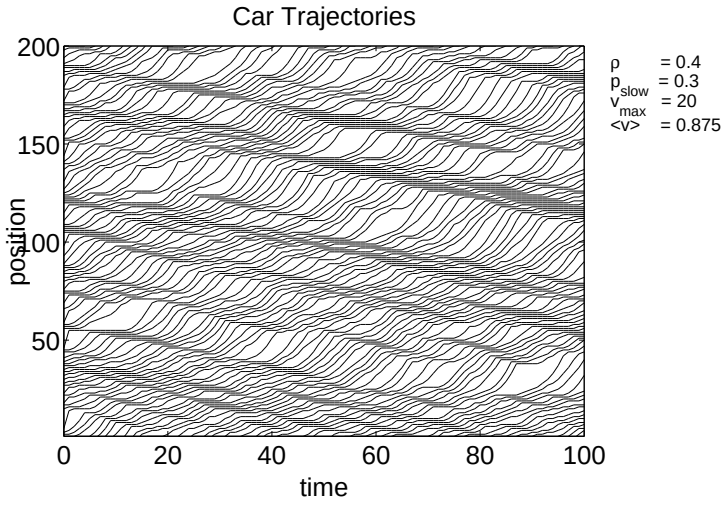

Figure 4.8: Parameters are $\rho = 0.4$, $p_{sb} = 0.3$, and $v_{\max} = 20$. A further increase of the traffic density leads to 'stop-and-go' waves and the average speed is merely $\langle v \rangle = 0.88$.

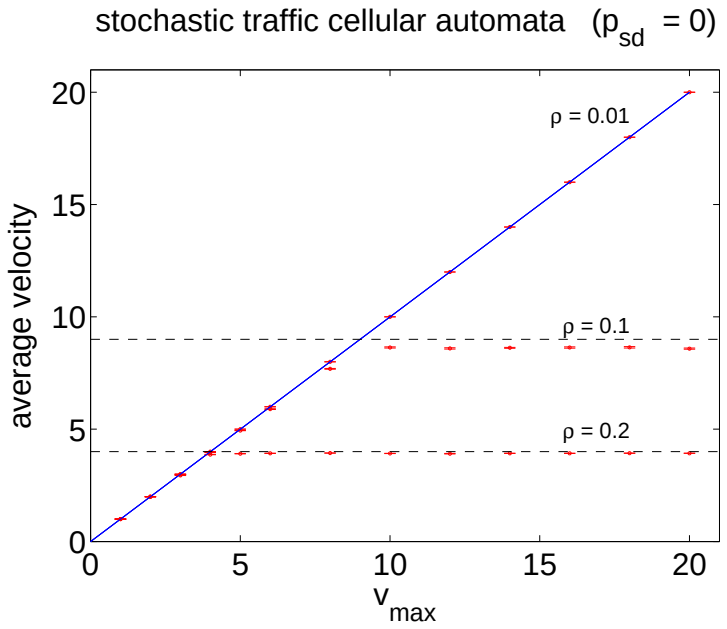

Figure 4.9: Average speed versus $v_{\max}$ for different densities without stochastic slowing down ($p_{sb} = 0$). The solid line shows the theoretical result for non-interacting cars.

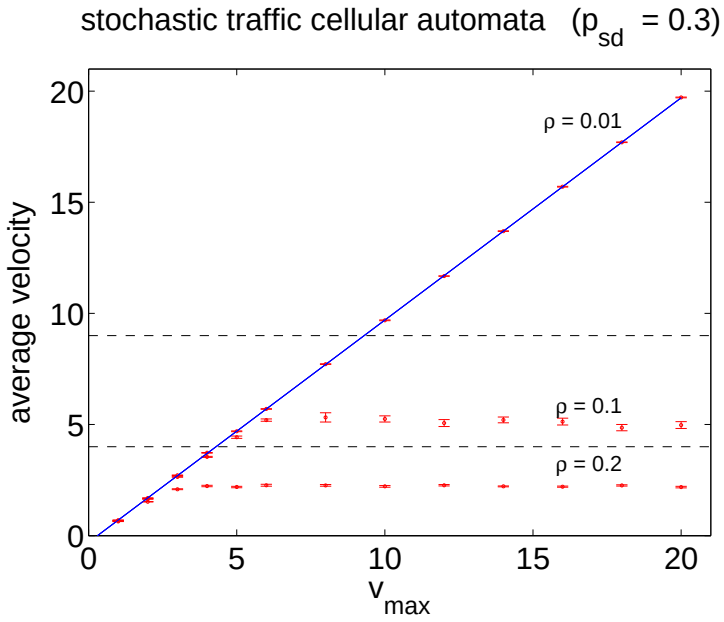

Figure 4.10: Average speed versus $v_{\max}$ for different densities with stochastic slowing down ($p_{sb} = 0.3$). The solid line shows the theoretical result for non-interacting cars.

Figure 4.9 depicts the average velocity as a functions of $v_{\max}$ in the absence of stochastic slowing down. In the low density limit the results agree with those for non-interacting cars. Since there is no stochastic slowing down, the cars drive with maximum speed. Also for higher densities the cars drive with the maximum speed allowed as long as $v_{\max}$ is small. Beyond a certain value $v^*_{\max}$ the average speed levels off at about $v^*_{\max}$. With increasing density the critical velocity $v^*_{\max}$ decreases. The behavior can be understood easily. If N_c cars are arranged equidistantly along the road of length L, then the average distance between cars is $d = \frac{L}{N_c} = \frac{1}{\rho}$. According to the STCA rules, the speed is limited to $d - 1$, which is the number of empty cells between successive cars. Hence we can estimate

$$v^*_{\max} \simeq d - 1 = \frac{1 - \rho}{\rho}.$$

Therefore, at large density ρ, the *throughput* of cars $v \cdot \rho$ behaves like $1 - \rho$. At small density, however, it is approximately $\rho \cdot v_{\max}$. Thus there must be an optimum density in between, for which the throughput is maximized. Beyond this density, the road gets increasingly clogged.

In figure 4.10 stochastic slowing down is included. We observe a similar overall behavior, merely the critical velocities are reduced.

4.5 Percolation: Forest Fires

A common question is whether two sides of a porous object are connected by a continuous path such that a liquid will go from one end to the other. This is called "percolation". It occurs in a multitude of incarnations, including e.g. the Ising model.

Here we look at a simple model of "forest fires". We start with a two-dimensional square arrangement of cells with periodic boundary conditions. Each cell can be in one of four states: Empty, living tree, burning tree, burnt-out tree. Initially we place living trees with occupation probability p in each cell; otherwise the cells are empty. We then light a fire in the center.

The update rules of the CA are as follows.

- A living tree catches fire if any of its nearest neighbors burns.
- Trees burn one time step, afterward they are burnt-out.

The system parameters are the system size L and the probability p for the presence of an inflammable tree. When p is low, the fire will stop quickly since only a few trees will be reached. When p is large, then the trees will be very dense and all or almost all of them will burn, within a time $\simeq L$. At intermediate probabilites p some trees will only be reached by the fire via a long winding path, and therefore the total burning time can be large. Indeed, there is a *critical* probability p_c, where paths of neighboring trees *percolate* through the lattice. At p_c, the burning time diverges (with growing L).

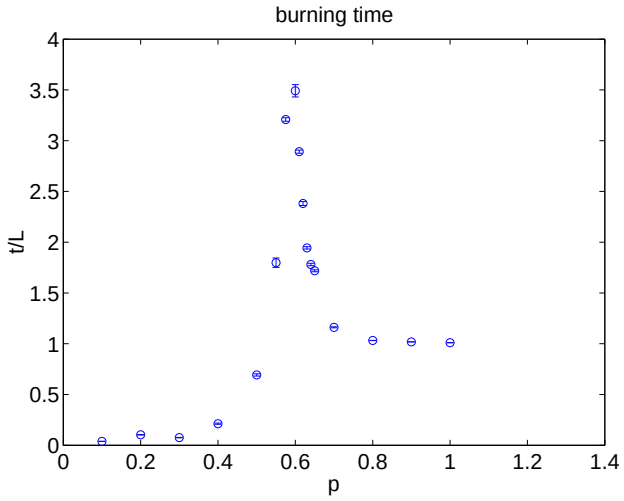

Figure 4.11: Dependence of the burning time on probability p. System size 200×200

This phenomenon is a sign of a phase transition, related to the phase transition in the Ising model, where length scales, as well as the time scales for simulations diverge. Indeed, the *disappearence* (divergence) *of all length and time scales* is the defining characteristic of criticality.

Algorithm 9 MATLAB Code: Forest Fire

```
p = 0.6;
L = 100;
i1 = [L, 1:L-1]; i2 = [2:L, 1];
            % n.n. tableaux
forest = (rand(L,L)<p);
            % randomly arranged trees
forest(forest == 0) = 4; % empty cells
forest(L/2,L/2) = 2;
            % start fire in center
fig = image(forest,'erasemode','xor');
colormap([.1 .7 .1; 1 0 0; 0 0 0; 1 1 1]);
            % green,red,black, white
while sum(forest(:)==2) > 0
  ind = find(forest==2);
            % indices of burning trees
  forest((forest==1) & ...
    (forest(i1,:)==2|forest(i2,:)==2|...
    forest(:,i1)==2|forest(:,i2)==2)) = 2;
  forest(ind) = 3;
  set(fig,'cdata',forest);
  drawnow;
end
```

4.6 Self-Organized Criticality

In the systems just discussed, like forest fires, the Ising model, or also water, criticality occurs when some parameter, like a temperature or the concentration of trees, is tuned to a specific value.

Amazingly, there are many natural systems which evolve towards criticality by themselves, without any tuning. Such Self-Organized Criticality (SOC) can be observed for e.g. earthquakes, river currents, sand piles, avalanches, etc. It is a frequent feature of *dissipative dynamical systems*.

The disappearance of all length (and time) scales implies *power law* behavior. For example, the size distribution of earth quakes does not follow a function $f(r/r_0)$ with some scale r_0, but instead a power law $r^{-\tau}$ with some characteristic exponent τ. The absence of a characteristic scale also implies *self-similarity* of the system at different lengths.

4.6.1 Sand piles

The paradigm example of self-organized critical systems is a pile of sand. Let us drop grains of sand on a horizontal plane at randomly chosen places, one grain at a time. At some point in time, the average slope of the pile reaches a steady state corresponding to an angle that cannot be exceeded no matter how long we carry on adding sand. The stationary state of the sandpile is not completely uniform since variations of the local slopes are possible. If we add a grain of sand, which causes the local slope to exceed the critical angle, an avalanche is triggered. Avalanches can have any size, without characteristic scale (within the limits of roughly molecule size and system size). They therefore exhibit a power law distribution of sizes. Similarly, the times of avalanches are extremely irregular. The time intervales have no characteristic scale between peaks and also obey a power-law distribution.

Sandpile Cellular Automaton

To examine these observations mathematically, BAK, TANG, and WIESENFELD proposed a simple CA model (*BTW model*). In this "sandpile" model on the two-dimensional square lattice it is not the slope but the *height* of sand which determines avalanches. Consider a rectangular lattice of linear dimension L. Each site i of the lattice is characterized by an integer z_i, the number of particles or the local height at this site. One drops a grain of sand on a site i chosen at random, thereby increasing its height by one:

$$z_i \rightarrow z_i + 1.$$

If this new height exceeds a maximum stable value, say 4, then the column of sand at site i becomes unstable and topples. The height z_i decreases by

4 and each of the four nearest neighbors j of the site i receives one particle:

$$z_i \to z_i - 4, \quad z_j \to z_j + 1, \qquad j : \text{n.n. of site } i.$$

(Here, 'n.n' means nearest neighbor.) If a toppling occurs at the edge of the lattice, the toppled site gives one particle to each of three neighbors while one grain drops out of the system.

To watch the evolution of the sandpile in time, we assume that one adds one particle to a stable configuration at each discrete point in time. If the height z_i reaches 5 somewhere, there is a toppling wherein 4 particles are transferred from the unstable site to its neighbors. The transferred particles may cause instabilities among new sites. The toppling of the latter perturbs next neighbors and a chain reaction propagates up to the moment when all sites get stable again. One assumes the updating to be done concurrently, with all sites updated simultaneously. The relaxation processes are assumed to be quick enough to be completed by the next discrete time. A collection of s distinct sites relaxed during an interval between two successive discrete moments of time forms an avalanche of size s. If a toppling at a given site causes instabilities at all nearest neighbors, the initial site receives 4 particles back and gets unstable after the next updating and therefore topples again. Typically, almost all sites inside a large avalanche undergo multiple topplings. The total amount of topplings in the given time interval is the mass m of the avalanche. The duration t of an avalanche is the number of updatings for the relaxation process to complete. The formulated rules describe a CA which is useful for computer simulations. The first investigations of sand piles already displayed power-law dependencies for distributions of all basic characteristics of the model:

$$\begin{aligned} D(s) &\propto s^{-\tau} \\ D(m) &\propto m^{-\kappa} \\ D(t) &\propto t^{-\alpha} \end{aligned}$$

and provided rough estimates for the critical exponents τ, κ, α in the size, mass, and duration distributions.

4.6.2 Chain of blocks and springs

The following simple model is another simple example of self organized criticality.

- One-dimensional arrangement of L blocks, connected by springs to their nearest neighbors.
- There is friction between the blocks and the underlying plane.
- The movement of the chain is driven by an external force.

- A block slips if the force on a block exceeds a threshold, the maximum static friction.
- The slip of a block changes the forces on its nearest neighbors, which results in further slips, so that a part of the chain moves together.

Question: If we place a glass of water on a block in the middle, is it possible to pull in such a way that the water in the glass would never be spilled? The answer is NO. If the length of the chain L becomes very large, the probability of very sudden movements of large parts of the chain becomes large, and the probability of spilling tends to unity.

In a more formal way, the motion of the chain in the steady state is characterized by an average velocity v_{av}. The quantity of interest, however, is the distribution of the velocities or of the kinetic energy of a block

$$P(\varepsilon) = P(|E - E_{\text{av}}| > \varepsilon).$$

One could think that the energy fluctuations might be characterized by a fixed parameter ε_0 independent of the number of blocks L. Then we would typically have

$$P(\varepsilon) \propto e^{-\varepsilon/\varepsilon_0},$$

where ε_0 is a cutoff independent of L. This exponential law corresponds to a smooth motion, if ε_0 is sufficiently small.

Actually, however, the sequences of blocks at rest form clusters of any size. When the force at the edge of a cluster exceeds the maximum static friction, the motion of the whole cluster is triggered. A block involved in this motion performs a big jump giving rise to a considerable fluctuation of the kinetic energy. The size distribution of the clusters has no characteristic length except L and 1. Therefore, the energy distribution for large L can be written in the form

$$P(\varepsilon) \propto \varepsilon^{-\tau},$$

where τ is a constant. This power law implies unlimited large fluctuations in the kinetic energy, similar to the avalanches of the sandpile model.

Chapter 5

Fractals

Literature

- J. SCHMELZER, G. RÖPKE, and R. MAHNKE, *Aggregation Phenomena in Complex Systems: Principles and Applications*, J. Wiley (1999).
- M.F. BARNSLEY, R.L. DEVANEY, B.B. MANDELBROT, H.O. PEITGEN, D. SAUPE, and R.F. VOSS, *The Science of Fractal Images*, Springer (1988).
- H. GOULD, J. TOBOCHNIK, and W. CHRISTIAN, *An Introduction to Computer Simulation Methods: Applications to Physical Systems*, Addison Wesley (2006).

5.1 Introduction

Fractals occur in nature in a multitude of incarnations. Yet, before the invention of computers, fractals were apparently recognized only a few times as an important phenomenon. One occasion was when British map makers discovered a problem with measuring the length of Britain's coast. On a zoomed out map, the coastline was measured to be about 5,000 (in some odd units). When measuring the coast on more zoomed-in maps, it became longer, like 8,000. And by looking at really detailed maps, the coastline was beyond twice the original.

A second instance of pre-computer fractals was noted by French mathematician G. JULIA. He wondered what a complex iterative map would look like, such as the one named after him, in the form of $z^2 + c$, where c is a complex constant. The idea of an iterative map is that one takes the x and y coordinates of a point and plugs them into z in the form $z = x + iy$, squares this number and then adds c, a constant. Then one plugs the resulting pair of real and imaginary numbers back into z, runs the equation again, and keeps doing so until the result is greater than some threshold, the 'orbit'.

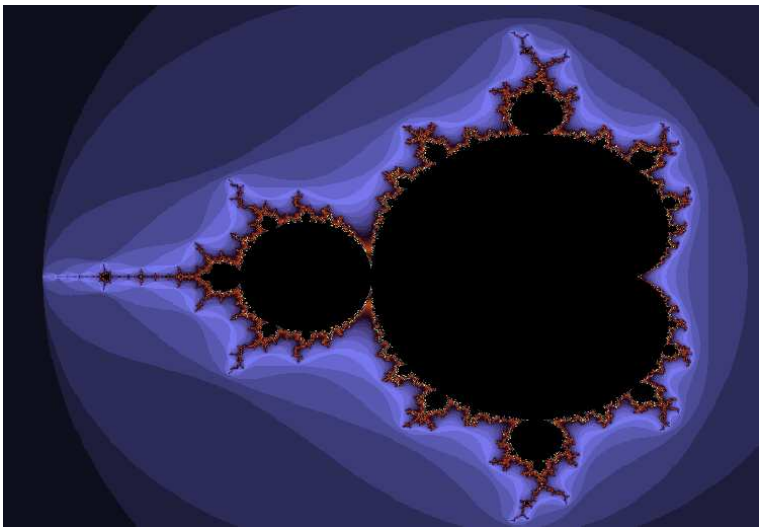

Figure 5.1: A typical MANDELBROT picture of a Julia set.

Later, B. MANDELBROT, working at IBM, implemented such iterative maps as programs. He assigned a color to the number of times one has to run the equations to get out of the 'orbit' and displayed each pixel (x, y) by the corresponding color. When the map starting at (x, y) cannot get out of the orbit, the point is made black. He obtained famous pictures of Julia sets, such as figure 5.1. Mandelbrot also coined the notion *fractal*.

The basic concept of fractals is that they contain a large degree of *self similarity*. This means that they usually contain little copies of themselves buried deep within the original and they also have infinite detail. Like the coastal problem, the more one zooms in on a fractal, the more detail (coastline) one gets.

We have already seen self similar structures in the critical systems mentioned earlier, some of them self-organized. They include e.g. percolation at the threshold and the Ising model at its phase transition. These structures have no intrinsic scale (between "atomic" and system size) and are also fractal, although there is no regularity in them.

Regular fractal properties occur in a wide variety of natural objects. Examples can be found in plants, sea shells, polymers, thin films, colloids,[1] and aerosols. Often these structures have intruiging shapes.

We will see that these shapes have non-integer dimensions. Some geometric objects are exact fractals with the same dimension for all their points, while for other objects the dimension can be defined only locally or on the average. We will not study the theories that lead to fractal geometry, but we will rather look at how some simple models and rules produce fractal structures. To the extent that these models generate structures like

[1] *Colloid*: a substance consisting of very tiny particles that are usually between 1 nanometer and 1000 nanometers in diameter and that are suspended in a continuous medium, such as a liquid, a solid, or a gaseous substance.

those occurring in nature, it is reasonable to assume that the natural processes may be governed by similar rules.

When we deal with complicated objects that have fractional dimensions, different definitions of dimension are conceivable, and each may give a somewhat different answer. In addition, the fractal dimension is often defined by using a measuring box the size of which approaches zero. In realistic applications there is in general a smallest and a largest scale, respectively, which also hampers the precise determination of the fractional dimension.

One definition of a fractional dimension d_f (the HAUSDORFF dimension) is based on our knowledge that a line is of dimension 1, a rectangle of dimension 2, and a cube of dimension 3. Let's assume we have a mathematical formula, that yields results in agreement with our experience for regular objects. It seems perfectly legitimate, then, to apply this formula to fractal objects, resulting in non-integer values for d_f. For simplicity, let us consider objects that have the same length L on each side, as do equilateral triangles and squares. We postulate that the dimension of an object is determined by the dependence of its mass upon its length.

$$M(L) = AL^{d_f}. \tag{5.1}$$

Here A is a constant and the power d_f is the fractal dimension. We will see that when we apply this rule to some unusual objects, it produces fractional values for d_f.

Fractals have technological applications. Antennas have always been a tricky subject. A single wire of some length is an antenna tuned to a specific frequency. It is not good for accessing a large range of frequencies, which is often necessary. It is also less efficient than an array of antennas in tapping the electromagnetic field. Antennas of fractal shape provide both high efficiency and a wide range of useable frequencies. They are for example used in many mobile phones.

5.2 The SIERPINSKI Gasket

We generate our first fractal, shown in Fig. 5.2, by the following rule. We start with an equilateral triangle, filled with black color. We remove an inverted equilateral triangle of size $L/3$. The resulting figure consists of three black equilateral triangles. We iteratre this procedure, removing inverted triangles from the center of the filled triangles at each step. The result is shown in Fig. 5.2. (The name is due to the fact that a gasket ("Dichtungsring" in German) for an automobile cylinder head has some remote resemblance to the Sierpinski gasket.)

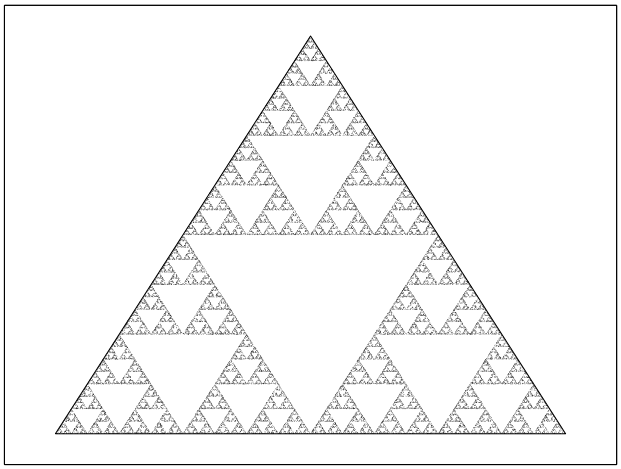

Figure 5.2: A SIERPINSKI gasket. Such a pattern has been found in the tile work of medieval monasteries and on the shells of sea animals. Each filled part of this figure is self-similar.

5.3 Analytic Determination of the Fractal Dimension

The topology of Fig. 5.2 was first analyzed by the Polish mathematician SIERPINSKI. Observe that there is the same structure in a small region as there is in the entire figure. In other words, if the figure were infinitely dense, any point of the figure could be scaled up in size and would be similar to the whole. In the context of fractals, this property is called self-similarity.

We now analyze how the density $\rho = \frac{\text{"mass"}}{\text{area}}$ of dots depends on size. Here the "mass" inside some area means the total black area inside (which we might think of as made up of points of some atomic scale, for definiteness). We start with some small triangle of length r and of a density of dots which we call ρ_0, implying a mass which we call m_0. For convenience we call r^2 the "area" (omitting a factor $\sqrt{3/4}$). Then

$$\rho(L = r) = \frac{M = m_0}{r^2} =: \rho_0.$$

Next, for the triangle with side $L = 2r$ the density is

$$\rho(L = 2r) = \frac{M = 3m_0}{(2r)^2} = \frac{3m_0}{4r^2} = \frac{3}{4}\,\rho_0.$$

We see that the extra white space leads to a density that is 3/4 the density of the previous stage. In the next step we obtain

$$\rho(L = 4r) = \frac{M = 9m_0}{(4r)^2} = \left(\frac{3}{4}\right)^2 \frac{m_0}{r^2} = \left(\frac{3}{4}\right)^2 \rho_0.$$

We see that as we continue the construction process, the density of each new structure is $3/4$ the density of the previous one. This is unusual. For ordinary objects the density is an insensitive quantity, independent of the size of the object. For this strange object, there is a power-law dependence of the density on the size of the object (with discrete steps of L) :

$$\rho = cL^{\alpha},$$

where c is some constant. The power α is determined via:

$$\alpha = \frac{\Delta \log \rho(L)}{\Delta \log(L)} = \frac{\log(1) - \log(3/4)}{\log(1) - \log(2)} = \frac{\log(3)}{\log(2)} - 2 \simeq -0.41504.$$

This means that, as the gasket gets larger and larger, it contains more and more open space. So even though its mass approaches infinity, its density approaches zero! And since a two-dimensional figure like a solid triangle has a constant density as its length increases, a 2D figure would have $\alpha = 0$. Since the SIERPINSKI gasket has a nonzero α value, it is not a 2D object! The fractional dimension d_f is defined by

$$M(L) = \rho(L) * L^2 = cL^{\alpha+2} = cL^{d_f}. \tag{5.2}$$

Hence

$$d_f = \alpha + 2 \simeq 1.58496.$$

We see that the SIERPINSKI gasket has a dimension between that of a 1D line and a 2D triangle; that is, it has a fractional dimension.

We can also determine the fractal dimension numerically. Algorithm 10 measures the exponent α. It first maps the dots of the fractal onto a grid of size 1024×1024 and generates a corresponding array A with entries 0 and 1. It then counts the number of dots in a square of size L. The procedure is repeated 100 times, and the results are fitted according to eq. (5.2). The numerical result for the fractal dimension is

$$\alpha = 1.59 \pm 0.01.$$

which is in perfect agreement with the analytical result.

Amazingly, one can define a 3-dimensional analogue of the Sierpinski gasket, consisting of tetraeders inside tetraeders. This object, although 3-dimensional, has a fractal dimension of exactly $\frac{\log 4}{\log 2} = 2$!

5.4 Length of a Coastline

MANDELBROT asked the classic question "What is the length of the coastline of Britain?". MANDELBROT's answer introduces another definition to our study of fractals, namely using box counting to determine fractal dimension.

Algorithm 10 MATLAB Code: Fractal Dimensions

```
N_pts = 15000;
N_rep = 100;
L = 10; N = 2^L;
alpha = zeros(N_rep,1);
for ir = 1: N_rep
  X = sierp_fct(P,N_pts);
  X = ceil(X*N); % map onto grid
  A = zeros(N,N);
  A(sub2ind([N,N],X(:,1),X(:,2))) = 1;
  for i = 1: L
    LL(i) = 2^i;
    m(i) = sum(sum(A(1:LL(i),1:LL(i))));
  end
  ind = find(m > 0);
  ln_LL = log(LL(ind));
  ln_m = log(m(ind));
  [p,S] = polyfit(ln_LL,ln_m,1);
  alpha(ir) = p(1);
end
fprintf('alpha = %10.3f +/- %10.3f\n',...
  mean(alpha),std(alpha)/sqrt(N_rep));
```

As illustrated in Fig. 5.3, let us divide the plane into squares of size s and we count the number of cells N which are crossed by the object under consideration. Then the scale s is changed and the box counting is repeated leading to the dependence of the number of crossed cells $N(s)$ on the scale s. For 1D objects, we have

$$N(s) \propto s^{-1},$$

and for 2D objects the relation is:

$$N(s) \propto s^{-2}.$$

The dimension d enters into the power law as

$$N(s) \propto s^{-d}, \tag{5.3}$$

and we extend this formula to fractal objects.

The fractal dimension is then determined from a straight line fit to the $N(s)$ data on a log-log scale. Points close to the scales $s = 1$ and $s = L$ have to be omitted, as the self-similarity breaks down at these points when the surface is constructed with a finite resolution $s = 1$ and has finite size $s = L$.

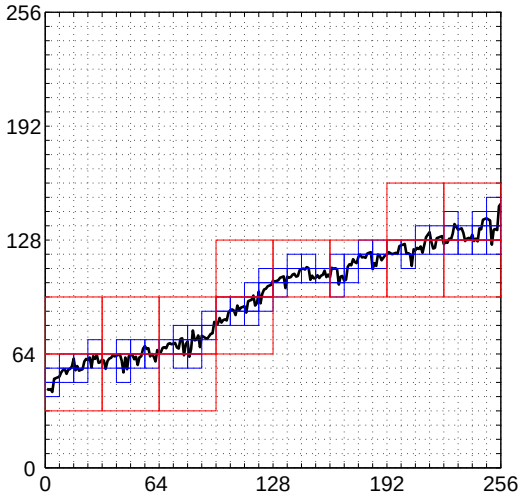

Figure 5.3: Illustration of the box counting method. The surface has been tilted to make the counting procedure more obvious. On scale $s = 8$ the curve passes through $N_8 = 70$ (blue) boxes, while $N_{32} = 14$ (red) boxes are crossed on the scale $s = 32$.

5.5 Ballistic deposition

There are numerous physical processes in which particles are deposited on a surface to form a film, e.g. Molecular Beam Epitaxy (MBE). Here we consider particles that are evaporated thermally from a hot filament. The emission, the propagation to the surface and the diffusion on the surface are random processes. Nonetheless, the films produced by deposition turn out to have well-defined structures. We will simulate this growth process on the computer by simplified rules.

Simulation

For simplicity, we consider particles falling onto and sticking to a horizontal line of length L (instead of an actual surface). The emission and propagation process to the final destination on the line is mimicked by the following rules.

1. Start with a flat substrate and zero film thickness $h_i = 0;\ \forall i$.
2. Determine at random the site i at which the particle(s) will stick eventually.
3. Decide how many particles shall be added to this place. We choose

$$h_i = \begin{cases} h_i + 1, & \text{if } h_i \geq \max(h_{i-1}, h_{i+1}) \\ \max(h_{i-1}, h_{i+1}), & \text{otherwise} \end{cases}$$

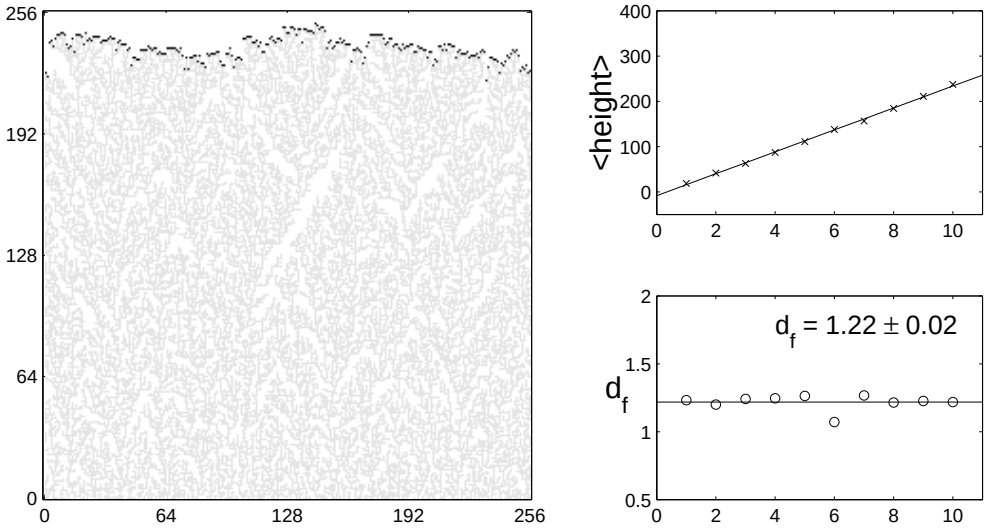

Figure 5.4: Simulation of the ballistic deposition on a 1D substrate (left panel). The top (black curve) represents the final "surface". The other marks indicate intermediate surfaces during the growth process. The right panel shows the fractal dimensions of the surface during the growth process as a function of time.

The reason for the last step is to accelerate of the time consuming diffusion process on the surface. The sticking probability is higher at edges than on plane surfaces patches. To model this effect (in a drastic way), the height is increased by one if the particle lands on a flat surface patch, otherwise in this version of ballistic deposition the height at site i is set to the maximum height of its neighbors.

A representative result of a simulation is shown in Fig. 5.4. Below the surface, which is indicated by black dots, all columns are actually completely filled. The fractal internal structure which is shown instead contains information about the growth process. Grey dots indicate surfaces of previous iterations. The empty parts of the columns occur when particles hit an edge, which is subsequently filled in one time step according to deposition rule (3). The average height increases linearly with time (see right panel of Fig. 5.4). The fractal dimension d_f for different surfaces during the growth process, computed according to eq. (5.3), is also shown. Due to the finite range of the surface, the fractal dimension is a random variable and varies during the growth process. The average fractal dimension is $d_f = 1.22$.

5.6 Diffusion-Limited Aggregation

Diffusion-limited aggregation (DLA) takes place in non-living (mineral deposition, lightning paths) or living nature (corals) and results in objects with unusual geometry. We will first discuss the meaning of the terms in the notion 'DLA'.

Diffusion is a random motion of particles. Individual particles typically move far away from their original position. The distance, measured by the square-root of the variance, grows as:

$$d = \sqrt{\mathrm{var}(\mathbf{x})} \propto \sqrt{t}.$$

In contrast to a normal flow, where all particles under consideration move more or less into the same direction, the average distance $\langle \mathbf{x} \rangle$ covered by the particles within a random walk (Brownian motion) is zero. In diffusion there might be a net transport of material, when the starting density is not uniform. If you pour a drop of ink into a glass of water, the ink spreads. But diffusion is not only a phenomenon in fluids, it can also occur in solids. It just takes much more time in the latter case.

The driving force for diffusion is the entropy. The energy of a state where all ink molecules are piled up in one corner could be the same as the energy for a state in which the ink is spread homogeneously. Then each 'microstate' has the same statistical (BOLTZMANN-) weight. However, there are overwhelmingly more states with a nearly homogeneous density then there are states yielding a significant inhomogeneity. In equilibrium, the latter therefore has vanishing odds to be observed.

Aggregations are formed when particles attract each other and stick together. (Then the energies of the above microstates are not equal to each other.) Depending on the strength of the forces the resulting aggregates differ. Strong forces lead to compact and well ordered crystalline structures. When the forces are weaker it may happen that particles stick together for a while and then travel around again. The resulting aggregates have no distinct shape. Each aggregate is unique. Fluffy, not compact, maybe tree like clusters emerge, like e.g. snow-flakes.

DLA-clusters are aggregates, where the shape of the cluster is controlled by the criterion of whether particles coming from far away can reach the cluster in finite time. When they do reach it, they always stick. DLA-clusters are ideal objects for computer simulations. One approach is to simulate the random walk of the particles and their aggregation. Typically one uses a lattice, puts an initial seed particle at some origin and another particle somewhere on the lattice. Then the second particle moves around in random motion, step by step from lattice site to lattice site. Finally it may meet the first particle and stick next to it. Then another particle is thrown onto the lattice, it walks around and after a while meets the first two. This is continued for as many particles as one likes, one after the other.

There are many variations of the DLA model with more realistic properties depending upon the application of interest.

Simulation

Here we study the most simple DLA simulation on a 2D lattice:

1. Define a simple square lattice of vacant grid points.
2. The linear size L of the lattice should be 'sufficiently large' in order to avoid boundary effects.
3. Place a seed particle (first element of the cluster) at the center of the lattice.
4. Draw a circle C_1 that just fits into the square and map it onto the grid points.
5. The points in and on C_1 define the area A_1.
6. Add a particle at random on C_1.
7. Let the particle perform a random walk, with equal probability in the four nearest neighbor directions.
8. The random walk stops if
   (a) the particle escapes from A_1.
   (b) the particle touches the aggregate.
   Then add the particle to the aggregate.
9. If the aggregate has not yet the desired size go to 6.

In this form, the algorithm is highly inefficient as it takes a long time until the particle eventually touches the aggregate. Since we are not interested in the dynamics itself but rather in the form of the aggregate, the simulation can be accelerated considerably by the following reasoning. Consider a circle of radius r_1 centered around the seed particle that is only slightly bigger than the aggregate at a given time. The situation is depicted in Fig. 5.5.

In order to reach the aggregate the random walk particle has to cross the circle. Due to symmetry, all points on the circle are crossed with equal probability. Hence, the particle can be added straight away somewhere on the circle with equal probability. This circle plays the role of circle C_1 defined above. However, now we cannot stop the random walk if a particle leaves A_1. This would imply a bias since the escape probability is smaller on parts of the circle which are close to the aggregate than at parts which

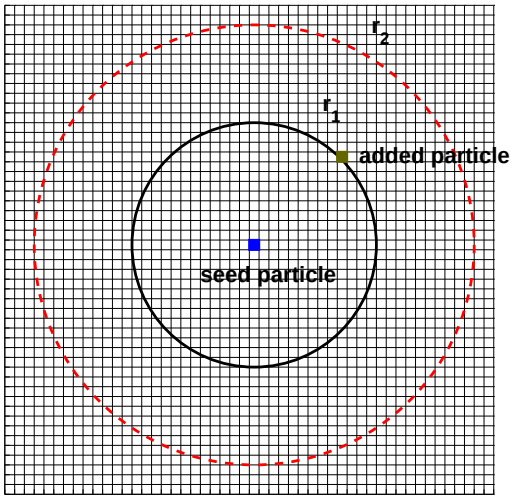

Figure 5.5: Setup of the DLA simulation.

are far away. Instead of using C_1, we approximate its effect by introducing an outer circle C_2 of radius $r_2 > r_1$ which defines the escape radius. If a particle crosses C_2 it is considered lost and a new particle is added on C_1.

Figure 5.6 shows a typical result of a DLA simulation . The fractal dimension is determined analogously to the definition (5.1) via the mass $M(s)$ or rather the density $\rho(s)$. Here it is sensible to consider the mass contained in concentric circles $C(s)$ of radius s around the seed particle. The mass $M(s)$ is defined as the number of aggregate cells inside the circle of radius s. The corresponding volume $V(s)$ is the total number of cells within $C(s)$. The density reads $\rho(s) = M(s)/V(s)$. The fractal dimension is given by the power law dependence

$$M(s) \propto s^{d_f}.$$

In Fig. 5.6 we observe that the fractal dimension of the bulk of the graph is $d_f \simeq 1.7$ while it decreases towards zero at the outer fringes. It is reasonable that the dimension decreases once the outer fringes of the aggregate are reached. A fractal dimension $d_f = 0$ means that the mass is constant beyond a certain radius.

Applications

DLA structures occur for example in the following applications:

- When metals like copper or gold are separated electrolytically out of a solution, shapes like DLA-cluster form under certain conditions.
- When metals are deposited onto surfaces from the gaseous phase to get very thin films a DLA-growth is observed.

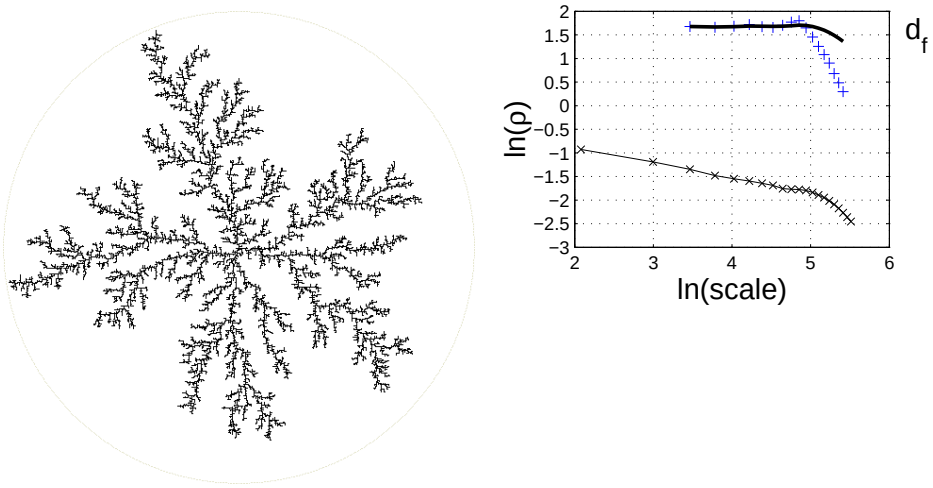

Figure 5.6: The left panel shows an aggregate with $N = 16700$ particles on a grid of linear size $L = 3000$ constructed with $r_2/r_1 = 6$. The right panel exhibits the density ρ as a function of scale s (lower curve) along with the local fractal dimension determined from the slope of 5 neighboring points and the cumulative average of the latter.

- Deposition of carbon on the walls of a Diesel engine exhibit DLA structures.
- Generation of polymers out of solutions can follow a DLA-mechanism.
- Catalyst forming. These materials, of great value in chemical engineering, may show strongly branched surfaces with many holes and channels. The very large surface area is often relevant for the catalytic process.
- Exploitation of oil resources embedded in sand by means of water pressed into the sand. The resulting water-oil-surface may or may not exhibit shapes which resemble those of DLA.